12-2019

Influence of Single and Multiple Histidine Residues and their Ionization Properties on Transmembrane Helix Dynamics, Orientations and Fraying

Fahmida Afrose
University of Arkansas, Fayetteville

Influence of Single and Multiple Histidine Residues and their Ionization Properties on Transmembrane Helix Dynamics, Orientations and Fraying

A dissertation submitted in partial fulfillment
of the requirements for the degree of
Doctor of Philosophy in Chemistry

by

Fahmida Afrose
University of Dhaka
Bachelor of Science in Applied Chemistry and Chemical Engineering, 2011
University of Dhaka
Master of Science in Applied Chemistry and Chemical Engineering, 2013

December 2019
University of Arkansas

This dissertation is approved for recommendation to the Graduate Council.

_____
Roger E. Koeppe II, Ph.D.
Dissertation Director

_____
Frank Millett, Ph.D.
Committee Member

_____
Colin D. Heyes, Ph.D.
Committee Member

_____
Susanne Striegler, Ph.D.
Committee Member

_____
Josh Sakon, Ph.D.
Committee Member

Abstract

Since aromatic and charged residues are often present in various locations of transmembrane helices of integral membrane proteins, their impacts on the molecular properties of transmembrane proteins and their interactions with lipids are of particular interest in many studies. In this work, I used solid-state deuterium NMR spectroscopy in designed model peptide GWALP23 [GGALW$(LA)_6$LWLAGA] with selective deuterium labels to addresses the pH dependence and influence of single and multiple "guest" histidine residues in the orientation and dynamic behaviors of transmembrane proteins. The mutations include Gly to His (G2/22 to H2/22), Trp to His (W5/19 to H5/19) and Leu to His (L8/16 to H8/16). For the glycine to histidine substitutions, either one or both, the peptides show similar biophysical properties to the host GWALP23 peptide, with modest motional averaging and tilted transmembrane orientations that scale with bilayer thicknesses. Yet, the dynamic motion about the average azimuthal rotation increases significantly when the helix carries only H22. However, when the tryptophan residues, W5 and/or W19 are replaced by histidines, the new histidine residues effectively anchor the transmembrane α-helix, providing similar transmembrane topology. A consistent ~30° shift in helix rotation is observed for Trp to His substitutions and found to be terminal-dependent. Modifying the core sequence of GWALP23 with His residues at positions 8 and 16 provides some interesting insights. The peptide is significantly tilted in DLPC, has multiple orientations in DMPC and surface bound in DPoPC and DOPC lipid bilayers, where the bilayer thicknesses increase consecutively from DLPC to DOPC. Further analysis for peptide with only H8 was performed. Results indicate multiple signal resonances, similar to -$H^{8,16}$, but in a thicker lipid bilayer. Moreover, the helix with H8 alone significantly responds with pH in DLPC and DMPC lipids and two titration points for H8 was calculated. Finally, mutation of GWALP23 with two

adjacent histidines at the N-terminal end (positions 4 and 5) causes a large increase in the motional averaging about helix azimuthal rotation, which in turn obscures the actual orientation and the peptide is found to adopt a very small tilt angle (τ).

Acknowledgements

First and foremost, I would like to express my deepest appreciation to my advisor Dr. Roger E. Koeppe II. His valuable suggestions and persistent help in last five years have made this work successful. I thank him for his constant encouragement and support in both my personal and professional life. His knowledge and guidance have always motivated my work in the lab and helped me to build up my understanding in this fascinating field of research.

I also express my sincere gratitude to Dr. Denise Greathouse for her countless help and suggestions in day to day work. She taught me how to handle and troubleshoot the instruments we used in lab. I truly enjoyed our discussions on sharing recipes and all the group potlucks she arranged.

I thank my lab mate Dr. Matthew Mckay, who joined in the lab with me and has been immensely helpful throughout. Whenever I was not comfortable maintaining an instrument by myself, I never had to hesitate to ask him for help. I wish him the best in both his personal and professional life.

I would like to express my deepest appreciation to my committee members Dr. Frank Millett, Dr. Colin Heyes, Dr. Josh Sakon and Dr. Susan Striegeler. Their thoughtful and scientific discussions and guidance have been very useful.

Lastly, my heartful gratitude goes to my parents Md. Abul Basher and Fatema Begum, my sisters Farhana Afrose and Mariam Afrose for their moral support and encouragement. They are the primary reason for who and where I am now.

Dedication

I dedicate this dissertation to Md Foysal Zahid Khan, my loving husband and my best friend, who has been beyond supportive and encouraging to me throughout this work.

Table of Contents

List of Publications

Published Peer Reviewed Paper:

Fahmida Afrose, Matthew J. McKay, Armin Mortazavi, Vasupradha Suresh Kumar, Denise V. Greathouse, Roger E. Koeppe II. (2019.) Transmembrane helix integrity versus fraying to expose hydrogen bonds at a membrane–water interface. Biochemistry 58(6):633-645. **(Chapter 5)**

1. Chapter 1: Introduction

With the known significance of biological membrane and their constituent proteins, great efforts have been made for many years to understand the structures of lipid membranes and their interactions with membrane proteins. The lipid bilayers of biological membranes do not simply provide the matrix to embed proteins but they actively participate in the regulation of local structure, dynamics, and even the activity of a membrane [1]. Very early experiments showed the importance of lipid components for the glucose transport activity in red blood cells [2]. Another relevant example is the loss of activity for mitochondrial respiratory complex I when extracted with depletion of some lipid elements [3-4]. Hence, the importance of the protein–lipid interactions in biology and medicine encourages the need to preserve the lipid environment while extracting proteins from membranes or even when studying membrane proteins.

Membrane proteins, covering an estimated 30% of the entire human proteome [5], are a crucial class of macromolecules in living systems. Their functional roles including transferring specific molecules, ions and other types of signals into and out of the cell as well as being involved in enzyme catalysis make them one of the main focal points of pharmaceutical research recently. About 60% of the current drug and therapeutic targets nowadays are membrane proteins [6]. However, membrane proteins have been much less studied than globular proteins since their structural analysis is extremely challenging. Most of the membrane proteins fold into their native structures with proper amount of stability only when associated with lipids. These issues cause difficulties to crystallize and solubilize such proteins and hence complicates the experimental X-ray crystallographic system. Until now most high resolution structures of membrane protein are from X-ray crystallography (although cryo-electron microscopy has recently contributed 3.4 Å resolution range structures), whereas another powerful technique called solid-state nuclear

magnetic resonances (ss-NMR) spectroscopy provides unique, detailed, dynamically sensitive and biologically authentic information about membrane protein structure and dynamics while avoiding the complexities of crystallography. As an added bonus, with solid-state NMR experiments it is possible to study membrane proteins in their native-like membrane environments using a variety of lipid compositions ranging from lipid vesicles to bicelles, planar or stacked bilayers, and sometime even mimicking the cellular membrane environment.

Among the important segments of membrane proteins are the transmembrane domains that may constitute ~20-30 amino acids with an overall hydrophobic character. This hydrophobicity [7-9] as well as the thermodynamic equilibrium [10] are the primary driving forces for transmembrane domains to form α-helical structures and insert into the membrane. Then the orientation of a such segment relative to the bilayer plane is determined largely by positive-inside rule [11], which states that the positively charged extra-membrane domain should be exposed to the cytoplasmic side, while the neutral or negatively charged extra-membrane domain should orient on the opposite outer side of the membrane. But these rules are not always strictly followed by all transmembrane domains. In many proteins functionally important positively charged Lys and Arg residues can be found within the bilayer core. For example, in the four-helix voltage sensor of voltage-gated potassium channels multiple Lys and Arg residues reside in their charged state and their movement with the membrane potential is vital for channel opening and closing [12-13].

As mentioned earlier, the structures of lipid molecules and their compositions in the surrounding membrane modulate the functional activities of membrane proteins, but this is not the only factor to consider when researching membrane proteins. Membrane proteins are associated with a complex mixture of other proteins and are prone to aggregation in solution [14].

Moreover, most membrane proteins are quite large in size and often contain multiple membrane spanning domains bundled together. Thus, the orientation of each transmembrane domain is affected by the inter- or intra-molecular interactions between neighboring domains and lipids in the bilayer as well [15]. All of these factors make this system very complicated to study and that is why the interaction of membrane protein with lipid molecules and how it affects the overall activity of a protein are still not understood properly. To simplify the overall environment of the cell membrane system, several model systems that mimic the actual cell have been developed. This approach allows one to substitute the complex biological lipid bilayer membrane with individual synthetic lipids of particular hydrocarbon chain length. For mimicking the transmembrane segments of membrane proteins small single span α-helical peptides can be used. These model systems are simple enough to experimentally derive a fundamental understanding of the underlying mechanisms of cell biology, and yet can still approximate aspects of biological processes only emergent in more complex systems. The short alpha-helical model peptides are also advantageous for labeling selective residues isotopically through solid phase peptide synthesis. Because these systems provide results that are very comparable with the natural protein folding and unfolding behavior and allow for specific well-defined changes in the peptide sequence, these systems can be utilized to investigate the direct consequences of single- residue sequence changes on the interactions with the surrounding lipid membrane.

A model WALP peptide sequence ($GWW(LA)_nLWWA$) was an early model peptide that was primarily developed to study the general rules that govern peptide-lipid interactions such as hydrophobic mismatch and lipid phase behavior [16-18].The WALP peptides do not appear to aggregate, are strongly α-helical and consist of a repeating hydrophobic Leu-Ala core sequence flanked by two amphipathic Trp residues on each end. The next generation peptide framework,

GWALP23, which I have employed to initiate my research, is a WALP-like analog, that features only a single Trp residue on each end, with Gly replacing the other Trp residues [19]. This newer peptide has the same benefits of the WALP model yet with advantages of demonstrating much greater sensitivity to the lipid bilayer. GWALP23 also exhibits less dynamic averaging of solid-state NMR observables including the ^{2}H quadrupolar splitting and the ^{15}N-^{1}H dipolar coupling [19-20]. Therefore, it has been successfully used for various type of experimental research to study protein-lipid interactions and related features such as the anchoring properties of different interfacial aromatic residues [21-23], the influence of "guest" residues in the hydrophobic core of the peptide [24-27] and terminal α-helical fraying [28-29]. This system is also utilized to elucidate the titration properties and pKa values of several amino acid residues present at various depths of the bilayer [24, 26-27]. In this dissertation model peptide GWALP23 has acted as a host framework for studying the influence of aromatic residues, particularly histidine, in different locations throughout the sequence.

Histidine is a crucial residue in several functional roles of proteins. The unique structural characteristic of histidine is its side chain imidazole ring that is an aromatic motif which also is ionizable. The ring can coordinate metallic cations (such as Ca^{2+} and Zn^{2+}) and serve as a hydrogen bond donor and acceptor. These features of histidine side chains make this residue play multiple roles in molecular interactions. This residue has been shown to stabilize proteins through long range aromatic and electrostatic interactions with neighboring residues [30-33].

A well characterized histidine-containing transmembrane helix is the M2 proton channel from Influenza A virus [34-35] that plays a critical role in virus replication. This tetrameric channel opens upon acidification and allows protons to flow from the endosome into the virion, which further leads to release of the virus's genetic material into the cytoplasm. The histidine residue

(His 37) present near the center of the transmembrane helix of each segment of the channel serves as the gating mechanism for the proton flow [36-37].

The identified histidine residues in transmembrane domains of several membrane proteins have been found to play meaningful functional roles. Histidine is frequently present in protein active or binding sites. Its roles include the binding of prosthetic groups in the photosynthetic reaction center [38] and hemes in cytochrome *c* oxidase [39], participating in rat prostaglandin receptor $PGF_{2\alpha}$ binding and forming a series of stacked rings in the pore formed by the mammalian copper transporter 1 homo-trimer that is required for maximal copper transport. Histidine also stabilizes the protein folding by forming a salt bridge with a negatively charged residue or by hydrogen bonding [39-40]. The pH sensitivity of histidine is also critical for proteins. With the imidazole side chain pKa of about 6.5, it is a key catalytic residue in many enzymes. One of the most interesting examples is the catalytic triad of serine proteases that is comprised of residues His57, Asp102 and Ser195. The histidine residues (His57) in the triad acts as the general acid and base during the enzymatic reaction and makes Ser195 an unusually strong nucleophile and permits peptide bond hydrolysis [41]. Histidine also has important participation in pH sensing of ion channels, especially the acid-sensing ones. Multiple histidine residues, located adjacent to one another [42] or in nearby positions [43-44], are present in the acid-sensing component of these channels. These important aspects of histidine have driven this research work to understand the particular impact of this versatile amino acid in protein-lipid interactions when present at different depths in lipid bilayer membranes and also when present by itself or in conjunction with other aromatic amino acids (i.e. tryptophan).

Because the use of model peptides is an attractive way to study such protein-lipid interactions, including the orientations and dynamic properties of transmembrane peptides,

throughout this work GWALP23 has served the "parent" or host peptide where a histidine residue is inserted in different locations. Each section of this work addresses multiple related mutants of GWALP23 having single or pairs of histidine residues in different locations. The characterization of each of the new peptides was performed using solid-state ^{2}H NMR spectroscopy with peptides incorporated in macroscopically aligned lipid bilayers. This technique is a powerful tool for determining the orientation and dynamics adopted by a transmembrane α-helix [45] such as that of the GWALP23 family peptides, since the multiple alanine residues within the core of GWALP23 can be ^{2}H-labeled to produce unique signals from each of the ^{2}H-labels of the alanine methyl side chains. These signals, more specifically the quadrupolar splittings of ^{2}H can be used to calculate the overall tilt and azimuthal rotation of the helix as described previously [18].

Additionally, the ionization properties of histidine residues in different location of the sequence can be tested using solid-state deuterium NMR. Similar research work has revealed the titration behavior of other polar residues such as Lys, Arg [24], Glu [27] and even His in different locations [26]. Mutations involving histidine in this study are completely different from previous work [26] and hence these two studies do not merge. Rather, this work provides more detailed ideas about the overall behavior of histidine containing peptides, which was initially introduced in the previous work [26].

In Chapter 2, the histidine residue/s are introduced at the ends of peptide sequence, in positions 2 and/or 22, resulting three peptides, H$^{2, 22}$WALP23; H^{2}GWALP23 and H^{22}GWALP23 (sequences in Table 1). Previous research work performed with similar replacement involved charged (lysine, arginine) and aromatic (tryptophan) amino acid residues [19]. Results from those studies revealed that tryptophans at positions 2 and 22 led (surprisingly) to highly dynamic

behavior of the transmembrane peptide helix, while the polar and charged residues Lys and Arg do not affect the helix orientation significantly. The choice of histidine substitution into these positions allowed comparison of the effect of the imidazole ring to compared to the indole ring for the dynamics of the transmembrane helix. Additionally, it was possible to test whether the His residue acts more as an aromatic residue and shows results similar to Trp or behaves more as a polar residue like Lys and Arg. It turns out from the results of Chapter 2 that the orientations and motional averaging of $H^{2,22}$WALP are quite different from the Trp containing peptide ($W^{2,22}$WALP), but instead are rather similar to the properties of the $K^{2,22}$WALP and $R^{2,22}$WALP analogs. Removal of either H2 or H22 from the sequence of $H^{2,22}$WALP provides additional information. It is observed that an absence of H2 or H22 has no significant effect on peptide orientation, but interestingly the helix with only H22 (H^{22}WALP) possesses higher dynamic averaging than the peptides with only H2 (H^{2}GWALP23) or both H2 and H22 ($H^{2,22}$WALP).

Because interfacial aromatic or charged residues are notorious for anchoring transmembrane helices by forming hydrogen bonds with lipid head groups or with water molecules and thereby providing stable peptide orientation, tryptophan is frequently found at the interfaces of membrane proteins. The indole ring hydrogen bonding of Trp is important for the preference of this residue for an interfacial position. Histidine has an imidazole ring side chain which also forms hydrogen bonds in many proteins and helps in protein function (as explained in previous section). So, to obtain the probable "anchoring" properties of histidine, in Chapter 3 I have analyzed three peptides having one histidine (H5 or H19) and one tryptophan (W19 or W5), and then with only histidines (both H5 and H19) at positions 5 and 19 that are originally occupied by tryptophan residues in GWALP23 sequence (Table 1). Previous studies showed that single replacement of a Trp residue by Phe [46] or Tyr [23] near the N-terminal interface of the

GWALP23 results in similar transmembrane orientations. Replacement of only W19 or both W5 and W19 with tyrosine also retained the defined orientation and low dynamics [22]. Based on these precedents, in Chapter 3 peptides with H5 or H19 or both were examined to see the effect of such mutation on protein-lipid interactions. Results indicate that the orientations of all three peptides are essentially comparable, notably with an interesting aspect of the peptide fraying. When H5 is present in the helix, in both H^{5}GWALP23 and $GH^{5,19}$ALP23, the peptide experiences helical unwinding all the way up to core residue A7. This result is interesting since similar unwinding of residue 7 was also observed for a related mutant having histidine at position 5, $H^{4,5}$GWALP23 [29] (see Chapter 5).

Several membrane proteins contain multiple histidine residues within their transmembrane domains [42-44]. Histidine has the ability to shuttle protons with other functional groups or between two nitrogen atoms of its imidazole ring side chain. It also can transfer a proton with another histidine residue adjacent to it. This property of histidine could have an influence on the peptide-lipid interaction within the membrane bilayer. In Chapter 4, the possible effect of multiple histidine residues positioned within the hydrophobic core is tested, by incorporating a pair of histidine residues at positions 8 and 16 (Table 1). This results in the GWALP23-$H^{8,16}$ peptide with two partially buried histidine residues that are equidistant from the peptide center and from their corresponding ends. Arg residues were previously introduced into the same locations within the helix and produced some dramatic results [47]. Notably, the helix with R8 and R16 shifts orientations from transmembrane to surface-bound depending on the bilayer thickness. In the case of GWALP23-$H^{8,16}$ a similar transition of orientation is observed, but with a different lipid dependence, possibly due to the length of histidine residues. To further investigate such behavior, another similar peptide but with only histidine 8 (GWALP23-H^{8}) is

examined (Table 1). Results indicate that the orientation transition occurs also for this single histidine peptide helix, although the second target orientation remains unclear. In addition, this single His 8 mutant responded dramatically with pH, such that the titration point for H8 in the GWALP23 framework was determined in two different lipids.

Introduction of adjacent double aromatic residues at the N-terminal ends of GWALP-family peptides was previously studied using tyrosine and phenylalanine [23 46]. Results indicated that the presence of two neighboring Tyr residues leads to high dynamic averaging and makes it difficult to predict the azimuthal rotation (ρ) of the helix in membranes of different thickness. Moreover, the helix tilt angle becomes less sensitive to the bilayer thickness and the peptide exhibits high dynamics similar to $W^{2,317,18}$ALP19, $W^{2,3,21,22}$ALP23 and $W^{2,22}W^{5,19}$ALP23. But interestingly, Phe residues provides the peptide a well-defined and low-dynamic transmembrane orientation which is quite similar to GWALP23. To have some idea about the effect of adjacent aromatic residues, in Chapter 5 peptides with histidine residues at positions 4 and 5 were analyzed for comparison with a number of other peptides with pairs of identical residues at positions 4 and 5, including tryptophan, glycine and others. Results seem very promising. $H^{4,5}$ displays a high dynamic averaging with very low tilt in DMPC and DOPC lipid bilayers, but unlike $Y^{4,5}$ its tilt angle changes slightly with membrane thickness. The -$W^{4,5}$ peptide on the other hand, despite having adjacent tryptophans has no such issue with high dynamics and exhibits a well-defined tilted transmembrane orientation with low motional averaging. Importantly, the helix terminal unwinding or end "fraying" could also be assessed for each of the helices, by analyzing the signals from the juxta-terminal alanines A3 and A21. Interestingly, only $H^{4,5}$GWALP23 shows an exceptional unraveling that involves residue A7. These observations along with those from peptides discussed in Chapter 3 indicates the possible direct involvement

of residue H5 for the unwinding of peptides that draws residues A7 away from the helical geometry of the core transmembrane segment.

Overall, I have investigated multiple analogs of GWALP23 with single or pairs of histidine residue throughout various locations of the helix. As noted, these experiments are relevant for understanding fundamental properties of membrane proteins, generally speaking. Key findings include: i) terminal histidine residue/s present along with tryptophans preserve the overall properties of the parent peptide, with modest motional averaging and tilted transmembrane orientations that scale with the bilayer thickness; ii) in the absence of tryptophan anchors, the helices having histidine residues instead, exhibit similar orientations and other biophysical properties; iii) when a pair of histidine residues is inserted into the hydrophobic core of the membrane, the peptides become more sensitive to bilayer thickness than the parent GWALP23 helix and display transitions from one orientation to another; iv) helices with only one partially buried histidine reveal similar results but with a different lipid dependence; and v) two adjacent histidine residues at the N-terminus of a peptide helix promote unraveling, increase the overall dynamics of helix and therefore obscure the actual orientation. These features will be explored in the following chapters.

1.1 References

1. van Meer, G.; Voelker, D. R.; Feigenson, G. W., Membrane lipids: where they are and how they behave. *Nat Rev Mol Cell Biol* **2008,** *9* (2), 112-124.

2. Carruthers, A.; Melchior, D. L., Human erythrocyte hexose transporter activity is governed by bilayer lipid composition in reconstituted vesicles. *Biochemistry* **1984,** *23* (26), 6901-6911.

3. Phillips, R.; Ursell, T.; Wiggins, P.; Sens, P., Emerging roles for lipids in shaping membrane-protein function. *Nature* **2009,** *459* (7245), 379-385.

4. Henrich, E.; Ma, Y.; Engels, I.; Münch, D.; Otten, C.; Schneider, T.; Henrichfreise, B.; Sahl, H.-G.; Dötsch, V.; Bernhard, F., Lipid Requirements for the Enzymatic Activity of MraY Translocases and in Vitro Reconstitution of the Lipid II Synthesis Pathway. *J. Biol. Chem* **2016,** *291* (5), 2535-2546.

5. Fagerberg, L.; Jonasson, K.; von Heijne, G.; Uhlén, M.; Berglund, L., Prediction of the human membrane proteome. *Proteomics* **2010,** *10* (6), 1141-1149.

6. Bakheet, T. M.; Doig, A. J., Properties and identification of human protein drug targets. *Bioinformatics* **2009,** *25* (4), 451-457.

7. Harley, C. A.; Holt, J. A.; Turner, R.; Tipper, D. J., Transmembrane Protein Insertion Orientation in Yeast Depends on the Charge Difference across Transmembrane Segments, Their Total Hydrophobicity, and Its Distribution. *J. Biol. Chem* **1998,** *273* (38), 24963-24971.

8. Lee, E.; Manoil, C., Mutations eliminating the protein export function of a membrane-spanning sequence. *J. Biol. Chem* **1994,** *269* (46), 28822-28828.

9. White, S. H.; Ladokhin, A. S.; Jayasinghe, S.; Hristova, K., How Membranes Shape Protein Structure. *J. Biol. Chem* **2001,** *276* (35), 32395-32398.

10. Cymer, F.; von Heijne, G.; White, S. H., Mechanisms of integral membrane protein insertion and folding. *J Mol Biol* **2015,** *427* (5), 999-1022.

11. Heijne, G., The distribution of positively charged residues in bacterial inner membrane proteins correlates with the trans-membrane topology. *EMBO J* **1986,** *5* (11), 3021-3027.

12. Catterall, W. A., Ion channel voltage sensors: structure, function, and pathophysiology. *Neuron* **2010,** *67* (6), 915-928.

13. Jiang, Y.; Ruta, V.; Chen, J.; Lee, A.; MacKinnon, R., The principle of gating charge movement in a voltage-dependent K+ channel. *Nature* **2003,** *423* (6935), 42-48.

14. Kucik, D. F.; Elson, E. L.; Sheetz, M. P., Weak dependence of mobility of membrane protein aggregates on aggregate size supports a viscous model of retardation of diffusion. *Biophys J* **1999,** *76* (1 Pt 1), 314-322.

15. Aroca, J. D.; Sánchez-Piñera, P.; Corbalán-García, S.; Conesa-Zamora, P.; de Godos, A.; Gómez-Fernández, J. C., Correlation between the effect of the anti-neoplastic ether lipid 1-O-octadecyl-2-O-methyl-glycero-3-phosphocholine on the membrane and the activity of protein kinase Cα. *Eur. J. Biochem.* **2001,** *268* (24), 6369-6378.

16. de Planque, M. R. R.; Kruijtzer, J. A. W.; Liskamp, R. M. J.; Marsh, D.; Greathouse, D. V.; Koeppe, R. E.; de Kruijff, B.; Killian, J. A., Different Membrane Anchoring Positions of Tryptophan and Lysine in Synthetic Transmembrane α-Helical Peptides. *J. Biol. Chem* **1999,** *274* (30), 20839-20846.

17. Killian, J. A.; Salemink, I.; De Planque, M. R.; Lindblom, G.; Koeppe, R. E., II; Greathouse, D. V., Induction of non-bilayer structures in diacylphosphatidylcholine model membranes by transmembrane α-helical peptides. Importance of hydrophobic mismatch and proposed role of tryptophans. *Biochemistry* **1996,** *35*, 1037-1045.

18. van der Wel, P. C. A.; Strandberg, E.; Killian, J. A.; Koeppe, R. E., II, Geometry and intrinsic tilt of a tryptophan-anchored transmembrane alpha-helix determined by ^{2}H NMR. *Biophys. J.* **2002,** *83*, 1479-1488.

19. Vostrikov, V. V.; Daily, A. E.; Greathouse, D. V.; Koeppe, R. E., II, Charged or aromatic anchor residue dependence of transmembrane peptide tilt. *J. Biol. Chem.* **2010,** *285* (41), 31723-31730.

20. Vostrikov, V. V.; Grant, C. V.; Opella, S. J.; Koeppe, R. E., II, On the combined analysis of ^{2}H and $^{15}N/^{1}H$ solid-state NMR data for determination of transmembrane peptide orientation and dynamics. *Biophys. J.* **2011,** *101* (12), 2939-2947.

21. Vostrikov, V. V.; Koeppe, R. E., 2nd, Response of GWALP transmembrane peptides to changes in the tryptophan anchor positions. *Biochemistry* **2011,** *50* (35), 7522-7535.

22. Gleason, N. J.; Greathouse, D. V.; Grant, C. V.; Opella, S. J.; Koeppe, R. E., II, Single Tryptophan and Tyrosine Comparisons in the N-Terminal and C-Terminal Interface Regions of Transmembrane GWALP Peptides. *J. Phys. Chem. B* **2013,** *117* (44), 13786-13794.

23. Gleason, N. J.; Vostrikov, V. V.; Greathouse, D. V.; Grant, C. V.; Opella, S. J.; Koeppe, R. E., II, Tyrosine replacing tryptophan as an anchor in GWALP peptides. *Biochemistry* **2012,** *51* (10), 2044-2053.

24. Gleason, N. J.; Vostrikov, V. V.; Greathouse, D. V.; Koeppe, R. E., Buried lysine, but not arginine, titrates and alters transmembrane helix tilt. *Proc. Natl. Acad. Sci. U.S.A.* **2013,** *110* (5), 1692.

25. Vostrikov, V. V.; Hall, B. A.; Greathouse, D. V.; Koeppe, R. E.; Sansom, M. S. P., Changes in Transmembrane Helix Alignment by Arginine Residues Revealed by Solid-State NMR Experiments and Coarse-Grained MD Simulations. *J. Am. Chem. Soc.* **2010,** *132* (16), 5803-5811.

26. Martfeld, A. N.; Greathouse, D. V.; Koeppe, R. E., Ionization Properties of Histidine Residues in the Lipid Bilayer Membrane Environment. *J. Biol. Chem* **2016,** *291* (36), 19146-19156.

27. Rajagopalan, V.; Greathouse, D. V.; Koeppe, R. E., Influence of glutamic acid residues and pH on the properties of transmembrane helices. *Biochim. Biophys. Acta, Biomembr.* **2017,** *1859* (3), 484-492.

28. Mortazavi, A.; Rajagopalan, V.; Sparks, K. A.; Greathouse, D. V.; Koeppe, R. E., II, Juxta-terminal Helix Unwinding as a Stabilizing Factor to Modulate the Dynamics of Transmembrane Helices. *ChemBioChem* **2016,** *17* (6), 462-465.

29. Afrose, F.; McKay, M. J.; Mortazavi, A.; Suresh Kumar, V.; Greathouse, D. V.; Koeppe, R. E., Transmembrane Helix Integrity versus Fraying To Expose Hydrogen Bonds at a Membrane–Water Interface. *Biochemistry* **2019,** *58* (6), 633-645.

30. Loewenthal, R.; Sancho, J.; Fersht, A. R., Histidine-aromatic interactions in barnase: Elevation of histidine pKa and contribution to protein stability. *J Mol Biol* **1992,** *224* (3), 759-770.

31. Jasanoff, A.; Weiss, M. A., Aromatic-histidine interactions in the zinc finger motif: Structural inequivalence of phenylalanine and tyrosine in the hydrophobic core. *Biochemistry* **1993,** *32* (6), 1423-1432.

32. Fernández-Recio, J.; Vázquez, A.; Civera, C.; Sevilla, P.; Sancho, J., The Tryptophan/Histidine interaction in α-helices 11Edited by F. E. Cohen. *J Mol Biol* **1997,** *267* (1), 184-197.

33. Bhattacharyya, R.; Saha, R. P.; Samanta, U.; Chakrabarti, P., Geometry of Interaction of the Histidine Ring with Other Planar and Basic Residues. *J. Proteome Res.* **2003,** *2* (3), 255-263.

34. Pinto, L. H.; Holsinger, L. J.; Lamb, R. A., Influenza virus M2 protein has ion channel activity. *Cell* **1992,** *69* (3), 517-528.

35. Wang, J.; Qiu, J. X.; Soto, C.; DeGrado, W. F., Structural and dynamic mechanisms for the function and inhibition of the M2 proton channel from influenza A virus. *Curr Opin Struct Biol* **2011,** *21* (1), 68-80.

36. Hu, J.; Fu, R.; Nishimura, K.; Zhang, L.; Zhou, H.-X.; Busath, D. D.; Vijayvergiya, V.; Cross, T. A., Histidines, heart of the hydrogen ion channel from influenza A virus: Toward an understanding of conductance and proton selectivity. *Proc. Natl. Acad. Sci. U.S.A.* **2006,** *103* (18), 6865.

37. Takeuchi, H.; Okada, A.; Miura, T., Roles of the histidine and tryptophan side chains in the M2 proton channel from influenza A virus. *FEBS Lett* **2003,** *552* (1), 35-38.

38. Deisenhofer, J.; Epp, O.; Miki, K.; Huber, R.; Michel, H., Structure of the protein subunits in the photosynthetic reaction centre of Rhodopseudomonas viridis at 3Å resolution. *Nature* **1985,** *318* (6047), 618-624.

39. Iwata, S.; Ostermeier, C.; Ludwig, B.; Michel, H., Structure at 2.8 Å resolution of cytochrome c oxidase from Paracoccus denitrificans. *Nature* **1995,** *376* (6542), 660-669.

40. Zhou, F. X.; Merianos, H. J.; Brunger, A. T.; Engelman, D. M., Polar residues drive association of polyleucine transmembrane helices. *Proc. Natl. Acad. Sci. U.S.A.* **2001,** *98* (5), 2250.

41. Perona, J. J.; Craik, C. S., Structural basis of substrate specificity in the serine proteases. *Protein Sci* **1995,** *4* (3), 337-360.

42. Paukert, M.; Chen, X.; Polleichtner, G.; Schindelin, H.; Gründer, S., Candidate Amino Acids Involved in H+ Gating of Acid-sensing Ion Channel 1a. *J. Biol. Chem* **2008,** *283* (1), 572-581.

43. Rajan, S.; Wischmeyer, E.; Xin Liu, G.; Preisig-Müller, R.; Daut, J.; Karschin, A.; Derst, C., TASK-3, a Novel Tandem Pore Domain Acid-sensitive K+Channel: AN EXTRACELLULAR HISTIDINE AS pH SENSOR. *J. Biol. Chem* **2000,** *275* (22), 16650-16657.

44. Clarke, C. E.; Benham, C. D.; Bridges, A.; George, A. R.; Meadows, H. J., Mutation of histidine 286 of the human P2X4 purinoceptor removes extracellular pH sensitivity. *J Physiol* **2000,** *523 Pt 3* (Pt 3), 697-703.

45. Özdirekcan, S.; Rijkers, D. T. S.; Liskamp, R. M. J.; Killian, J. A., Influence of Flanking Residues on Tilt and Rotation Angles of Transmembrane Peptides in Lipid Bilayers. A Solid-State 2H NMR Study. *Biochemistry* **2005,** *44* (3), 1004-1012.

46. Sparks, K. A.; Gleason, N. J.; Gist, R.; Langston, R.; Greathouse, D. V.; Koeppe, R. E., II, Comparisons of Interfacial Phe, Tyr, and Trp Residues as Determinants of Orientation and Dynamics for GWALP Transmembrane Peptides. *Biochemistry* **2014,** *53* (22), 3637-3645.

47. Lipinski, K.; McKay, M. J.; Afrose, F.; Martfeld, A. N.; Koeppe Ii, R. E.; Greathouse, D. V., Influence of Lipid Saturation, Hydrophobic Length and Cholesterol on Double-Arginine-Containing Helical Peptides in Bilayer Membranes. *ChemBioChem* **2019,** *0* (0).

1.2 **Table**

Table 1: Sequence of GWALP23 with histidine substitutions studied here

Name of peptide	**Sequence**	**Chapter discussed**
GWALP23	Ac-GGALWLALALALALALALWLAGA-amide	
$H^{2,22}$WALP23	Ac-G**H**ALWLALALALALALALWLA**H**A-amide	Chapter 2
H^{2}GWALP23	Ac-G**H**ALWLALALALALALALWLAGA-amide	
H^{22}GWALP23	Ac-GGALWLALALALALALALWLA**H**A-amide	
$GH^{5,19}$ALP23	Ac-GGAL**H**LALALALALALAL**H**LAGA-amide	Chapter 3
H^{5}GWALP23	Ac-GGAL**H**LALALALALALALWLAGA-amide	
H^{19}GWALP23	Ac-GGALWLALALALALALAL**H**LAGA-amide	
GWALP23-$H^{8,16}$	Ac-GGALWLA**H**ALALALA**H**ALWLAGA-amide	Chapter 4
GWALP23-H^{8}	Ac-GGALWLA**H**ALALALALALWLAGA-amide	
$H^{4,5}$GWALP23	Ac-GGA**HH**LALALALALALALWLAGA-amide	Chapter 5
$W^{4,5}$GWALP23	Ac-GGA**WW**LALALALALALALWLAGA-amide	
$G^{4,5}$GWALP23	Ac-GGA**GG**LALALALALALALWLA**H**A-amide	

2. Chapter 2: Ionization Properties of Single and Paired Histidine Residues When Present Outside the Tryptophan Cage of a Transmembrane Alpha Helix.

2.1 Abstract

GWALP23, a constructive low-dynamic model peptide framework, widens the range of protein-lipid interactions that can be investigated when potentially charged residues are present. In this context, I have examined the effects of single or pairs of histidine residues when present in close proximity to the stabilizing interfacial tryptophan residues W5 and W19 of the GWALP23 helix. To this end, I substituted residues H2 and H22 into the parent sequence (acetyl- GGALW^{5}LALALALALALALW^{19}LAGA-amide) of GWALP23. Specific ^{2}H-labeled alanine residues within core of the helix were incorporated for detection by means of solid-state ^{2}H NMR. The signals from NMR spectroscopy and orientational analysis suggest marked differences between the peptide helices with H^{2,22} compared to those having W^{2,22} at the same positions. Notably, the properties of membrane-spanning H^{2,22}WALP23 helices are similar the those glycine, arginine or lysine at positions 2 and 22. Additionally, to address the effect of single histidine residue at the peptide terminus, I removed either H2 or H22 from the sequence of H^{2,22}GWALP23. Peptide helices having H2 or H22 display tilted transmembrane orientations in bilayers of DLPC or DOPC, with little or no pH dependence of the orientations from pH 2 to pH 8. Comparing the results from H^{2,22}WALP23 with those observed when only H2 or H22 is present, I surmise that the presence, locations and number of histidine residues is more important for the motional averaging of a transmembrane helix than for the average preferred helix orientation.

2.2 **Introduction**

Membrane-spanning proteins have distinct segments composed of hydrophobic amino acid residues flanked by interfacial loops that tend to be rich in aromatic amino acids. In integral membrane proteins and peptides, it has been found from statistical analysis [1-6] and genomic databases [6-8] that the aromatic amino acids are not uniformly distributed but rather are significantly localized at the membrane-water interfaces. The major driving force causing the aromatic amino acids to prefer the interfacial location is thought to be the hydrophobic effect, but their involvement in hydrogen bonding with lipid carbonyl groups or interfacial water molecules as well as the dipole-dipole interactions in the interface region are additional contributing factors [9-11].

Because membrane proteins are inherently complex in structure, there are difficulties for the structural and functional characterization of membrane proteins using experimental techniques. Implementation of synthetic model peptides has proven invaluable to overcome the difficulties of research focused on fundamental principles of protein-lipid interactions. A good example model peptide is GWALP23 [12]which not only solves the issues related to complexity of biological membrane proteins, but also allows for a wealth of information derived from single or multiple residue replacements throughout its sequence. In historical sequence, GWALP23 peptides were derived primarily from "WALP" model peptides [13] by reducing the number of tryptophan (W) residues [12]. Since the development of GWALP23, this peptide has been used as "host" for several amino acid residues to study the influence of particular amino acids such as those having aromatic, charged or polar residues in various locations on the scaffold of a transmembrane helix.

GWALP23 was developed by introducing two interfacial glycine residues G2 and G22, which were incorporated by removing two tryptophans from the original sequence of WALP23[14-15]. These paired W to G substitutions lead to less molecular dynamic averaging than was observed with the WALP23 and WALP19 helices [13]. Indeed, when four tryptophans flank a core helix, whether $W^{2,3,21,22}$ or $W^{2,5,19,22}$, the high dynamic behavior of the transmembrane peptide helix is maintained, indicating the probable incompatibility of more than one nearby aromatic ring at a membrane interface [12]. In this context, a choice of histidine for these positions allows me to verify this probability and to compare the effect of imidazole ring versus indole ring for the dynamics of the transmembrane peptide helix. Alternatively, charged residues such as lysine and arginine are known to have only minor effects on the peptide orientation and dynamics [12].

Here, I have incorporated histidine residues H2 and H22 in the sequence of GWALP23 (with G2 and G22) to address whether the high dynamic averaging in WWALP23 (with W2 and W22) is specific only for tryptophan residues or whether any aromatic residue can give rise to such behavior. Another important aspect to test here is the possibility of cation-π interactions involving histidine, that have been described to have a critical role in ligand binding [16-17] and catalysis in ion-channels [18-20] and G-protein-coupled receptors [21] The interaction between protonated histidine and an aromatic side chain can stabilize α-helices [22-23]. In my study, the H2 and W5, or H22 and W19, pairs within the modified version of GWALP23 are very close to each other in the helix geometry, such that the results from this system could provide insight into possible cation- π interactions between residues on adjacent helical turns. Moreover, I have expanded the experiments with two additional peptides that have either H2 or H22 (but not both), to understand which interaction (N-terminal or C-terminal) might have more effect in stabilizing a peptide helix. My results reveal that histidine residues at positions 2 and 22 behave quite

differently from the tryptophans observed previously [12], and this behavior also differs depending on the location of the histidine residue.

2.3 **Materials and Methods**

N-Fmoc protected amino acids and rink amide resins were purchased from NovaBiochem (San Diego, CA) and (Louisville, KY). Commercial L-alanine, deuterated at C_α and C_β carbons (Ala-d_4), from Cambridge Isotope Laboratories (Andover, MA) was derivatized with an Fmoc protecting group as described previously [24-25].^{1}H-NMR spectroscopy was then used to confirm the successful Fmoc-Ala-d_4 synthesis. DLPC and DOPC synthetic lipids were purchased from Avanti Polar Lipids (Alabaster, AL). Histidine and tryptophan side chains were protected with trityl and t-butoxycarbonyl protecting groups and were purchased from Novabiochem and Bachem.

Peptides were synthesized on a model 433A solid-phase peptide synthesizer (Applied Biosystems; Foster City, CA) using modified FastMoc® chemistry, with extended deprotection and coupling times where needed. Two deuterium-labeled alanines at ~50% and 100% isotope abundance levels were incorporated in a single peptide, allowing the NMR signals to be distinguished and assigned based upon the relative intensities. The final residue on each peptide was acetyl-Gly to yield a blocked, neutral N-terminal.

After synthesis, peptides were simultaneously deprotected and cleaved from rink amide resin with a peptide cleavage solution containing TFA:phenol:triisopropylsilane:water in a 85:5:5:5 ratio. Crude peptides were purified on a reversed-phase HPLC octyl-silica Zorbax Rx-C8 column with 9.4 x 250 mm dimensions and 5 μm particle size from Agilent Technologies (Santa Clara, CA). A gradient of 92-96% methanol (with 0.1% trifluoroacetic acid (v/v)) at a

flow rate of 1.7 ml/min or about 15 minutes was used for each peptide purification. Finally the peptides were lyophilized multiple times with 1:1 mixture of acetonitrile:water to ensure complete removal of TFA. The identity of peptide and deuteration pattern was then confirmed by MALDI mass-spectrometry (Fig. S1).

Circular dichroism measurements were performed on peptides incorporated into small unilamellar vesicles of DOPC at 1/60 (mol/mol) peptide/lipid (P/L) in unbuffered water, obtained by ultrasonic treatment. Spectra were recorded at 22 °C on a Jasco J-1500 spectropolarimeter, using a scan speed of 20 nm/min in a cell of1.0 mm path length, 1.0 nm band width, and 0.1 nm slit. An average of six scans were recorded to enhance the signal-to-noise ratio.

Solid-state NMR samples were prepared, as described previously [26] using macroscopically aligned lipid bilayers. After quantification of obtained purified peptides, 1.33 μmol (~ 3 mg) peptide was aliquoted and mixed with 80 μmol of lipid to achieve 1:60 P/L molar ratio. Solvents were removed under a stream of nitrogen and samples were dried under vacuum. The mixture peptide-lipid was redissolved in methanol:water 95:5 and distributed evenly among 34 glass slides (4.8 × 23 mm; Marienfeld, Germany) and then dried under vacuum for 48 h. The dried P/L films were then hydrated with buffers of required pH, made from ^{2}H-depleted water (Cambridge), sealed in a glass cuvette and incubated at 40°C for minimum 24 h (or more depending on pH) before measurement.

Solid-state NMR spectra were recorded at 50°C using two Bruker Avance spectrometers (Billerica, MA), each operating at a proton frequency of 300 MHz. For each NMR sample spectra were recorded with the membrane normal either parallel (β=0°) or perpendicular (β=90°)

to the applied magnetic field. At first the samples were subjected to ^{31}P NMR, decoupled with ^{1}H, to confirm bilayer alignment within each sample. For ^{2}H NMR spectroscopy, spectra were obtained using a quadrupole echo pulse sequence [27], with full phase cycling, 3.2 μs pulse length, 105 μs eco delays and 120 ms of recycle delay. Typically, 0.9 to 1.5 million free induction decays were recorded, with applied exponential weighting function of 100 Hz line broadening (prior to Fourier transformation). For a peptide with fast averaging around the lipid bilayer normal the ^{2}H quadrupolar splittings ($\Delta\nu_q$) observed at $\beta=90°$ have absolute magnitude of ½ those at $\beta=0°$ [28].

The signals of ^{2}H NMR, arose from $C_\beta D_3$ groups of Ala-d_4 residues of peptides were analyzed according to Geometric Analysis of Labeled Alanines (GALA) method described previously [26 29]. This is a semi-static analysis based on a relationship between the alanine $C_\beta D_3$ quadrupolar splitting ($\Delta\nu_q$) and the angle θ between the alanine C_α-C_β bond vector and the applied magnetic field [26]. GALA analysis provides information of helix orientation, by means of the average tilt τ of the helix axis, the azimuthal rotation ρ, and the principal order parameter S_{zz} as variables. Additionally, we have employed another method called "Modified Gaussian Analysis" [30] to reconfirm and elaborate the results from GALA analysis.

2.4 **Results**

In this study, I investigate the interactions of interfacial histidines, present alongside trypotophans, flanking a transmembrane segment that is similar to helices of biological proteins. I also examine the ionization and role of the His imidazole ring side chain in orienting the helix in a lipid bilayer. GWALP23 is an ideal model system for studying the ionization properties of charged residues as have been carried out in recent years with Arg, Lys, His and Glu residues [31-

[34]. Previous studies with Lys, Arg and Trp along with Gly in the positions 2 and 22 show some very interesting results. For peptides with positively charged Lys and Arg residues, the apparent tilt angle generally increases by a small amount in $X^{2,22}$WALP23, as compared to GWALP23 where X is Gly [12]. Furthermore, Arg causes marginally larger tilts than does Lys in the equivalent positions 2 and 22. The tilt direction and more importantly the dynamics change more dramatically when two Trp residues are incorporated in these two positions. Based on these results, I have decided to incorporate histidine residues at positions 2 and 22, outside the tryptophan cage of GWALP23, to give the sequence acetyl-GH^{2}ALW^{5}LALALALALALAL-W^{19}LAH^{22}A-amide (Table 1). Then, for comparison, I removed one histidine from either position 2 or 22 and replaced it with glycine, to yield peptides anchored by two aromatic chains (imidazole and indole) at one end, while the other side is anchored only Trp. This type of substitution resulted in two assymetrically anchored peptides, H2GWALP23 and H22GWALP23. The former one has two anchors at N-terminal side (H2GWALP23) and one anchor at the C-terminal side, while the later peptide has the reversed scenario. The sequences of each peptide mentioned here are listed in Table 1.

After successfully synthesizing the peptides, their molecular weights as well as deuteration patterns were verified by MALDI-TOF Mass Spectrometry (Figure S1). Because all of the peptides have a hydrophobic core composed of alternating Leu-Ala residues, they are expected to adopt an α-helical conformation. To check the secondary structures, I recorded CD spectra for the $H^{2,22}$WALP23, H^{2}GWALP23 and H^{22}GWALP23 peptides incorporated into hydrated DLPC bilayer membranes. Each peptide exhibited mean residue ellipticity profiles typical of an α-helix, characterized by minima at 208 and 222 nm and by the ratio $\varepsilon_{222}/\ \varepsilon_{208}$ between 0.74 and 0.86 (Figure S2). For the aligned samples, the sample orientation was checked

with solid-state ^{31}P NMR, performed on a 300 MHz Bruker spectrometer with broadband ^{1}H decoupling, to test for correct bilayer alignment. Figure S3 shows the peaks at β=0° and β=90° sample orientations for all three peptides considered in this study in DLPC lipid membranes. The DLPC bilayers that hold the embedded peptides are well aligned.

Comparison of H with G, K, R and W at positions 2 and 22

Solid-state ^{2}H NMR spectroscopy reveals well-defined signals for the ^{2}H-Ala methyl groups of H^{2,22}WALP23 in DLPC and DOPC lipid bilayers (Figure 2 top panel). Each ^{2}H-label at the core of this peptide also produces a distinct quadrupolar splitting magnitude ($|\Delta\nu_q|$). These signals as well as quadrupolar splitting values are indicative of a single predominant tilted transmembrane orientation in each lipid. The spectra observed previously for XWALP23 peptides with similar mutations, where X = G, R, K and W suggest that depending on the size and identity of side chains at positions 2 and 22, the overall peptide behavior can vary significantly [12]. For the G2 and G22 peptide, as mentioned earlier, the varying quadrupolar splittings for the alanine CD_3 groups suggest a relatively well-defined tilted transmembrane orientation, which changes with the thickness of bilayer. Very similar features are observed when the X residues are either arginine or lysine. However, when two additional tryptophans (W2 and W22) are present outside the anchoring tryptophan residues (W5 and W19), the spectra for core alanine ^{2}H-labels and their quadrupolar splitting magnitudes changes drastically, which eventually resulted in a peptide orientation with significant low apparent tilt and high dynamic averaging.

To investigate how histidine side chain in the same positions affect the peptide behavior, I have compared the spectra and ^{2}H quadrupolar splitting magnitudes of the H^{2,22} peptide with the

$G^{2,22}$; $K^{2,22}$; $R^{2,22}$ and $W^{2,22}$ analogs. I observe that the measured quadrupolar splittings (Table 2) for $H^{2,22}$ are quite different from the $W^{2,22}$ peptide, even though both carry aromatic side chains. HWALP displays a $|\Delta\nu_q|$ range from 4-35 kHz in DLPC and 1-17 kHz in DOPC (Table 2). Conversely, these ranges for WWALP are moderate in DOPC (about 2-14 kHz) and significantly narrow in DLPC (1-14 kHz). Interestingly, the $\Delta\nu_q$ magnitudes of HWALP are in close proximity to those for GWALP, RWALP or KWALP (Table 2 and [12]), which implies that the orientations of this double-histidine peptide in DLPC and DOPC lipid membranes are likely to be similar to those of the GWALP, RWALP and KWALP helices.

Using the Geometric Analysis of Labeled Alanines (GALA) method to plot quadrupolar splittings $|\Delta\nu_q|$ vs. radial locations, I have analyzed the apparent tilt (τ) and rotation (ρ) of the HWALP23 helix. Figures 6 and 7 show the wave plots of HWALP23 along with the control peptide GWALP23 (with G2 and G22) and two other single histidine peptides (which will be discussed later) in DOPC and DLPC lipid membrane respectively. These plots and the variables calculated from the GALA method (listed in Table 3) indicate minor changes in the orientations of peptides when G2 and G22 are replaced by histidines. The HWALP peptide exhibits a tilted transmembrane orientation that scales with the membrane thickness to adjust hydrophobic mismatches. In DLPC, the apparent tilt (τ) angle of HWALP in DLPC is 26^o, about 5^o higher than GWALP23. This minor change in tilt angle is absent when the helix is moved to thicker DOPC membrane, meaning the tilt angles of HWALP and GWALP are essentially identical (about 6^o). As expected, the modified Gaussian analysis [30] more accurately addresses the dynamic averaging and predicts slightly higher tilt angles, about 10^o for the $G^{2,22}$ and $H^{2,22}$ helices (Table 3). The observed azimuthal rotations (ρ) for H2 and H22, on the other hand, are

slightly different in DOPC and almost same in DLPC. Now these observations remain consistent when we compare the results of HWALP with RWALP and KWALP.

Comparison of $H^{2,22}$ with H^{2} and H^{22}

For further analyzing the residue/s that control the orientation of the HWALP23 peptide in lipid bilayers of DLPC and DOPC, I extended the study with two more peptides by removing either of the two histidines from the HWALP sequence and incorporating glycine in that position (Table 1 and Figure 1), resulting H^{2}GWALP23 and H^{22}GWALP23. Figure 2 displays and compares the ^{2}H NMR spectra for labeled core alanine residues 7, 9, 11, 13, 15 and 17 for $H^{2,22}$WALP, H^{2}GWALP and H^{22}GWALP peptides in DOPC lipid bilayer. The spectra for the same peptides in DLPC lipid membranes are shown in Figure S4. Each spectrum in Figures 2 and S4 represents signals for two deuterated alanines, labeled with different ^{2}H isotope abundancy (50% and 100%). Both H^{2} and H^{22} peptides exhibit sharp signals and well-resolved spectra for labeled core alanines, with wide ranges of ^{2}H quadrupolar splittings. In DOPC lipid membranes, these magnitudes range from 1.5 kHz to 19.5 kHz for the H^{2} peptide, slightly larger compared to the previous peptide with $H^{2,22}$ (1-17 kHz) (Table 1). Similar ranges of quadrupolar splittings are also observed in DLPC (1-36 kHz for H^{2} and 4-35 kHz for $H^{2,22}$). For the other peptide H^{22}, with histidine near C-terminal end, the $|\Delta\nu q|$ ranges are 1-14 kHz in DOPC and 7-26 kHz in DLPC. Although these ranges are not significantly narrow, they are somewhat reduced and one observes similarity of these magnitudes with those of the highly dynamic $W^{2,22}$ peptide, especially in DOPC (Table 2 and ref. [12]). This similarity suggests the possibility of an increased extent of motional averaging (discussed in next section) of the ^{2}H NMR signals when H22 is present.

Comparing the quadrupolar wave plots and the apparent tilt (τ) and azimuthal rotation (ρ), obtained from GALA analysis (Figure 6, Figure 7 and Table 3), it is evident that all three α-helices with single or a pair of histidine residues close to the termini adopt stable transmembrane orientations in bilayers of two different thicknesses (C12:0 and C18:1), without any significant change in overall orientation. To adjust the hydrophobic mismatch between lipid and peptide, all three peptides scale their tilt (τ) and rotation angles (ρ) when moved from thinner DLPC to thicker DOPC membranes. For the H^2 peptide in DLPC bilayers the resulting tilt angle is identical to the observed tilt for $H^{2,22}$ peptide (Table 3), whereas in DOPC it is ~3° more tilted. The H^{22} peptide, conversely, has same tilt magnitude to $H^{2,22}$ in DOPC but ~3° less in DLPC. The observed azimuthal rotation angle for both of these single histidine peptides remains similar to the peptide containing H2 and H22 in DLPC and about 10° – 15° different in DOPC. The combined results suggest that the presence of only one histidine, either at the N- or C-terminal, does not much affect the overall peptide orientation. Rather, the helices align themselves with an orientation similar to the helix carrying histidines at both ends. These features suggest that the more interior Trp residues at positions 5 and 19 remain the primary determinants of the helix tilt and rotation.

To further assess and verify the results obtained from the semi-static GALA analysis, I used a second three-variable method known as the modified-Gaussian approach [30](described in materials and method section). This approach generally agrees with the predictions of the GALA calculations and provides some additional information about the motional averaging of the peptides with histidine. I find that the helix with H2 displays only modest values of rotational slippage (σρ) ranging from about 36° in DLPC to 46° in DOPC (Table 3). The H22 isomer, on the other hand, has a very low σρ value of 8° in DLPC, which is lower than that observed for

GWALP23. Interestingly, nevertheless, the value of σρ increases significantly to about 70° in DOPC (Table 3). When the two histidines are combined in a single peptide to produce the $H^{2,22}$WALP helix, the rotational slippages are intermediate, with values of about 16° in DLPC and 56° in DOPC (Table 3). These results indicate significant motional differences, suggesting that although the apparent tilt and rotation of the H^2 and H^{22} isomers are not very different, their motional averaging changes markedly when the location of the histidine side chain is moved from position 2 to 22. Also notable, and perhaps due to an averaging of effects, the peptide having both H2 and H22 displays an intermediate range of dynamics.

Ionization of histidine in H^2, H^{22} and $H^{2,22}$ peptides

In attempts to determine the titration point of the histidine side chain/s present at different locations of the transmembrane α-helices, I have used solid-state NMR to monitor the changes in the quadrupolar splittings of ^{2}H-labeled alanine residues A7 and A9 of the three peptides studied here. The underlying concept is that a change in ionization might affect the properties of the global helix which in turn might alter aspects of the ^{2}H NMR spectra [32]. The spectral changes with pH are nevertheless small to nonexistent for these particular helices. Changing the pH environment of peptides from acidic to basic (pH 2-8) causes little change in the spectral quality or the magnitude of quadrupolar splittings $|\Delta\nu_q|$ of $GH^{2,22}$ALP23 (Figure 3B), H^2GWALP23 (Figure 4B) or H^{22}GWALP23 (Figure 5B) in DOPC bilayers. For the DLPC lipid, there are some minor changes in the signals between pH 4 and pH 6 in each peptide, with the A7 signal being more visible and slightly shifted from A9 signal (Figure 3A, 4A and 5A). But these changes are not enough to plot any titration curves. Therefore, it is probable that the helices with either H2 or H22 or both respond slightly with the titration of histidine side chains when the membrane is

thinner and thus the side chains are more exposed to the surface. In the thicker lipid DOPC, the loss of pH-dependent peptide response could be due to the lower amount of tilt displayed by the peptides.

2.5 **Discussion**

It has been well established that model peptides are useful tools for the investigation of fundamentals of protein–lipid interactions and their dynamic aspects [35-36]. An example of such a model system that has been widely used since the last decade is the GWALP23 family of peptides. With a developed single-span model peptide helix, with amino acid sequences typical of and similar to biological transmembrane protein segments, GWALP23 allows easier access to and interpretation of single or multiple-residue replacement experiments [32 31 30 37 33-34]. I have taken advantage of this feature of GWALP23 and performed some mutations at the N- and C-terminus of the helix. The analysis involved incorporation of histidine residues at positions 2 and 22 or either one of them, to analyze the direct consequences of histidine side chain interaction with neighboring tryptophan residues and surrounding lipid membrane as well. This approach also allows investigations of the ionization of histidine side chain/s present and how the peptides respond to it.

In GWALP23 peptide, when the two glycine residues from positions 2 and 22, are substituted by positively charged amino acids such as lysine or arginine, the properties of the peptide remain quite similar, with a small increase in apparent tilt angle and no change in tilt direction [12]. But when two tryptophan residues are incorporated in these positions, giving rise to extra tryptophan residues, the direction of tilt becomes less well defined and the magnitude of tilt also loses its tendency to scale with lipid bilayer thickness [12]. These behaviors are also observed

for few other GWALP-like peptides WALP19 and WALP23 [26] [29]. Notably, the common feature among these mentioned high dynamic peptides is the presence of multiple tryptophan residues at both ends of the transmembrane segment, which possibly compete with each other for a preferred position and thereby give rise to extensive dynamic averaging of solid-state NMR observables. Because no other aromatic residues at positions 2 and 22, one helical turn away from the Trp side chains at positions 5 and 19, have been investigated yet, I decided to perform the experimental investigations of the dynamics of peptide helices with histidine residues, which are both aromatic and positively charged (at low pH), in these two positions.

The experiments and analysis indicate that, although the histidine imidazole ring possesses some properties similar to the tryptophan indole ring, the presence of an imidazole ring close to a tryptophan indole ring causes very different properties than two closely located indole rings. The histidine side chain is quite compatible with a nearby tryptophan side chain, which is indicated by the sharp resonances and wide ranges of quadrupolar splitting magnitudes from ^{2}H-NMR (Figure 2 and Table 2). With the presence of H2 and H22, rather than G2 and G22, I expected this peptide to exhibit NMR observables similar to W2 and W22, but in actuality it is completely opposite. The GH^{2,22}ALP peptide adopts a well-defined tilt in lipid bilayers and expresses only moderate levels of dynamic averaging ($\sigma\rho$). Its tilt (τ_0) also scales with bilayer thicknesses, from 26^{o} in DLPC to 6^{o} in DOPC. The rotational preferences (ρ_0) also remain very similar to those of the host peptide GWALP23. This means that histidine despite being aromatic residue, prefers orientations displayed previously by non-aromatic residues such as glycine, lysine or arginine [12]. These results suggest favorable interactions between the tryptophan and histidine side chains (both H2, W5 and W19, H22), positioned approximately one helical turn apart (4.5 Å) and near the membrane interface

Now these types of interactions between histidine and tryptophan side chains are not unusual. A relevant example of such an interaction is in the M2 proton channel of Influenza-A virus. The transmembrane segment of the M2 proton channel contains a HxxxW motif with a His residue at position 37, which interacts with Trp41, and this interaction is essential for the proton selective activity of M2 channels [38-39]. The protonated form of the imidazole ring of His37 of one helix interacts with the indole ring of Trp 41 to facilitate the activity of channel gating [19-20, 38 39]. The presence of the same sequence motif in the Influenza-B M2 channel (His19 and Trp23) [40-41] strengthens the importance of this type of interaction. With the HxxxW motif, the B/M2 channel has an additional histidine residue His27 [22], which indicates an interaction also between Trp23 and His27. Indeed, it is found that the proton conductance decreases to about 60% for a mutation of His27 to Ala [42].

My results strongly support the stabilizing effect of such interactions. Rather than competing for favorable interactions with the polar head groups as observed for the tryptophan side chains in $W^{2,22}$WALP, the histidine side chains are able to find proper orientation to interact possibly more with tryptophan side chains than lipid head groups. This preference toward Trp side chain over lipid head group could be due to a continued protonation state up to pH 8, giving rise to His-aromatic cation-π interaction, but at this point it is complicated to explain as we do not observe much change in the resonances in DOPC lipid bilayers. Nevertheless, in DLPC the spectra below pH 6 are comparatively better resolved, which may indicate the change in ionization state of His between pH 4 and 6. Another possibility could be that both Trp and His find favorable positions to interact with lipid groups as their radial separation is not exactly one helical turn but rather 300°. The α-carbons of H2 and H22 are about 4.5 Å apart from the α-carbons of W5 and W19.

Removal of H22 from the sequence of $H^{2,22}$WALP23 does not affect the helix dynamics or orientation much. The peptide continues to display well-defined tilted transmembrane orientations in DLPC and DOPC membranes, which do not change over a pH range of 2-8 in DOPC. In DLPC, there are some changes in the spectral resolution which agrees with the similar observations for $H^{2,22}$WALP and therefore may provide additional support about the deprotonation of histidine at pH above 4. The key variables defining the dynamic properties remain similar, especially the "rotational slippage" ($\sigma\rho$) of the helix, which remains below 50^o in both lipid bilayers.

In the case of H^{22}GWALP23, with only one aromatic Trp ring at N-terminal end, all the interactions between histidine and tryptophan are at the C-terminus of the helix. I found that although the orientations and pH dependent behaviors are almost same when H22 is introduced in the absence of H2, in DLPC and DOPC lipids, their dynamic behavior changes significantly. The $\sigma\tau$ "wobble" value drastically increases from 8^o to a very large 70^o when the helix is moved from DLPC to DOPC membrane (Table 3). This means that the interactions between W19 and H22 stabilize the helical motions in thinner lipid when the helix is more tilted. Conversely in thicker DOPC lipid, due to the low tilt angle (τ_0), there may arise some competitions between two aromatic rings (imidazole and indole) for interaction with lipid head groups, which add more motion in the helix. Now more interestingly, this type of competition is diminished when a second histidine is added to position 2 (producing $H^{2,22}$WALP). As mentioned earlier, the helix wobble ($\sigma\rho$) of $H^{2,22}$WALP in both DLPC and DOPC is somewhat in between the respective values observed for H^2GWALP and H^{22}GWALP. The results indicate that H2 and H22 may affect only the motional averaging of the helix, while the actual preferred mean orientations are still controlled by tryptophans W5 and W19. When a total of four aromatic rings are present near

the interface, each of them possibly finds a suitable position to either interact with a lipid head group or each other, which could result in a well-behaved moderately dynamic tilted transmembrane orientation.

In the present work, I have sought to understand the effect of adding a histidine residue outside the hydrophobic core sequence of a transmembrane helix and near the anchoring tryptophan residues. The findings reveal that a single or pair of histidine residues near the tryptophan anchors does not greatly affect the overall orientation of a transmembrane peptide. Histidine side chain play relatively little effect in defining the peptide tilt and rotation as these magnitudes are probably controlled primarily by the tryptophan side chains. Yet the dynamic properties of the peptide helices are somewhat altered by the presence and location of histidine residues as well as the bilayer thickness.

2.6 **Acknowledgement**

This work was supported in part by NSF MCB grant 1713242, and by the Arkansas Biosciences Institute. The peptide, NMR and mass spectrometry facilities were supported in part by NIH grant GM103429.

2.7 **References**

1. Ulmschneider, M. B.; Sansom, M. S. P., Amino acid distributions in integral membrane protein structures. *Biochim. Biophys. Acta, Biomembr.* **2001,** *1512* (1), 1-14.

2. Granseth, E.; von Heijne, G.; Elofsson, A., A Study of the Membrane–Water Interface Region of Membrane Proteins. *J. Mol. Biol.* **2005,** *346* (1), 377-385.

3. Ulmschneider, M. B.; Sansom, M. S. P.; Di Nola, A., Properties of integral membrane protein structures: Derivation of an implicit membrane potential. *Proteins: Struct., Funct., Bioinf.* **2005,** *59* (2), 252-265.

4. Adamian, L.; Nanda, V.; DeGrado, W. F.; Liang, J., Empirical lipid propensities of amino acid residues in multispan alpha helical membrane proteins. *Proteins: Struct., Funct., Bioinf.* **2005,** *59* (3), 496-509.

5. Senes, A.; Chadi, D. C.; Law, P. B.; Walters, R. F. S.; Nanda, V.; DeGrado, W. F., Ez, a Depth-dependent Potential for Assessing the Energies of Insertion of Amino Acid Side-chains into Membranes: Derivation and Applications to Determining the Orientation of Transmembrane and Interfacial Helices. *J. Mol. Biol.* **2007,** *366* (2), 436-448.

6. Wimley, W. C., Toward genomic identification of beta-barrel membrane proteins: composition and architecture of known structures. *Protein Sci.* **2002,** *11* (2), 301-312.

7. Landolt-Marticorena, C.; Williams, K. A.; Deber, C. M.; Reithmeier, R. A., Non-random distribution of amino acids in the transmembrane segments of human type I single span membrane proteins. *J. Mol. Biol.* **1993,** *229* (3), 602-608.

8. Wallin, E.; von Heijne, G., Genome-wide analysis of integral membrane proteins from eubacterial, archaean, and eukaryotic organisms. *Protein Sci.* **1998,** *7* (4), 1029-1038.

9. Wimley, W. C.; Creamer, T. P.; White, S. H., Solvation Energies of Amino Acid Side Chains and Backbone in a Family of Host−Guest Pentapeptides. *Biochemistry* **1996,** *35* (16), 5109-5124.

10. Wimley, W. C.; White, S. H., Membrane partitioning: Distinguishing bilayer effects from the hydrophobic effect. *Biochemistry* **1993,** *32* (25), 6307-6312.

11. Yau, W.-M.; Wimley, W. C.; Gawrisch, K.; White, S. H., The Preference of Tryptophan for Membrane Interfaces. *Biochemistry* **1998,** *37* (42), 14713-14718.

12. Vostrikov, V. V.; Daily, A. E.; Greathouse, D. V.; Koeppe, R. E., II, Charged or aromatic anchor residue dependence of transmembrane peptide tilt. *J. Biol. Chem.* **2010,** *285* (41), 31723-31730.

13. Killian, J. A.; Salemink, I.; De Planque, M. R.; Lindblom, G.; Koeppe, R. E., II; Greathouse, D. V., Induction of non-bilayer structures in diacylphosphatidylcholine

model membranes by transmembrane α-helical peptides. Importance of hydrophobic mismatch and proposed role of tryptophans. *Biochemistry* **1996,** *35*, 1037-1045.

14. Vostrikov, V. V.; Grant, C. V.; Opella, S. J.; Koeppe, R. E., II, On the combined analysis of ^{2}H and $^{15}N/^{1}H$ solid-state NMR data for determination of transmembrane peptide orientation and dynamics. *Biophys. J.* **2011,** *101* (12), 2939-2947.

15. Strandberg, E.; Esteban-Martin, S.; Ulrich, A. S.; Salgado, J., Hydrophobic mismatch of mobile transmembrane helices: Merging theory and experiments. *Biochim. Biophys. Acta.* **2012,** *1818*, 1242-1249.

16. Feinberg, H.; Torgersen, D.; Drickamer, K.; Weis, W. I., Mechanism of pH-dependentN-Acetylgalactosamine Binding by a Functional Mimic of the Hepatocyte Asialoglycoprotein Receptor. *J. Biol. Chem* **2000,** *275* (45), 35176-35184.

17. Williams, S.; Bledsoe, R. K.; Collins, J. L.; Boggs, S.; Lambert, M. H.; Miller, A. B.; Moore, J.; McKee, D. D.; Moore, L.; Nichols, J.; Parks, D.; Watson, M.; Wisely, B.; Willson, T. M., X-ray Crystal Structure of the Liver X Receptor β Ligand Binding Domain: REGULATION BY A HISTIDINE-TRYPTOPHAN SWITCH. *J. Biol. Chem* **2003,** *278* (29), 27138-27143.

18. Li, H.-L.; Galue, A.; Meadows, L.; Ragsdale, D. S., A Molecular Basis for the Different Local Anesthetic Affinities of Resting Versus Open and Inactivated States of the Sodium Channel. *Mol. Pharmacol* **1999,** *55* (1), 134.

19. Okada, A.; Miura, T.; Takeuchi, H., Protonation of Histidine and Histidine−Tryptophan Interaction in the Activation of the M2 Ion Channel from Influenza A Virus. *Biochemistry* **2001,** *40* (20), 6053-6060.

20. Takeuchi, H.; Okada, A.; Miura, T., Roles of the histidine and tryptophan side chains in the M2 proton channel from influenza A virus. *FEBS Lett.* **2003,** *552* (1), 35-38.

21. Inoue, Y.; Nakamura, N.; Inagami, T., A review of mutagenesis studies of angiotensin II type 1 receptor, the three-dimensional receptor model in search of the agonist and antagonist binding site and the hypothesis of a receptor activation mechanism. *J Hypertens* **1997,** *15* (7), 703-714.

22. Fernández-Recio, J.; Vázquez, A.; Civera, C.; Sevilla, P.; Sancho, J., The Tryptophan/Histidine interaction in α-helices *J. Mol. Biol.* **1997,** *267* (1), 184-197.

23. Fernández-Recio, J.; Romero, A.; Sancho, J., Energetics of a hydrogen bond (charged and neutral) and of a cation-π interaction in apoflavodoxin. *J. Mol. Biol.* **1999,** *290* (1), 319-330.

24. Greathouse, D. V.; Koeppe, R. E., II; Providence, L. L.; Shobana, S.; Andersen, O. S., Design and characterization of gramicidin channels. *Methods Enzymol.* **1999,** *294*, 525-550.

25. Kortenaar, P. B. W.; Dijk, B. G.; Peeters, J. M.; Raagen, B. J.; Adams, P. J.; Tesser, G. I., Rapid and efficient method for the preparation of Fmoc-amino acids starting from 9-fluorenylmethanol. *Int. J. Pept. Prot. Res.* **1986,** *27*, 398-400.

26. van der Wel, P. C. A.; Strandberg, E.; Killian, J. A.; Koeppe, R. E., II, Geometry and intrinsic tilt of a tryptophan-anchored transmembrane alpha-helix determined by ^{2}H NMR. *Biophys. J.* **2002,** *83*, 1479-1488.

27. Davis, J. H.; Jeffrey, K. R.; Valic, M. I.; Bloom, M.; Higgs, T. P., Quadrupolar echo deuteron magnetic resonance spectroscopy in ordered hydrocarbon chains. *Chem. Phys. Lett.* **1976,** *42*, 390-394.

28. Aisenbrey, C.; Bechinger, B., Investigations of Polypeptide Rotational Diffusion in Aligned Membranes by 2H and 15N Solid-State NMR Spectroscopy. *J. Am. Chem. Soc.* **2004,** *126* (50), 16676-16683.

29. Strandberg, E.; Özdirekcan, S.; Rijkers, D. T. S.; van der Wel, P. C. A.; Koeppe, R. E., II; Liskamp, R. M. J.; Killian, J. A., Tilt angles of transmembrane model peptides in oriented and non-oriented lipid bilayers as determined by ^{2}H solid-state NMR. *Biophys. J.* **2004,** *86*, 3709-3721.

30. Sparks, K. A.; Gleason, N. J.; Gist, R.; Langston, R.; Greathouse, D. V.; Koeppe, R. E., II, Comparisons of Interfacial Phe, Tyr, and Trp Residues as Determinants of Orientation and Dynamics for GWALP Transmembrane Peptides. *Biochemistry* **2014,** *53* (22), 3637-3645.

31. Vostrikov, V. V.; Hall, B. A.; Greathouse, D. V.; Koeppe, R. E.; Sansom, M. S. P., Changes in Transmembrane Helix Alignment by Arginine Residues Revealed by Solid-State NMR Experiments and Coarse-Grained MD Simulations. *J. Am. Chem. Soc.* **2010,** *132* (16), 5803-5811.

32. Gleason, N. J.; Vostrikov, V. V.; Greathouse, D. V.; Koeppe, R. E., Buried lysine, but not arginine, titrates and alters transmembrane helix tilt. *Proc. Natl. Acad. Sci. U. S. A.* **2013,** *110* (5), 1692.

33. Martfeld, A. N.; Greathouse, D. V.; Koeppe, R. E., Ionization Properties of Histidine Residues in the Lipid Bilayer Membrane Environment. *J. Biol. Chem* **2016,** *291* (36), 19146-19156.

34. Rajagopalan, V.; Greathouse, D. V.; Koeppe, R. E., Influence of glutamic acid residues and pH on the properties of transmembrane helices. *Biochim. Biophys. Acta, Biomembr.* **2017,** *1859* (3), 484-492.

35. de Planque, M. R. R.; Bonev, B. B.; Demmers, J. A. A.; Greathouse, D. V.; Koeppe, R. E.; Separovic, F.; Watts, A.; Killian, J. A., Interfacial anchor properties of tryptophan residues in transmembrane peptides can dominate over hydrophobic matching effects in peptide-lipid interactions. *Biochemistry* **2003,** *42* (18), 5341-5348.

36. van der Wel, P. C. A.; Reed, N. D.; Greathouse, D. V.; Koeppe, R. E., 2nd, Orientation and motion of tryptophan interfacial anchors in membrane-spanning peptides. *Biochemistry* **2007,** *46* (25), 7514-7524.

37. Gleason, N. J.; Greathouse, D. V.; Grant, C. V.; Opella, S. J.; Koeppe, R. E., II, Single Tryptophan and Tyrosine Comparisons in the N-Terminal and C-Terminal Interface Regions of Transmembrane GWALP Peptides. *J. Phys.Chem. B* **2013,** *117* (44), 13786-13794.

38. Tang, Y.; Zaitseva, F.; Lamb, R. A.; Pinto, L. H., The Gate of the Influenza Virus M2 Proton Channel Is Formed by a Single Tryptophan Residue. *J. Biol. Chem* **2002,** *277* (42), 39880-39886.

39. Venkataraman, P.; Lamb, R. A.; Pinto, L. H., Chemical Rescue of Histidine Selectivity Filter Mutants of the M2 Ion Channel of Influenza A Virus. *J. Biol. Chem* **2005,** *280* (22), 21463-21472.

40. Paterson, R. G.; Takeda, M.; Ohigashi, Y.; Pinto, L. H.; Lamb, R. A., Influenza B virus BM2 protein is an oligomeric integral membrane protein expressed at the cell surface. *Virology* **2003,** *306* (1), 7-17.

41. Mould, J. A.; Paterson, R. G.; Takeda, M.; Ohigashi, Y.; Venkataraman, P.; Lamb, R. A.; Pinto, L. H., Influenza B Virus BM2 Protein Has Ion Channel Activity that Conducts Protons across Membranes. *Dev. Cell* **2003,** *5* (1), 175-184.

42. Otomo, K.; Toyama, A.; Miura, T.; Takeuchi, H., Interactions Between Histidine and Tryptophan Residues in the BM2 Proton Channel from Influenza B Virus. *J. Biochem.* **2009,** *145* (4), 543-554.

43. DeLano, W. L., The PyMOL Molecular Graphics System. *Delano Scientific, San Carlos, CA* **2002**.

2.8 **Tables**

Table 1: Sequence of GWALP23 peptides with single and double substitutions of tryptophan to histidine

Name of peptide	**Sequence**	**Reference**
GWALP23	acetyl-GGAL**W**LALALALALALALAL**W**LAGA-amide	[12]
$H^{2,22}$WALP23	acetyl-G**H**AL**W**LALALALALALALAL**W**LA**H**A-amide	This work
H^{2}GWALP23	acetyl-G**H**AL**W**LALALALALALALAL**W**LAGA-amide	This work
H^{22}GWALP23	acetyl-GGAL**W**LALALALALALALAL**W**LA**H**A-amide	This work

Table 2: ^{2}H-NMR quadrupolar splitting magnitudes of labeled core alanines of GWALP23 family peptides with single and double histidine substitution

Lipid	**Peptide**	**pH**	**[d4] Ala CD3 quadrupolar splittings[a]**					
			7	9	11	13	15	17
DLPC	GWALP23	-	26.4	25.5	26.9	14.6	20.7	3.4
	$H^{2,22}$	4	30.8	35	29.3	19.4	24.7	4.2
	H^{2}		31.9	35.6	31.4	23.7	25.8	1.2
	H^{22}		26.3	24.3	25.4	11.7	19.0	7.2
DOPC	GWALP23	-	16.6	1.7	16.7	1.5	15.4	2.6
	$H^{2,22}$	4	15.4	1.2	17.0	1.6	16.0	2.1
	H^{2}		19.1	6.3	19.5	5.2	17.4	1.6
	H^{22}		14.0	1.4	14.1	1.1	12.5	4.1

[a] Values listed are for $\beta = 0^{0}$ sample orientations

Table 3: Semistatic GALA and Modified Gaussian analysis results for $H^{2,22}$WALP23, H^{2}GWALP23, and H^{22}GWALP23

Peptide	**Lipid**	**GALA Analysis Results**				**Modified Gaussian Analysis Results**				
		τ	**ρ**	**Szz**	**RMSD**	**τ_0**	**ρ_0**	**στ**	**σρ**	**RMSD**
GWALP	DLPC	20.7	307	0.71	0.66	23	304	15	33	0.7
H2,22		26	304	0.74	1.05	24	303	10	16	1.43
H2		26	308	0.77	0.86	33	305	10	36	0.61
H22		22.7	297	0.67	0.66	17	299	10	8	1.22
GWALP	DOPC	6	323	0.87	0.61	9	321	9	48	0.7
H2,22		6	329	0.86	0.33	10	326	10	56	0.56
H2		8.7	319	0.83	0.52	12	318	10	46	0.52
H22		6	315	0.73	0.35	9	319	10	70	0.45

2.9 **Figure Legends**

Figure 1: Pymol [43] representations of oriented helices of GWALP23, G $H^{2,22}$ALP23, H^{2}GWALP23, and H^{22}GWALP23. The sequences are shown in Table 1

Figure 2: ^{2}H NMR spectra of $H^{2,22}$WALP23, H^{2}GWALP23 and H^{22}GWALP23in DOPC lipid bilayer. The samples were hydrated with acetate buffers of pH 4. Spectra for $\beta = 90^{o}$ sample orientations are shown

Figure 3: Selected ^{2}H NMR spectra to show the titration of $H^{2,22}$WALP23 in DLPC (A) and DOPC (B) lipid bilayers. Sample orientation is $\beta = 90^{o}$ and temperature is 50^{o}C

Figure 4: Selected ^{2}H NMR spectra to show the titration of H^{2}GWALP23 in DLPC (A) and DOPC (B) lipid bilayers. Sample orientation is $\beta = 90^{o}$ and temperature is 50^{o}C

Figure 5: Selected ^{2}H NMR spectra to show the titration of H^{22}GWALP23 in DLPC (A) and DOPC (B) lipid bilayers. Sample orientation is $\beta = 90^{o}$ and temperature is 50^{o}C

Figure 6: Quadrupolar wave plot for oriented GWALP23 family peptides with terminal single and double histidine residues in DOPC lipid bilayer

Figure 7: Quadrupolar wave plot for oriented GWALP23 family peptides with terminal single and double histidine residues in DLPC lipid bilayer

2.10 **Figures**

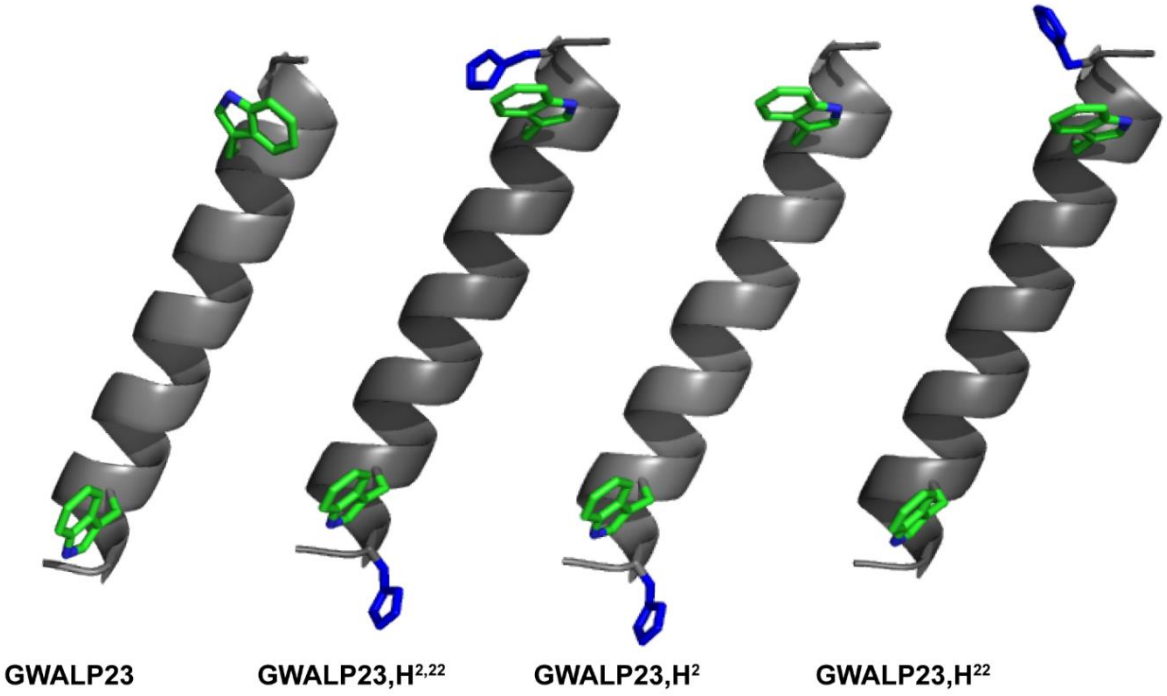

Figure 1: Pymol [43] representations of oriented helices of GWALP23, G $H^{2,22}$ALP23, H^{2}GWALP23, and H^{22}GWALP23. The sequences are shown in Table 1

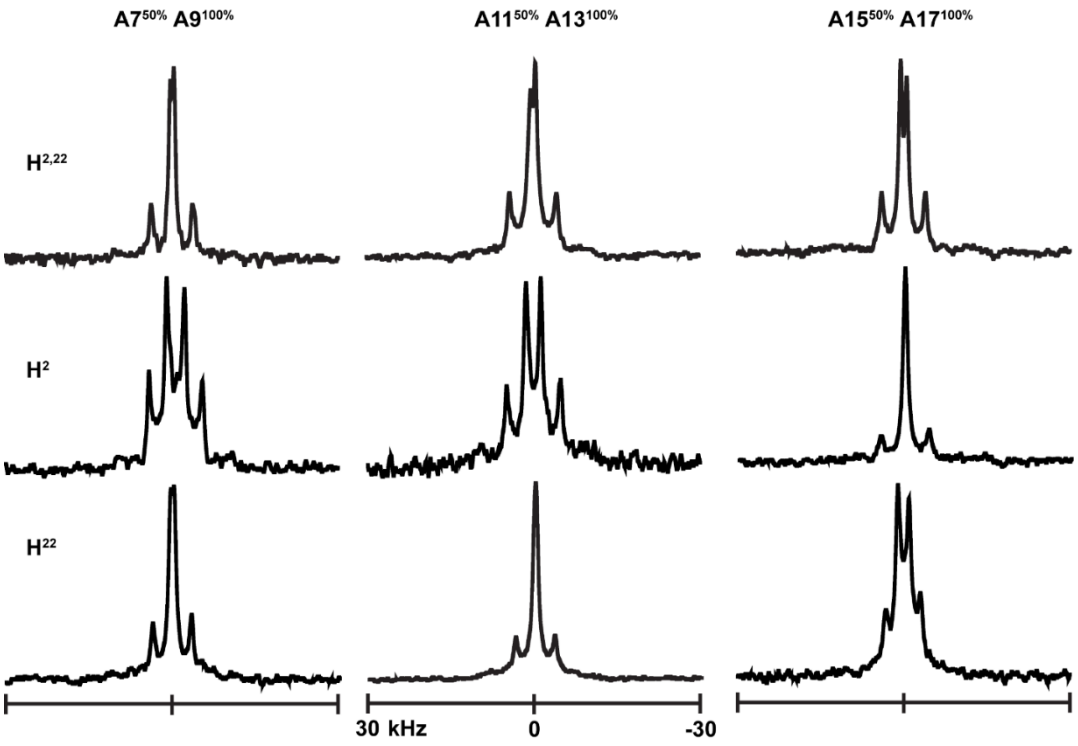

Figure 2: ^{2}H NMR spectra of $H^{2,22}$WALP23, H^{2}GWALP23 and H^{22}GWALP23in DOPC lipid bilayer. The samples were hydrated with acetate buffers of pH 4. Spectra for $\beta = 90^{o}$ sample orientations are shown

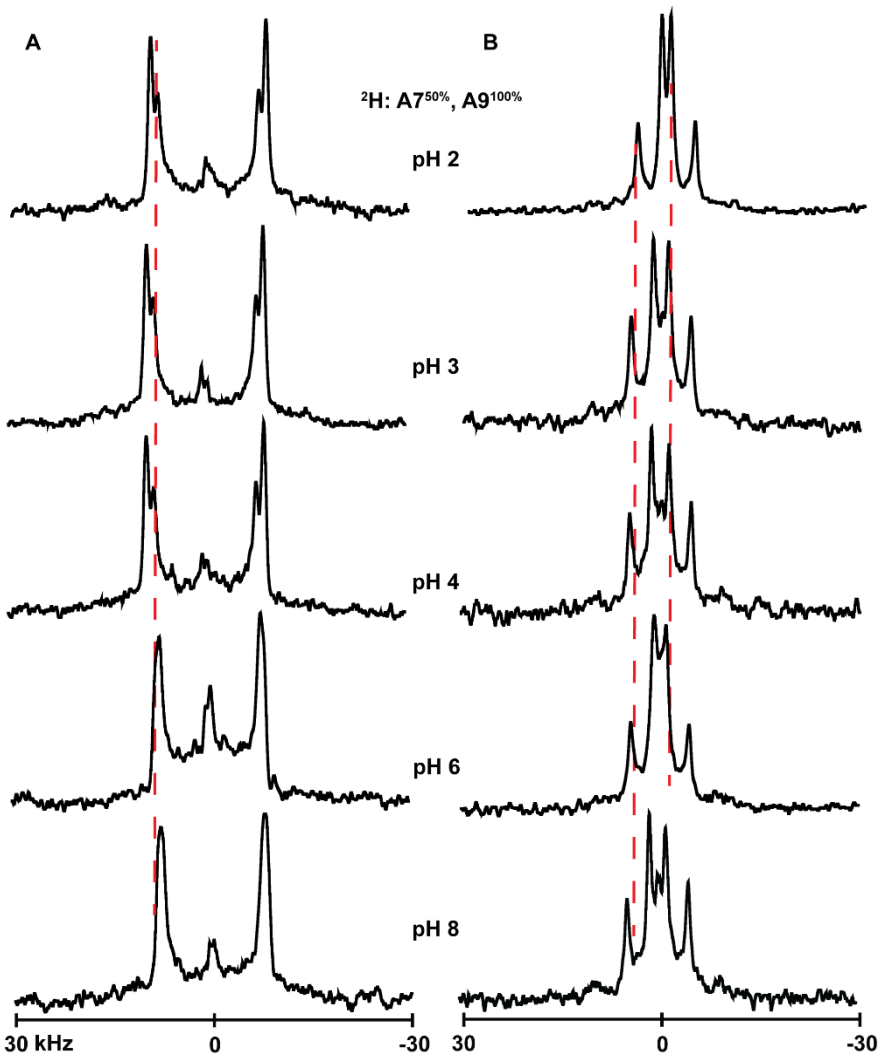

Figure 3: Selected ^{2}H NMR spectra to show the titration of H^{2,22}WALP23 in DLPC (A) and DOPC (B) lipid bilayers. Sample orientation is $\beta = 90^o$ and temperature is 50^oC

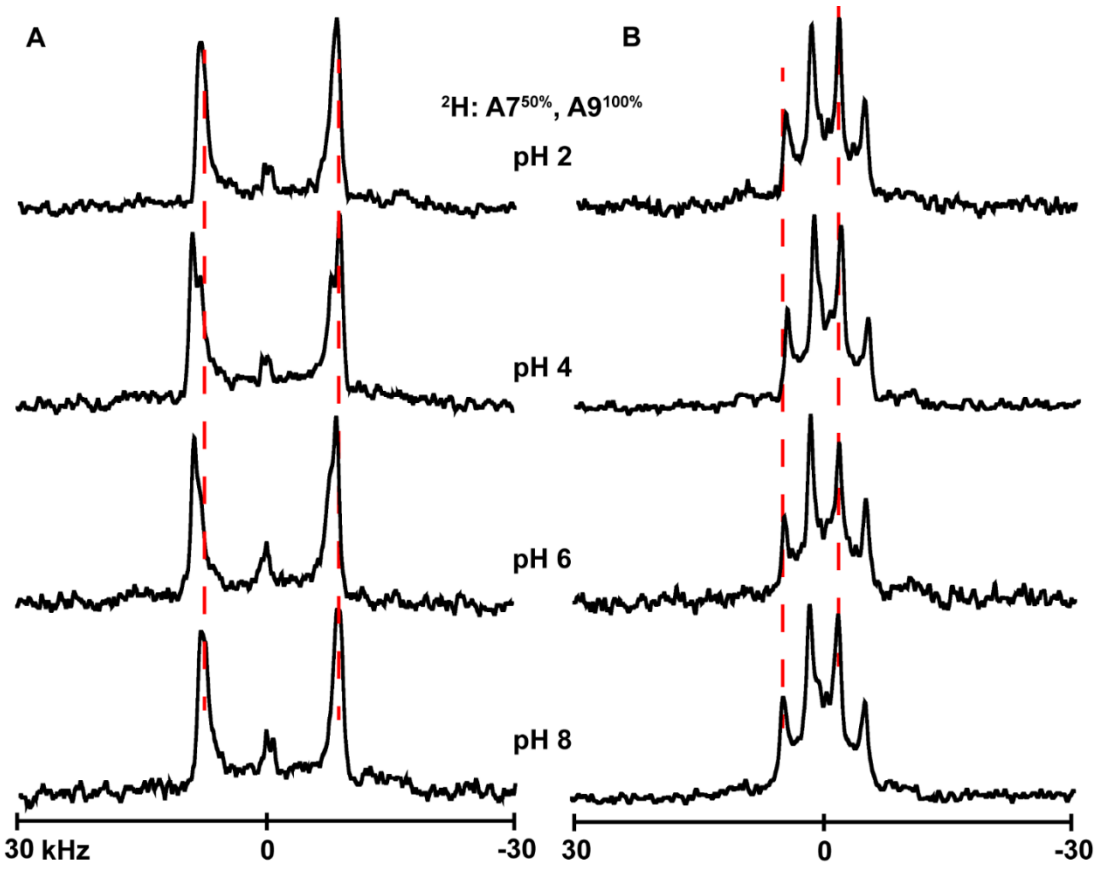

Figure 4: Selected ^{2}H NMR spectra to show the titration of H^{2}GWALP23 in DLPC (A) and DOPC (B) lipid bilayers. Sample orientation is $\beta = 90^o$ and temperature is 50^oC

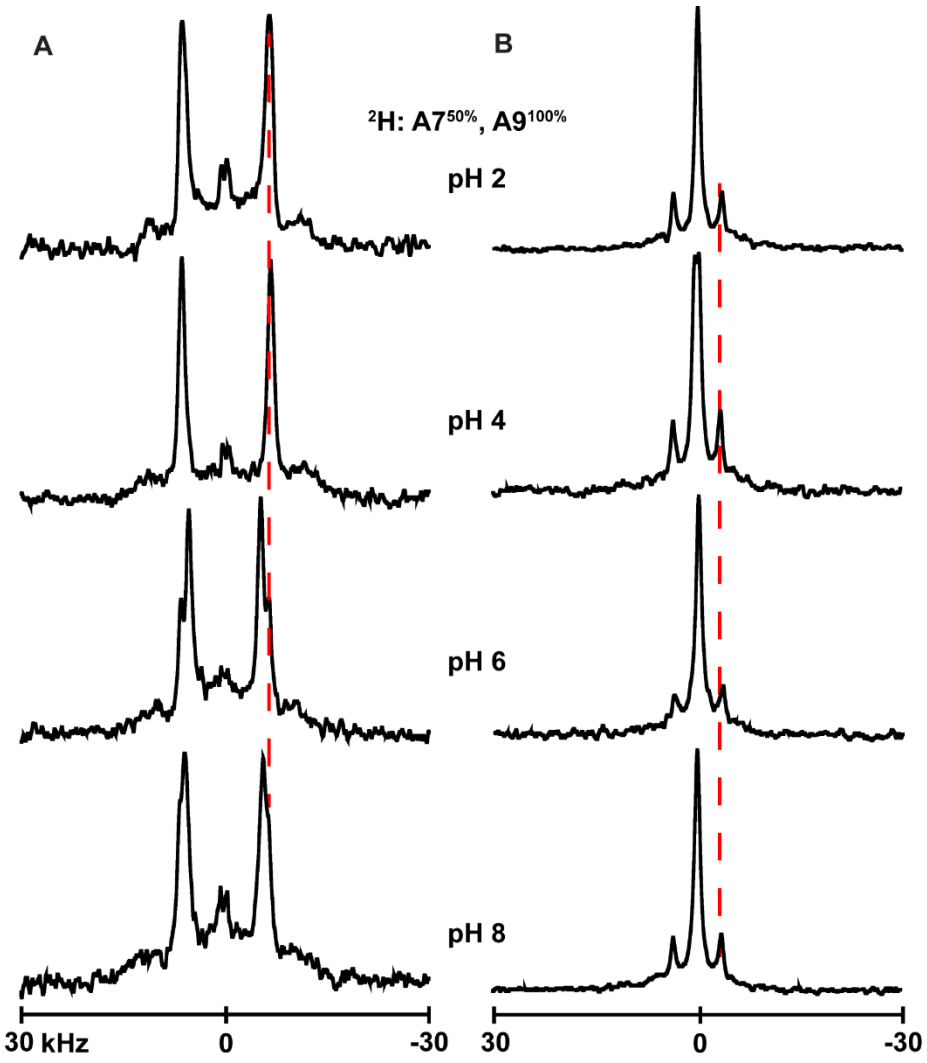

Figure 5: Selected ^{2}H NMR spectra to show the titration of H^{22}GWALP23 in DLPC (A) and DOPC (B) lipid bilayers. Sample orientation is $\beta = 90^o$ and temperature is 50^oC

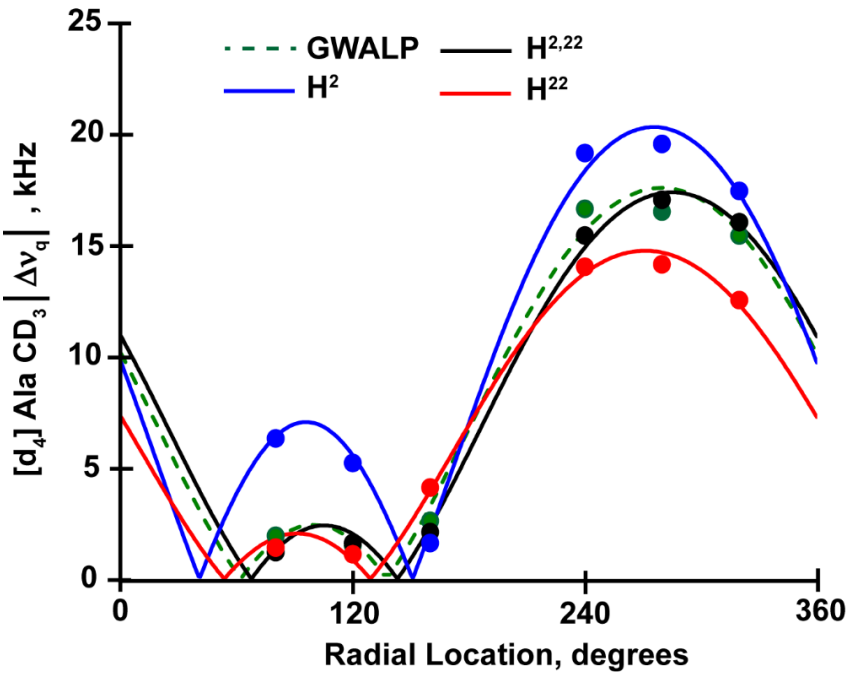

Figure 6: Quadrupolar wave plot for oriented GWALP23 family peptides with terminal single and double histidine residues in DOPC lipid bilayer

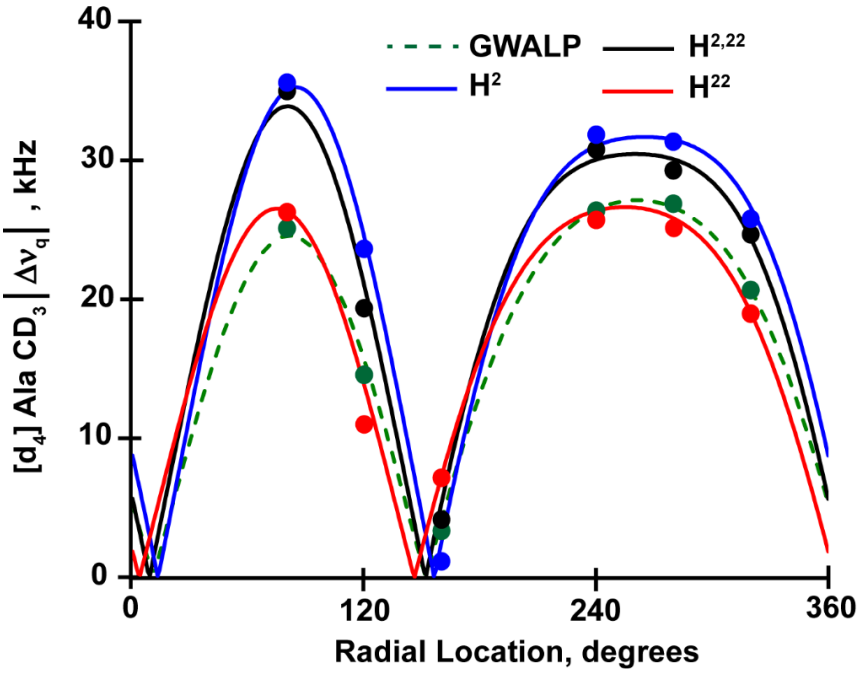

Figure 7: Quadrupolar wave plot for oriented GWALP23 family peptides with terminal single and double histidine residues in DLPC lipid bilayer

2.11 **Supporting Figures**

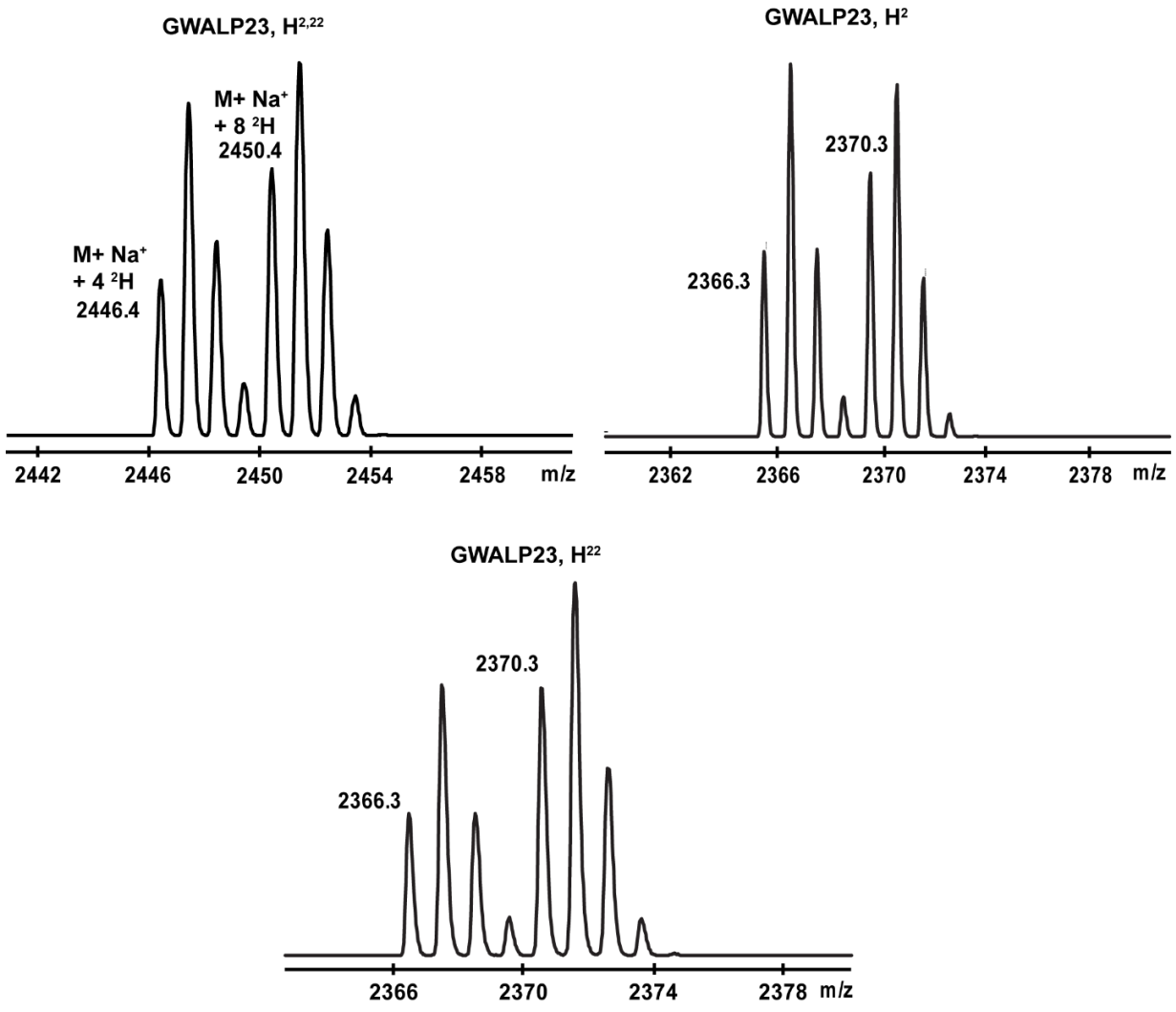

Figure S1: MALDI mass spectrum of synthesized $H^{2,22}$WALP23, H^{2}GWALP23 and H^{22}GWALP23

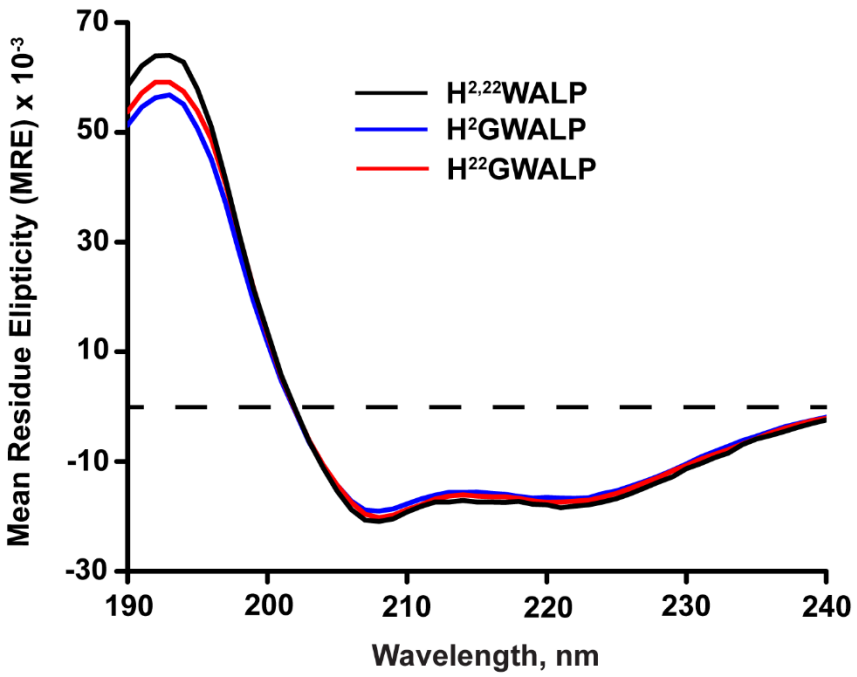

Figure S2: Circular Dichroism spectra of $H^{2,22}$WALP23; H^{2}GWALP23, and H^{22}GWALP23 helices in DLPC lipid vesicles

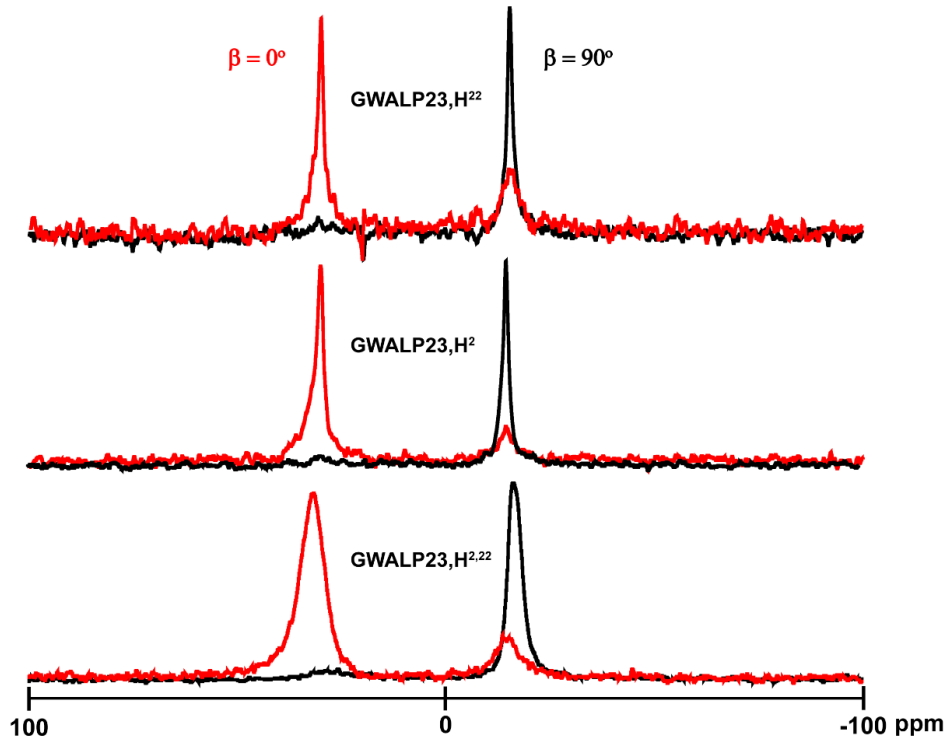

Figure S3: ^{31}P NMR spectra of $H^{2,22}$WALP23, H^{2}GWALP23 and H^{22}GWALP23 in DLPC lipid bilayers

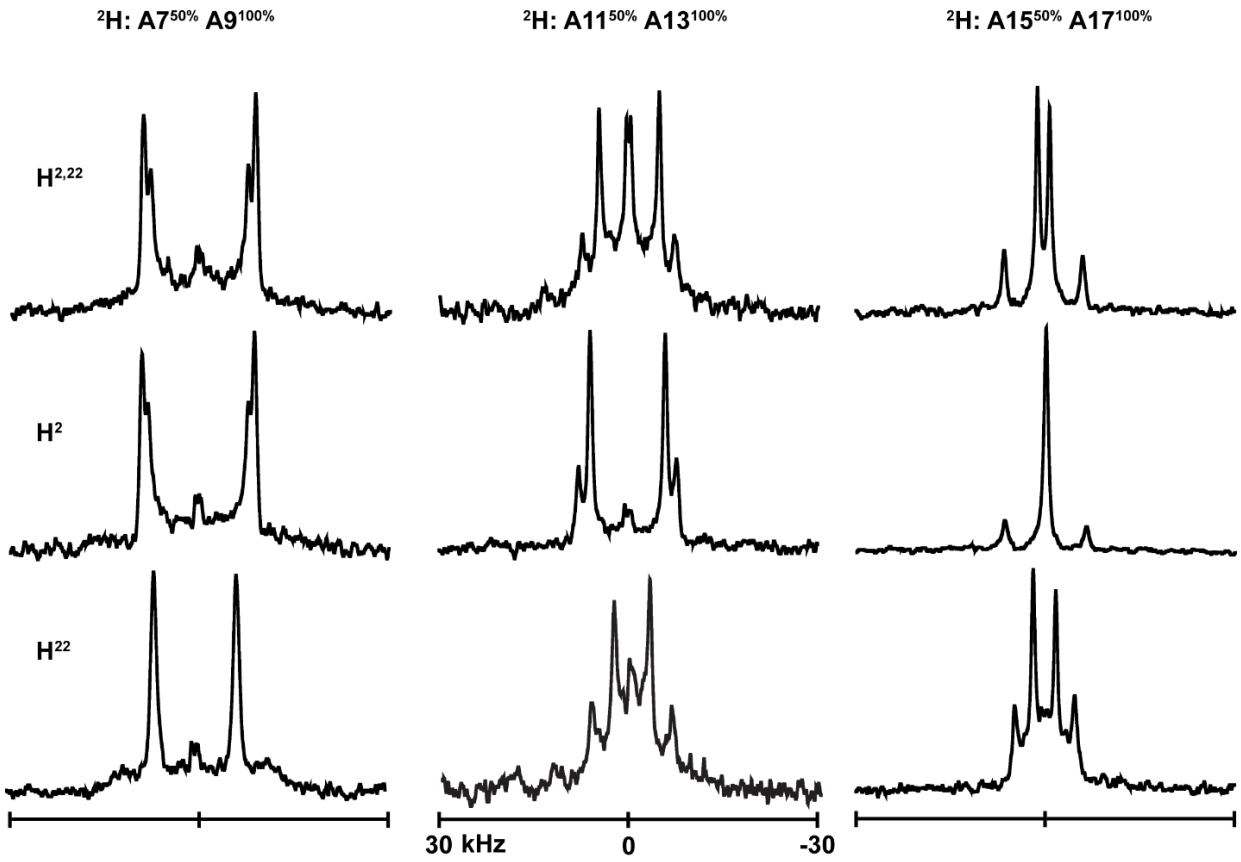

Figure S4: ^{2}H NMR spectra of H^{2,22}WALP23, H^{2}GWALP23, H^{22}GWALP23 in DLPC lipid bilayer. The samples were hydrated with acetate buffers of pH 4. Spectra for $\beta = 90^o$ sample orientations are shown

3. Chapter 3: Comparing the Mutations of Tryptophan to Histidine at the Terminal Regions of GWALP23 and pH Dependent Orientations of Transmembrane Peptides Flanked by Histidine Anchors.

3.1 Abstract

For better understanding of the orientation and dynamic interactions between a transmembrane protein segment and a lipid bilayer, a variety of model membrane systems are widely used for different experimental applications. One such model peptide that has been used extensively for characterizing peptide-lipid interaction is alpha-helical transmembrane peptide GWALP23 (acetyl-GGALW^{5}(LA)$_{6}$W^{19}LAGA-amide), that contains six Leu-Ala repeats in the core and single Trp flanking residues near each end. This model peptide, due to its reduced dynamic properties, demonstrates sensitivity to the lipid identity and bilayer thickness and has been useful in elucidating the importance of "anchoring" residues. GWALP23 furthermore illustrates well the effects of hydrophobic matching. In this work, I have modified GWALP23 to include one or two histidine residues that replace either W5 or W19 or both tryptophans within the sequence of GWALP23. The variations in dynamics and helix orientation of peptides anchored by only histidine or both histidine and tryptophan have been addressed, in addition to the ionization properties of single or double histidines and their effects on peptide helix behavior. Application of solid-state ^{2}H NMR spectroscopy to detect deuterium-labeled alanines in the core of the helix allowed us to report the effect of terminal histidine residues on the orientation of the transmembrane segment when present with or in absence of tryptophan anchors in DOPC lipid membranes. We observe that the presence of either H5 or H19 or both does not greatly affect the apparent tilt magnitude, but some changes in the helix rotational preference are noticeable. Nevertheless, the presence of only H5 in the helix (with W19) does affect the helical integrity,

which also has been found previously when H4 and H5 are both present. In an attempt to titrate the histidine residue(s), we found that the peptide doesn't change its orientation over a pH range from 2 to 8. Therefore, the analysis of orientation and dynamic properties shows little sensitivity to pH and reveals that the behavior of the model transmembrane helices with interfacial histidines remains very similar to the tryptophan and tyrosine analogs with similar mutations.

3.2 **Introduction**

Generally, transmembrane α-helices are composed primarily of hydrophobic residues with a very few strongly polar amino acids. Hydrophilic residues, if present in transmembrane domain, tend to be highly conserved. This conservation suggests their necessity either in structure or function of the specific protein [1]. Many transmembrane proteins have bands of aromatic and/or positively charged residues near the membrane interface which could serve as "anchors" for a particular protein orientation and promote favorable protein-lipid interactions. It has been found that aromatic residues such as Trp are localized to the carbonyl region of phospholipids, whereas charged residues such as Lys or Arg tend to be positioned outside of the membrane, interacting with lipid phosphate moieties [2] as well as with water.

The indole ring hydrogen bonding of Trp, which is invariable with pH, is important for stabilizing the transmembrane orientation and allows this amphipathic residue to be located in interfacial positions [34]. Histidine, with an imidazole ring in its side chain, also has the ability to form hydrogen bond with surface water. But the histidine imidazole group can be charged or neutral depending on the pH, which might have some effects on the interactions with lipid head groups, leading to peptide stability in membrane. As histidine usually has a pKa value close to physiological pH, it is able to function as both acid and base in many enzymes, including serine

proteases and some other unconventional proteases such as cytomegalovirus protease and rhomboid protease. The cytomegalovirus protease has a catalytic triad containing one serine and two histidines, in which both histidines are critically important for catalytic activity of the enzyme under certain conditions [5]. Multiple histidine residues, either directly adjacent [6] or closely located [7-8], were identified in the pH sensing components of acid-sensing ion channels, which implies the importance of histidine in pH sensing. Replacement of a specific histidine residue with alanine in specific ion channels causes lower sensitivity [9] and in some cases elimination of sensitivity [6 7] to proton concentration. These mutations may cause some conformational or structural changes which directly affect the function of protein. Therefore, it is crucial to investigate how this aromatic residue with the ability of being ionized interacts with the hydrophobic environment of a lipid membrane.

The understanding of how membrane proteins interact with the bilayer of a lipid membrane [10] has been aided by studies of "simple" model transmembrane (TM) α-helices such as the WALP series of peptides having the prototype sequence of $GWW(LA)_nLWWA$[11]. The modified version of WALP peptide, GWALP23 (acetyl-$GGALW(LA)_6LWLAGA$-amide) [12-13] has only two interfacial Trp residues. This arrangement contributes to a preferred and well-defined tilted transmembrane helix orientation for GWALP23 with low dynamic averaging of the helix [14-15]. These properties of GWALP23 provide exceptional opportunities for investigating the influence of guest residues upon the properties and lipid interactions of membrane-spanning peptide helices. Previously, this framework has been used to study several guest residues including arginine [16 17], lysine [18], tyrosine [19 20], histidine [21] and glutamic acid [22] in various locations throughout the sequence of transmembrane helix. Now this type of study is crucial because the identity, number and position of such residues greatly influence the overall peptide

orientation in the membrane. For example, peptides with single Trp → Tyr substitution at either end of the GWALP sequence (Y^{5} or Y^{19}) exhibit similar transmembrane orientations and dynamics as those of GWALP23 or a double Tyr mutant $GY^{5,19}$ALP23. However, with two adjacent Tyr residues ($Y^{4,5}$GWALP23) the peptides exhibit very high levels of dynamic averaging [23], which is comparable to the earlier WALP peptides. When two His residues are introduced in the same positions to produce $H^{4,5}$GWALP23 peptides, the extent of dynamic averaging also increases and gives rise to very low "apparent" tilt angles, similar to $Y^{4,5}$GWALP23. In this context, it is important to determine the biophysical properties of peptides carrying a single interfacial histidine residue and compare them with the peptide with two adjacent interfacial histidines as well as with tryptophan and tyrosine in the membrane-water interface.

In this study I focus on examining the similarities and differences between His, Trp and Tyr as interfacial aromatic anchoring residues at the interfacial positions of 5 and/or 19, flanking a core hydrophobic helix, in bilayer membranes of DOPC. I furthermore examined the ionization behavior of the histidine imidazole side chains when present alone or as a pair. My key findings indicate that when one or both Trp residues are replaced by one or two His residues from the sequence of GWALP23, the overall orientation and dynamics of the transmembrane helix remains nevertheless quite similar. Histidine 5, however, may disrupt the core helix under some conditions. While the His residues may titrate, the core helix often shows little response to the titration of His residues near the membrane interface. This minimal response to pH contrasts with the larger response of similar transmembrane helices to the titration of more buried His residues [21].

3.3 **Materials and methods**

Synthesis of ^{2}H-labeled peptides in solid phase

The ^{2}H isotope enriched alanines were purchased from Cambridge Isotope Laboratories (Andover, MA) and then were modified by manual derivatization with the N-fmoc protecting group, using a protocol that was optimized previously [24-25]. ^{1}H-NMR spectroscopy was used to confirm the successful Fmoc-Ala-d_4 synthesis. Other N-fmoc amino acids and acid-labile "Rink" amide resins were purchased from Novabiochem (San Diego, CA). Histidine and tryptophan side chains were protected with trityl and t-butoxycarbonyl protecting groups, respectively. All peptides were synthesized using an Applied Biosystems 433A Peptide Synthesizer from Life Technologies (Foster City, CA), in solid phase on a 0.1 mmol scale with monitoring of the deprotection reaction. Extended times were employed for deprotection or coupling where needed. Typically, d_4-alanines were introduced into the synthetic sequence in pairs at 50% and 100% isotope abundance levels, respectively, to distinguish and assign the ^{2}H signals when observed later by solid-state deuterium NMR spectroscopy. The N-terminal end of each peptide was blocked by adding an acetyl-Gly as final residue.

Following the completion of synthesis, the peptide cleavage from Rink amide resin was accomplished by treatment at 22 °C for over a 2 h period using a mixture of trifluoroacetic acid/triisopropyl silane/water/phenol (85/5/5/5, v/v/v/w). This treatment yielded a neutral, amidated C-terminal. The crude peptides were then precipitated by adding ice-cold 50/50 methyl-t-butyl ether/hexane solution and lyophilized several times from acetonitrile:water (50:50) to remove traces of solvent. After lyophilization, peptides were purified by reversed-phase HPLC on an octyl-silica Zorbax Rx-C8 column (9.4 x 250 mm, 5 μm particle size) from

Agilent Technologies (Santa Clara, CA) using a gradient of 88–92% (for H5H19) or 94-98% methanol (for both H5W19 and W5H19 peptides) with 0.1% trifluoroacetic acid (v/v). Due to the absence of tryptophan groups in H5H19 peptides, the detector wavelength was set to 220 nm while purifying and quantifying this peptide, whereas the Trp-containing peptides (H5W19 and W5H19) were detected based on absorbance at 280 nm, using a molar extinction coefficient of 5,600 $M^{-1}cm^{-1}$ for each Trp in the sequence. MALDI-TOF mass spectrometry was used to verify the molecular masses and deuteration patterns.

^{2}H and ^{31}P NMR Spectroscopy using Oriented Bilayer samples

Samples for solid-state ^{2}H NMR were prepared by mechanical alignment, as described previously [20, 23]. Bilayers were formed using 1.33 μmol peptide and 80 μmol (1:60 mol:mol) DOPC lipid (Avanti Polar Lipids, Alabaster, AL) and hydrated (45%, w/w) with 20 mM buffer at specified pH values between pH 2 and pH 8. Alignment of phospholipid head groups in bilayers within each sample was confirmed by means of ^{31}P NMR in a wide-line probe from Doty Scientific (Columbia, SC) with broad-band ^{1}H decoupling on a Bruker Avance 300 spectrometer (Billerica, MA) at 50 ˚C. Signals for both β = 0˚ (bilayer normal parallel to magnetic field) and β = 90˚ macroscopic sample orientations (Figure S3) were collected. Deuterium (^{2}H) NMR spectra, at both β = 90° and β = 0° sample orientations, were recorded at 50 °C by employing a quadrupolar echo pulse sequence [26] with full phase cycling, 105 μs echo delay, 3.2 μs pulse length and 120 ms recycle delay. During each ^{2}H NMR experiment approximately 0.9 to 1.5 million free induction decays were recorded. An exponential weighting function with 100 Hz line broadening was applied prior to Fourier transformation.

Buffers used for hydrating the oriented samples were prepared at room temperature using vacuum-dried reagents and prepared in deuterium-depleted water. Buffers include: pH 2-3.5 glycine-HCl buffer, pH 4 acetate buffer (sodium acetate and acetic acid, MilliporeSigma, St. Louis, MO); pH 6 Citrate buffers (EMD, Gibbstown, NJ); pH 8 HEPES buffer (MilliporeSigma)

Analysis of helix orientation and dynamics from ^{2}H NMR data

Geometric Analysis of Labeled Alanines (GALA) [27] [28] was employed to analyze the orientation of peptides in lipid bilayers. This is a semi-static analysis method that uses the quadrupolar splitting values from ^{2}H-NMR spectra to fit a generalized order parameter S_{zz}, and the apparent peptide tilt magnitude (τ) and direction (ρ), to a model of a tilted α-helical peptide, with an $\varepsilon_{//}$ angle between the alanine C_α-C_β bond vector and peptide helix axis equal to 59.4° [27]. We additionally employed a modified Gaussian approach [29] involving three variables, τ_0, ρ_0 and $\sigma\rho$ (rotational slippage), with fixed values for S_{zz} and $\sigma\tau$ (helix wobble), as described previously [20]. This method provides more detailed results toward the dynamic properties of α-helical peptides.

Circular Dichroism (CD) Spectroscopy

Samples for circular dichroism spectroscopy were prepared by forming small lipid vesicles incorporating 0.0626 μmol peptide and 3.75 μmol lipid (1/60 peptide:lipid) using ultrasonication in unbuffered water. The peptide concentrations were determined by UV-Vis spectroscopy using a molar extinction coefficient of ε_{280}=5600 $M^{-1}cm^{-1}Trp^{-1}$. An average of ten scans was recorded on a Jasco J-1500 spectropolarimeter, using a 1 mm cell path length, 1.0 nm bandwidth, 0.1 nm slit and a scan speed of 20 nm/min.

3.4 **Results**

Previous studies on insertion of aromatic residues like Phe and Tyr in place of Trp anchors indicate similar transmembrane orientations for the helix as that of the GWALP23 helix [19-20]. These findings along with evidence that aromatic amino acids play crucial roles in anchoring transmembrane protein function prompted us to employ GWALP23 as a host peptide for insertion of the other aromatic and potentially charged amino acid histidine. Our recent study reveals that the peptide dynamic properties change drastically when a pair of adjacent histidine residues at the N-terminal end ($H^{4,5}$) are incorporated [30]. To address this further, I have now replaced H4 with L4, which resulted in a GWALP23 mutant with a single histidine (H5) residue at the N-terminal end. Then I replaced the W19 from GWALP23 with H19 to compare the similarities and/or differences of histidine with tryptophan or tyrosine, which was previously studied [19] as well as its H5 counterpart. In addition to comparing the N- and C-terminal single histidine placements, pair of histidines were introduced to replace W5 and W19 to examine the properties displayed by a transmembrane helix flanked only by two histidines, rather than tryptophans.

The designed peptides (Figure 1 and Table 1) were successfully synthesized and their molecular masses confirmed by MALDI-TOF mass spectrometry (Figure S1). All three peptides contain single or pair of histidine in presence (for H5W19 and W5H19 mutants) or absence (H5H19) of tryptophan residues. To confirm that the expected α-helical secondary structure of peptides is retained with the substitution of tryptophan to histidine residue/residues, CD spectra were recorded in DOPC vesicles (Figure S2). The mean residue ellipticity (MRE) profiles of each peptide were generally found comparable and displayed double minima at wavelengths 208 and 222 nm, indicative of α-helical secondary structures.

We have applied solid-state NMR spectroscopy in mechanically-aligned samples of peptides incorporated within hydrated DOPC lipid-bilayer membranes to investigate the ionization properties and influence of histidine imidazole side chain on transmembrane peptide in lipid bilayers. We first analyzed the alignment of phospholipid head groups using ^{31}P NMR. The spectra from all peptide-lipid systems exhibit characteristic resonances of ^{31}P isotopes located close to -14.5 ppm for $\beta = 90°$ and +29 ppm for $\beta = 0°$ sample orientations.

Helix orientation and dynamic behavior of folded transmembrane peptides were studied with the help of solid-state ^{2}H NMR spectroscopy. In addition, the responses of each peptides with the ionization of histidine imidazole side chain, which in turn provide information of the pKa values of histidine in varying locations throughout the membrane, were also examined. Finally, I have compared the results of transmembrane peptides flanked by both histidine and tryptophan as well as only by histidine.

In each of the GWALP23 peptides with single or double Trp to His mutations, pairs of alanines within the core $(LA)_6$ helix were ^{2}H-labeled to different extents (50% and 100% deuteration). Figures. 2, 3 and 4 show examples of ^{2}H-NMR spectra for labeled core alanines A7 and A9 of H^{5}GWALP23 with Y^{5}GWALP23 (Figure 2), H^{19}GWALP23 with Y^{19}GWALP23 (Figure 3) and $GH^{5,19}$ALP23 with $GY^{5,19}$ALP23 and $GW^{5,19}$ALP23 (Figure 4) cousins. For the Y and W analogs, the spectra for labeled A7 and A17 are shown in Figures 2, 3 and 4, which were studied previously [13, 19]. The ^{2}H-NMR spectra recorded for oriented samples of -H^{5}, -H^{19} and -$H^{5,19}$ peptides display the two expected pairs of resonances corresponding to the quadrupolar splittings from the two labeled core Ala methyl side chains in DOPC lipid bilayers (Figures 2, 3 4 S4). For some cases such as A15 and A17 spectra of H^{5}GWALP23 (Figure S4), single set of

peaks with attached shoulders were observed due to spectral overlap arising from similar ^{2}H quadrupolar splittings from the two alanines.

Now examining the quadrupolar splittings magnitudes $|\Delta\nu_q|$ of the ^{2}H signals for peptides listed in Table 2, it is evident that H^{5}GWALP23 produced a relatively large range of ^{2}H quadrupolar splitting magnitudes, from 1 to 22 kHz in DOPC membrane than the parent GWALP23 (1-17 kHz) and two other similar peptides Y^{5}GWALP23 (0.5-16 kHz) and F^{5}GWALP23 (1-18 kHz) [19 20] (Table 2). This wide range of quadrupolar splittings suggests a tilted orientation of the peptide helix with low dynamic averaging in DOPC membrane. When compared the individual $\Delta\nu_q$ values of all core alanines of H^{5}GWALP23 with -W^{5}, -Y^{5} and -F^{5} analogs we see that these magnitudes are within 1−5 kHz in each case. These results indicate relatively similar membrane orientations and dynamic properties for the -H^{5}, -Y^{5}, -F^{5} and GWALP23 model peptides, with possibly a slight increase in the helix tilt when histidine is present at the N-terminal membrane water interface.

In case of C-terminal replacement of Trp to His, the range of quadrupolar splittings for H^{19}GWALP23 (4-21 kHz) is slightly smaller compared to the N-terminal histidine mutant H^{5}GWALP23 (Table 2), but are relatively consistent with those seen previously for GWALP23 and Y^{19} (0.5-15 kHz) analogue, implying that all these GWALP23-like peptides are tilted to similar extents, and exhibit similar dynamics, in the DOPC lipid bilayer membranes.

Moving forward to the double mutation of GWALP23 peptides, where both W5 and W19 are substituted by H5 and H19, producing $GH^{5,19}$ALP peptide, the sets of ^{2}H quadrupolar splittings for the six labeled alanines of the Leu-Ala core, indeed are comparable to those of H^{5}

and H^{19}GWALP23. Thus, the results for single and double histidine trading are consistent when compared them with similar tyrosine and tryptophan analogs.

To address the ionization of N-terminal histidine and its effect on the peptide behavior, we have recorded ^{2}H NMR signals for A7 and A9 of all three histidine containing peptides under consideration here at pH range from 2-8. Results indicate that each peptide exhibit sharp signals in DOPC membrane over this pH range, meaning they adopt well-defined transmembrane orientations, but there is no observable change in the spectra of H^{5}, H^{19} or $H^{5,19}$ peptides (Figure 5, 6,7) when the pH is lowered from 8 to 2. This implies that the peptide doesn't respond to the titration of histidine residue/residues present at the terminus of the helix. Thereby a titration plot of quadrupolar splittings versus pH would show straight lines, which is why the pKa values of histidines possibly cannot yet be calculated by means of ^{2}H quadrupolar splittings. Another way to determine the titration dependency is by observing the signal intensity, but similar to quadrupolar splitting magnitude the signal intensities remain unchanged under pH conditions from 2 to 8.

To analyze and verify the helix orientations and motional averaging, we used "Geometric Analysis of Labeled Alanines (GALA)" method, described previously [27]. The results from this analysis, listed in Table 3 and illustrated in Figure 8, demonstrate that the hydrophobic α-helices anchored by one histidine and one tryptophan as well as two histidines with no tryptophan adopt very similar transmembrane orientations. The resulting tilt angles for these new peptides are in the proximity of 9^{o} (8.7^{o} for H^{5} and $H^{5,19}$; 9.7^{o} for H^{19}) which is slightly larger (~ 3^{o}) than the $W^{5,19}$ peptide (Table 3) , The W/Y5, W/Y19 and W5,19/Y5,19 mutations of GWALP23 produce very minimal change in tilt ($\Delta\tau$). These comparisons suggest that the presence of H5 or H19 or

both results in very similar scaling of τ with the other two aromatic residues tyrosine and tryptophan in the same positions.

With very minor change in tilt angles, the Trp to His mutations display some changes in azimuthal rotations (ρ) about the helix axis. The H5 and H19 peptides show approximately 30^o and 20^o changes in rotation in DOPC lipid membrane compared to the W5,19 counterpart, but the direction of rotation is opposite for the H5 and H19 substitutions (Table 3). When both H5 and H19 are present, the changes in peptide rotation appear to cancel each other and thereby the helix rotation of double-histidine peptide does not differ much from that of the parent GWALP23 helix. These results are again consistent when the tryptophans were substituted by tyrosine residues in Y5, Y19 and Y5,19 peptides [19, 23].

To re-evaluate the results from semi-static analysis, we used a second method known as the modified-Gaussian approach.[20, 29] As mentioned previously this method uses τ, ρ, a distribution width σρ, and a fixed στ, to find the lowest RMSD and gives a more detailed idea on the dynamic averaging of peptides. For each peptide under consideration here the modified Gaussian approach shows further agreement, with similar values for tilt (τ_0) and rotation (ρ_0) with low slippage (σρ) values not exceeding 40^o.

A noteworthy feature observed here is the ^{2}H $|\Delta\nu_q|$ magnitude for deuterated A7, near the beginning of the core helix fails to fit the core helix backbone geometry, when only H5 or both H5 and H19 are present, in bilayers of DOPC and is therefore markedly unraveled from the transmembrane core helix (Figure 8). This type of unravelling involving an additional core residue was observed previously for H^{4,5}GWALP23, when two adjacent histidine residues are present at the N-terminal end [30]. Now more interestingly, this unraveling disappears when only

H19 is present with a tryptophan at N-terminal end (W5) and A7 fits into the GALA plot. Because the behavior of unraveling or unwinding has been observed for several GWALP23-like model peptides and is thought to have a significant contribution to the dynamic stability of transmembrane peptides [30-32], it is very likely that the extended unwinding in H5 and H5,19 peptides involving residue A7 plays important role in helical stability. Since histidine is not as bulky as tryptophan the peptide achieves stability by fraying residue 5 to accommodate the N-terminal histidine toward the interface while the C-terminal residue, either histidine or tryptophan anchors the peptide. This scenario is different in case of H19 peptide, where H19 probably anchors the peptide and W5 finds a better position to access to interface by only changing the rotation and without any additional structural change due to the size of tryptophan side chain. These results could also imply the importance of having a tryptophan at the N-termini, at position 5 in case of GWALP23, of a transmembrane peptide to obtain a more perfect helix.

3.5 **Discussion**

With the ability to provide interaction between a positively charged imidazole side chain and negatively charged lipid head groups, histidine offers the potential to promote protein-lipid interaction at the interface in membrane proteins [21 33 34 35]. Yet this residue is not as frequently present as tyrosine or tryptophan at the membrane-water interface, possibly due to its less thermodynamically favorable nature [36 37 38 39]. Another recent study tested this hypothesis by mutating the highly conserved F161 residue of eight-stranded OMP enzyme PagP to H161 and generating a library of PagPX160H mutants with X160 being any amino acid. Their analysis resulted in thermodynamically unstable PagP β-barrel because of the absence of a compact

structure [40]. The stabilization was then recovered partially by incorporating a hydrophobic residue (Y, M, I, V, L) at the X position.

To readdress such instability of membrane proteins with interfacial histidine residues, I have employed the well-established GWALP23 host peptide framework, with the replacement of tryptophan residue/s that help in maintaining a defined orientation, with moderate to low dynamics, to adjust the hydrophobic mismatch. My aim has been to the compare the anchoring properties of histidine when present at the interface of a transmembrane peptide, alone or in pair. I also have focused on titrating the imidazole side chain of histidine located in various positions. Titration could possibly orient the His side chain in a different manner and could influence the aggregation or unfolding of the resulting transmembrane α-helical peptide.

A similar comparison involving another potential aromatic residue Tyr was accomplished previously [19] where the two aromatic residues, Tyr and Trp were found to behave quite similarly in each position considered. Here we have further analyzed the system by comparing histidine with tryptophan as well as tyrosine at the N- and/or C-terminal interfaces of the α-helical segment.

My investigations reveal that neither histidine nor tyrosine alters fundamentally the behavior of GWALP-like peptides. The alanine ^{2}H quadrupolar splittings for GWALP23 with single or a pair of interfacial histidines do not vary much. The resulting ^{2}H quadrupolar wave plots observed for the core helices of H^{5}GWALP23, H^{19}GWALP23 and GH^{5,19}ALP23 are similar to those of the parent helix GWALP23. The helix of GWALP23 is moderately dynamic with tilted transmembrane orientations that changes with lipid thicknesses [13]. With H5 at N-terminal end and W19 at C-terminal end the new helix adopts a very similar well-defined

orientation in DOPC, with a 3° higher tilt (τ_o) and 30° change in azimuthal rotation. The rotational slippage remains modest of about 35°, meaning that the replacement of indole ring side chain with an imidazole one doesn't affect the helix dynamics. The only important difference we notice for H5GWALP23 and the host peptide is a long-unwound N-terminal end which not only unravels a portion of the core helix but also includes the mutated H5 residue. When the histidine is moved from position 5 to 19 (with tryptophan occupying position 5), we observe almost no change in peptide tilt but about 50° change compared to its H5 isomer. The dynamic properties, by means of $\sigma\rho$ value, also remain lower and unchanged. But very interestingly, for this histidine mutant no unwinding or helix fraying is observed. The H^{19}GWALP23 peptide stays helical from at least residue 7 to 17 unlike H^5GWALP23. Furthermore, when both H5 and H15 are present, the predicted $\sigma\rho$ doesn't increase, rather displays very identical tilted orientation with moderate rotational slippage and helical wobbling. Surprisingly, for this $GH^{5,19}$ALP23 peptide, residue A7 falls off the helical plot and deflects by about 5.0 kHz, resulting in extended N-terminal unraveling, possibly from residue 1 to 7, which is also observed for the H^5GWALP23 peptide. Thus, we confer that the N-terminal histidine residue may contribute more in determining the helical integrity for such transmembrane peptide segments, than the C-terminal residue. At this point as we do not have additional data to examine the terminal unwinding involving residue 3 and 21, which were found to participate in helix to non-helix transitions for most of the GWALP family peptides studied previously [30, 32], it is not possible to complete the study of unwinding in these cases. Rather we can speculate that because terminal unwinding is a very common feature for transmembrane proteins, the histidine analogs of GWALP23 doesn't differ from this general feature. Their unwinding behavior may be modified by the number and locations of interfacial histidine residues.

Now why does the loss of one or two tryptophan indole rings not affect the helix dynamics? I speculate that the histidine imidazole ring/s at the interfaces may behave as a combination of aromatic as well as polar rings in the absence of tryptophan indole rings, to accommodate the hydrophobic lipids and simultaneously anchor the peptide helix by forming stable interactions with lipid head groups and surface water molecules through hydrophilic interactions, including hydrogen bond formation. Since the imidazole ring is smaller than the indole ring, the helices with imidazole rings (in case of H5, H19 and H5,19 mutations) are slightly more tilted than their indole or tyrosyl cousins, suggesting an adjustment to the lipid bilayer thickness. Thus, the histidines may be able to find appropriate orientations at the interface and minimize the consequences of the loss of tryptophan anchors.

Even though histidine is a polar residue, its behavior depends on the polarity of its environment. With two –NH groups and a pKa of around 6-7, the imidazole ring can be charged as well as neutral depending on small changes in pH. Additionally, the pKa may be modulated by the local membrane environment and can drop by 2 to 4 units when the imidazole side chain is buried withing the hydrophobic core of a lipid bilayer [21]. To test whether I observe any change in the histidine pKa when present at the membrane-water interface, I have employed buffers of varying pH, ranging from acidic to basic, attempting to titrate the interfacial imidazole side chain of histidine residues. The properties of the global helix, as detected from the ^{2}H NMR spectra for the labeled alanines, serve as an indirect "read-out" for the titration behavior as the pH is changed. The one or two histidine residues in these peptides are the only titratable groups. NMR spectral changes will require two events; namely, (i) a His residue would need to change its ionization state, and (ii) the global helix would need to respond to the change in the His ionization. If the helix does not respond to a change in His ionization, then the titration will not

be detected. Indeed, there is no observable change in the ^{2}H NMR spectra from pH 2 to 8 for any of the labeled alanines in the peptides with the H5, H19 or H5,19 substitutions. This could imply that when present at the interface, the histidine side chains prefer only one ionization state, either charged or neutral, although such a scenario would seem unlikely. Another possibility, as noted, is that the interfacially located imidazole ring of histidine does titrate with the change of pH, but the peptide helix does not respond with any change in its preferred orientation or dynamics from pH 2-8. Notably, a similar helix does respond to the titration of more buried His residues [21].

In this study, I have characterized three peptides, H^{5}GWALP23, H^{19}GWALP23 and GH^{5,19}ALP23 each containing one or a pair of interfacial histidine residues in DOPC lipid membranes. I note that the identities and locations of the interfacial aromatic residues govern the azimuthal rotation of the transmembrane helix. It was previously seen that introduction of two adjacent histidine residues at N-terminal end, in the case of the H^{4,5}GWALP23 peptide, increases the rotational slippage ($\sigma\rho$) around helix axis in DOPC membranes [30]. Here I observe that removal of H4 drastically reduces $\sigma\rho$, while maintaining a well-defined helix tilt angle and azimuthal rotation. The present experiments also show that a change from W5 to H5 causes a shift of -30^{o} in ρ_{o}, while the change from W19 to H19 causes a shift of +20^{o} in ρ_{o}, compared to the parent GWALP23 helix with W5 and W19 as a control. Overall, the rotational preferences of H5W19 and W5H19 peptides differ by ~50°. Notably, residues 5 and 19 project 40° apart on a helical wheel. With both H5 and H19 present in the same helix, the rotational "corrections" cancel, and the rotational preference then once again matches that for GWALP23, when W5 and W19 are present. Moreover, these results projecting the trend of helix rotation are consistent with similar previously studied peptides in which tyrosines replace the tryptophan residues [19].

Therefore, the differences in orientation in terms of helix tilt and rotation with respect to anchor group identity (H or W or Y) and location (position 5 or 19) remain similar. Only one difference I have observed here is the helical unwinding, that involves a portion of core helix (alanine 7), that is displayed in the presence of histidine H5, but not with tryptophan or tyrosine in the same position. Indeed, this particular helix unraveling is only observed when H5 is present in the helix, as in the case of H^{5}GWALP23 and $GH^{5,19}$ALP23, even for another histidine analog $H^{4,5}$GWALP23 [30]. Such behavior is absent when the histidine is moved to the C-terminal end (in the case of H^{19}GWALP23).

In summary, the present study indicates that single or multiple histidine residues at the interfacial region of a transmembrane peptide does not significantly perturb the orientation or dynamics of a transmembrane alpha helix. Apparently, the His side chains do not cause crowding of aromatic rings at either of the membrane interfaces. The identity of the aromatic seems not to affect the helix dynamics as long as there are not "too many" aromatic rings. Histidine H5 does nevertheless extend the N-terminal unraveling up to residue 7. The influence of pH furthermore becomes complicated when the His residues, either one or both, are present at the membrane-water interface.

3.6 **Acknowledgements**

The peptide, NMR, and mass spectrometry facilities were supported in part by National Institutes of Health Grants GM103429 and GM103450. We thank Vitaly Vostrikov for software for semi-static GALA methods for analysis of helix orientations and dynamics.

3.7 **References**

1. Zhou, F. X.; Merianos, H. J.; Brunger, A. T.; Engelman, D. M., Polar residues drive association of polyleucine transmembrane helices. *Proc Natl Acad Sci* **2001,** *98* (5), 2250.

2. de Planque, M. R. R.; Kruijtzer, J. A. W.; Liskamp, R. M. J.; Marsh, D.; Greathouse, D. V.; Koeppe, R. E.; de Kruijff, B.; Killian, J. A., Different Membrane Anchoring Positions of Tryptophan and Lysine in Synthetic Transmembrane α-Helical Peptides. *J. Biol. Chem* **1999,** *274* (30), 20839-20846.

3. Connell, A. M.; Koeppe, R. E.; Andersen, O. S., Kinetics of gramicidin channel formation in lipid bilayers: transmembrane monomer association. *Science* **1990,** *250* (4985), 1256.

4. Yau, W.-M.; Wimley, W. C.; Gawrisch, K.; White, S. H., The Preference of Tryptophan for Membrane Interfaces. *Biochemistry* **1998,** *37* (42), 14713-14718.

5. Tong, L.; Qian, C.; Massariol, M.-J.; Bonneau, P. R.; Cordingley, M. G.; Lagacé, L., A new serine-protease fold revealed by the crystal structure of human cytomegalovirus protease. *Nature* **1996,** *383* (6597), 272-275.

6. Paukert, M.; Chen, X.; Polleichtner, G.; Schindelin, H.; Gründer, S., Candidate Amino Acids Involved in H+ Gating of Acid-sensing Ion Channel 1a. *J. Biol. Chem* **2008,** *283* (1), 572-581.

7. Clarke, C. E.; Benham, C. D.; Bridges, A.; George, A. R.; Meadows, H. J., Mutation of histidine 286 of the human P2X4 purinoceptor removes extracellular pH sensitivity. *J Physiol* **2000,** *523 Pt 3* (Pt 3), 697-703.

8. Rajan, S.; Wischmeyer, E.; Xin Liu, G.; Preisig-Müller, R.; Daut, J.; Karschin, A.; Derst, C., TASK-3, a Novel Tandem Pore Domain Acid-sensitive K+Channel: AN EXTRACELLULAR HISTIDINE AS pH SENSOR. *J. Biol. Chem* **2000,** *275* (22), 16650-16657.

9. Wang, Y.; Park, S. H.; Tian, Y.; Opella, S. J., Impact of histidine residues on the transmembrane helices of viroporins. *Mol Membr Biol* **2013,** *30* (7), 360-369.

10. Killian, J. A.; von Heijne, G., How proteins adapt to a membrane–water interface. *Trends Biochem Sci* **2000,** *25* (9), 429-434.

11. Killian, J. A.; Salemink, I.; De Planque, M. R.; Lindblom, G.; Koeppe, R. E., II; Greathouse, D. V., Induction of non-bilayer structures in diacylphosphatidylcholine model membranes by transmembrane α-helical peptides. Importance of hydrophobic mismatch and proposed role of tryptophans. *Biochemistry* **1996,** *35*, 1037-1045.

12. Vostrikov, V. V.; Grant, C. V.; Daily, A. E.; Opella, S. J.; Koeppe, R. E., II, Comparison of "Polarization Inversion with Spin Exchange at Magic Angle" and "Geometric Analysis

of Labeled Alanines" methods for transmembrane helix alignment. *J. Am. Chem. Soc.* **2008,** *130* (38), 12584-85.

13. Vostrikov, V. V.; Daily, A. E.; Greathouse, D. V.; Koeppe, R. E., II, Charged or aromatic anchor residue dependence of transmembrane peptide tilt. *J. Biol. Chem.* **2010,** *285* (41), 31723-31730.

14. Vostrikov, V. V.; Grant, C. V.; Opella, S. J.; Koeppe, R. E., II, On the combined analysis of ^{2}H and $^{15}N/^{1}H$ solid-state NMR data for determination of transmembrane peptide orientation and dynamics. *Biophys. J.* **2011,** *101* (12), 2939-2947.

15. Grage, S. L.; Strandberg, E.; Wadhwani, P.; Esteban-Martin, S.; Salgado, J.; Ulrich, A. S., Comparative analysis of the orientation of transmembrane peptides using solid-state ^{2}H and ^{15}N NMR: Mobility matters. *Eur. Biophys. J. Biophy* **2012,** *41* (5), 475-482.

16. Vostrikov, V. V.; Hall, B. A.; Greathouse, D. V.; Koeppe, R. E.; Sansom, M. S. P., Changes in Transmembrane Helix Alignment by Arginine Residues Revealed by Solid-State NMR Experiments and Coarse-Grained MD Simulations. *J. Am. Chem. Soc* **2010,** *132* (16), 5803-5811.

17. Vostrikov, V. V.; Hall, B. A.; Sansom, M. S. P.; Koeppe, R. E., 2nd, Accommodation of a central arginine in a transmembrane peptide by changing the placement of anchor residues. *J Phys Chem B* **2012,** *116* (43), 12980-12990.

18. Gleason, N. J.; Vostrikov, V. V.; Greathouse, D. V.; Koeppe, R. E., Buried lysine, but not arginine, titrates and alters transmembrane helix tilt. *Proc Natl Acad Sci* **2013,** *110* (5), 1692.

19. Gleason, N. J.; Greathouse, D. V.; Grant, C. V.; Opella, S. J.; Koeppe, R. E., II, Single Tryptophan and Tyrosine Comparisons in the N-Terminal and C-Terminal Interface Regions of Transmembrane GWALP Peptides. *J. Phys. Chem. B* **2013,** *117* (44), 13786-13794.

20. Sparks, K. A.; Gleason, N. J.; Gist, R.; Langston, R.; Greathouse, D. V.; Koeppe, R. E., II, Comparisons of Interfacial Phe, Tyr, and Trp Residues as Determinants of Orientation and Dynamics for GWALP Transmembrane Peptides. *Biochemistry* **2014,** *53* (22), 3637-3645.

21. Martfeld, A. N.; Greathouse, D. V.; Koeppe, R. E., Ionization Properties of Histidine Residues in the Lipid Bilayer Membrane Environment. *J. Biol. Chem* **2016,** *291* (36), 19146-19156.

22. Rajagopalan, V.; Greathouse, D. V.; Koeppe, R. E., Influence of glutamic acid residues and pH on the properties of transmembrane helices. *Biochim. Biophys. Acta, Biomembr.* **2017,** *1859* (3), 484-492.

23. Gleason, N. J.; Vostrikov, V. V.; Greathouse, D. V.; Grant, C. V.; Opella, S. J.; Koeppe, R. E., II, Tyrosine replacing tryptophan as an anchor in GWALP peptides. *Biochemistry* **2012,** *51* (10), 2044-2053.

24. Kortenaar, P. B. W.; Dijk, B. G.; Peeters, J. M.; Raagen, B. J.; Adams, P. J.; Tesser, G. I., Rapid and efficient method for the preparation of Fmoc-amino acids starting from 9-fluorenylmethanol. *Int. J. Pept. Prot. Res.* **1986,** *27*, 398-400.

25. Greathouse, D. V.; Koeppe, R. E., II; Providence, L. L.; Shobana, S.; Andersen, O. S., Design and characterization of gramicidin channels. *Methods Enzymol.* **1999,** *294*, 525-550.

26. Davis, J. H.; Jeffrey, K. R.; Valic, M. I.; Bloom, M.; Higgs, T. P., Quadrupolar echo deuteron magnetic resonance spectroscopy in ordered hydrocarbon chains. *Chem. Phys. Lett.* **1976,** *42*, 390-394.

27. van der Wel, P. C. A.; Strandberg, E.; Killian, J. A.; Koeppe, R. E., II, Geometry and intrinsic tilt of a tryptophan-anchored transmembrane alpha-helix determined by ^{2}H NMR. *Biophys. J.* **2002,** *83*, 1479-1488.

28. Strandberg, E.; Özdirekcan, S.; Rijkers, D. T. S.; van der Wel, P. C. A.; Koeppe, R. E., II; Liskamp, R. M. J.; Killian, J. A., Tilt angles of transmembrane model peptides in oriented and non-oriented lipid bilayers as determined by ^{2}H solid-state NMR. *Biophys. J.* **2004,** *86*, 3709-3721.

29. Strandberg, E.; Esteban-Martin, S.; Ulrich, A. S.; Salgado, J., Hydrophobic mismatch of mobile transmembrane helices: Merging theory and experiments. *Biochim. Biophys. Acta.* **2012,** *1818*, 1242-1249.

30. Afrose, F.; McKay, M. J.; Mortazavi, A.; Suresh Kumar, V.; Greathouse, D. V.; Koeppe, R. E., Transmembrane Helix Integrity versus Fraying To Expose Hydrogen Bonds at a Membrane–Water Interface. *Biochemistry* **2019,** *58* (6), 633-645.

31. Strandberg, E.; Grau-Campistany, A.; Wadhwani, P.; Bürck, J.; Rabanal, F.; Ulrich, A. S., Helix Fraying and Lipid-Dependent Structure of a Short Amphipathic Membrane-Bound Peptide Revealed by Solid-State NMR. *J. Phys. Chem. B* **2018,** *122* (23), 6236-6250.

32. Mortazavi, A.; Rajagopalan, V.; Sparks, K. A.; Greathouse, D. V.; Koeppe, R. E., II, Juxta-terminal Helix Unwinding as a Stabilizing Factor to Modulate the Dynamics of Transmembrane Helices. *ChemBioChem* **2016,** *17* (6), 462-465.

33. Lee, S. A.; Eyeson, R.; Cheever, M. L.; Geng, J.; Verkhusha, V. V.; Burd, C.; Overduin, M.; Kutateladze, T. G., Targeting of the FYVE domain to endosomal membranes is regulated by a histidine switch. *Proc Natl Acad Sci* **2005,** *102* (37), 13052.

34. Kampmann, T.; Mueller, D. S.; Mark, A. E.; Young, P. R.; Kobe, B., The Role of Histidine Residues in Low-pH-Mediated Viral Membrane Fusion. *Structure* **2006,** *14* (10), 1481-1487.

35. Bustad, H. J.; Skjaerven, L.; Ying, M.; Halskau, Ø.; Baumann, A.; Rodriguez-Larrea, D.; Costas, M.; Underhaug, J.; Sanchez-Ruiz, J. M.; Martinez, A., The peripheral binding of 14-3-3γ to membranes involves isoform-specific histidine residues. *PLoS One* **2012,** *7* (11), e49671-e49671.

36. Wimley, W. C.; Creamer, T. P.; White, S. H., Solvation Energies of Amino Acid Side Chains and Backbone in a Family of Host−Guest Pentapeptides. *Biochemistry* **1996,** *35* (16), 5109-5124.

37. Hessa, T.; Kim, H.; Bihlmaier, K.; Lundin, C.; Boekel, J.; Andersson, H.; Nilsson, I.; White, S. H.; von Heijne, G., Recognition of transmembrane helices by the endoplasmic reticulum translocon. *Nature* **2005,** *433* (7024), 377-381.

38. Moon, C. P.; Fleming, K. G., Side-chain hydrophobicity scale derived from transmembrane protein folding into lipid bilayers. *Proc Natl Acad Sci* **2011,** *108* (25), 10174.

39. Lin, M.; Gessmann, D.; Naveed, H.; Liang, J., Outer Membrane Protein Folding and Topology from a Computational Transfer Free Energy Scale. *J. Am. Chem. Soc* **2016,** *138* (8), 2592-2601.

40. Iyer, B. R.; Vetal, P. V.; Noordeen, H.; Zadafiya, P.; Mahalakshmi, R., Salvaging the Thermodynamic Destabilization of Interface Histidine in Transmembrane β-Barrels. *Biochemistry* **2018,** *57* (48), 6669-6678.

41. DeLano, W. L., The PyMOL Molecular Graphics System. *Delano Scientific, San Carlos, CA* **2002**.

3.8 **Tables**

Table 1: Sequence of GWALP23 peptides with single and double substitutions of tryptophan to histidine[a]

Name of peptide	Sequence	Reference
GWALP23	acetyl-GGAL**W**^{5}LALALALALALAL**W**^{19}LAGA-amide	[13]
H^{5}GWALP23	acetyl-GGAL**H**LAH^{8}ALALALALALWLAGA-amide	This work
H^{19}GWALP23	acetyl-GGALWLAH^{8}ALALALALAL**H**LAGA-amide	This work
GH^{5,19}ALP23	acetyl-GGAL**H**LALALALALALAL**H**LAGA-amide	This work
Y^{5}GWALP23	acetyl-GGALYLALALALALALALWLAGA-amide	[23]
Y^{19}GWALP23	acetyl-GGALWLALALALALALALYLAGA-amide	[19]
GY^{5,19}ALP23	acetyl-GGALYLALALALALALALYLAGA-amide	[19]

[a] Mutations with histidine performed in this study are shown as bold and underlined

Table 2: ^{2}H-NMR quadrupolar splitting magnitudes ($|\Delta\nu_q|$) of labeled core alanines of GWALP23 family peptides with single and double interfacial histidine residue in DOPC lipid bilayers[a]

Alanine positions	DOPC						
	H^{5}	**H^{19}**	**H^{5,19}**	**Y^{5}**	**Y^{19}**	**Y^{5,19}**	**W^{5,19}**
7	22.1	17.3	22.3	16.2	14.2	13.9	16.6
9	6.0	4.6	7.3	0.5	0.5	0.5	1.7
11	16.8	19.8	18.6	13.6	14.9	14	16.7
13	1.2	8.2	3.8	0.5	0.5	0.5	1.5
15	11.7	20.5	17.5	13.6	14.9	14	15.4
17	8.5	5.4	1.1	4.8	1.0	3.9	2.6

[a] The values listed are for $\beta = 0^{o}$ sample orientations

Table 3: Semi-static GALA and modified Gaussian analysis results for H^{5}GWALP23, H^{19}GWALP23 and $GH^{5,19}$ALP23 in DOPC lipid bilayer

Peptide	pH	GALA				Modified Gaussian[a]					Ref
		τ_0	ρ_0	S_{zz}	RMSD	τ_0	ρ_0	σ_τ	σ_ρ	RMSD	
$W^{5,19}$		6.0°	323°	0.87	0.57	9°	321°	9	48°	0.7	[13]
[b]H^{5}	4	8.7°	292°	0.76	0.37	9°	290°	10°	32°	0.6	This work
H^{19}		9.7°	343°	0.83	0.97	11°	342°	10°	28°	0.84	This work
[b]$H^{5,19}$		8.7°	319°	0.80	0.97	10°	319°	10°	34°	1.1	This work
Y^{5}	-	5°	310°	0.81	0.88						[23]
Y^{19}		5°	336°	0.83	0.77						[19]
$Y^{5,19}$		5°	325°	0.83	0.50						[19]

[a] The modified Gaussian analysis was followed Sparks et al [20], with fixed σ_τ value of 10° and S_{zz} of 0.88.

[b] Calculations were performed without the A7 data point

3.9 **Figure Legends**

Figure 1: Pymol [41] representation of GWALP23 family peptides with histidine mutations in different locations

Figure 2: ^{2}H NMR spectra of labeled alanines A7(50%) and A9 (100%) of H^{5}GWALP23 (A) and A7(50%) and A17(100%) of Y^{5}GWALP23 (B) in DOPC lipid bilayer. For the H^{5}GWALP23 peptides, samples were hydrated with acetate buffers of pH 4. Spectra for both $\beta = 90^{o}$ and $\beta = 0^{o}$ sample orientations are shown

Figure 3: ^{2}H NMR spectra of labeled alanines A7(50%) and A9 (100%) of H^{19}GWALP23 (A) and A7(50%) and A17(100%) of Y^{19}GWALP23 (B) in DOPC lipid bilayer. For the H^{19}GWALP23 peptides, samples were hydrated with acetate buffers of pH 4. Spectra for both $\beta = 90^{o}$ and $\beta = 0^{o}$ sample orientations are shown

Figure 4: ^{2}H NMR spectra of labeled alanines A7(50%) and A9 (100%) of GH^{5,19}ALP23 (A) and A7(50%) and A17(100%) of GY^{5,19}ALP23 (B) and GW^{5,19}ALP23 (C) in DOPC lipid bilayer. For the histidine peptide, samples were hydrated with acetate buffers of pH 4. Spectra for both $\beta = 90^{o}$ and $\beta = 0^{o}$ sample orientations are shown

Figure 5: Selected ^{2}H NMR spectra to show the titration of H^{5}GWALP23 in DOPC lipid bilayer. Sample orientation is $\beta = 90^{o}$ for each spectrum and temperature is 50^{o}C

Figure 6: Selected ^{2}H NMR spectra to show the titration of H^{19}GWALP23 in DOPC lipid bilayer. Sample orientation is $\beta = 90^{o}$ for each spectrum shown and temperature is 50^{o}C

Figure 7: Selected ^{2}H NMR spectra to show the titration of GH^{5,19}ALP23 in DOPC lipid bilayer. Sample orientation is $\beta = 90^{o}$ and temperature is 50^{o}C

Figure 8: Quadrupolar wave analysis for oriented H^{5}GWALP (red), H^{19}GWALP (blue) and GH^{5,19}ALP23 (black) peptides in DOPC lipid bilayer. The analysis for host peptide GW^{5,19}ALP23 in the same lipid membrane id shown as dotted green plot.

3.10 **Figures**

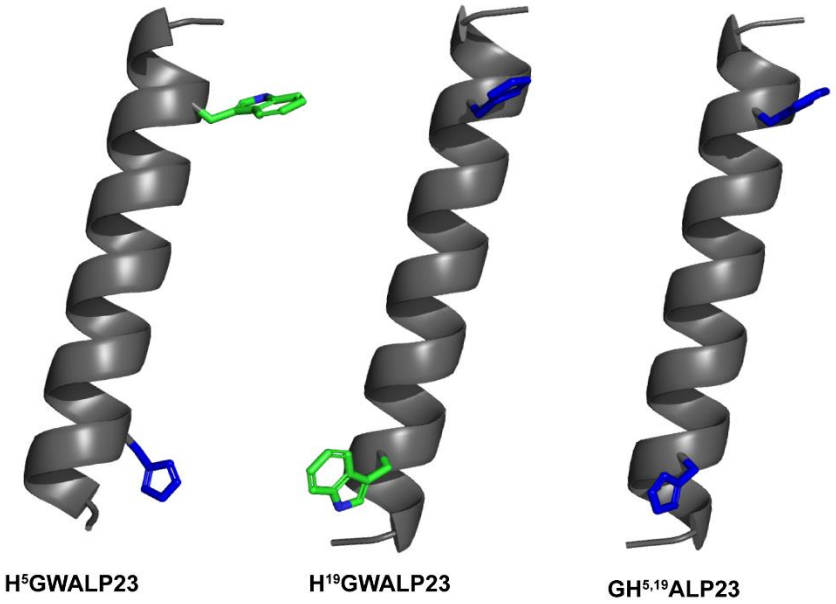

Figure 1: Pymol [41] representation of GWALP23 family peptides with histidine mutations in different locations

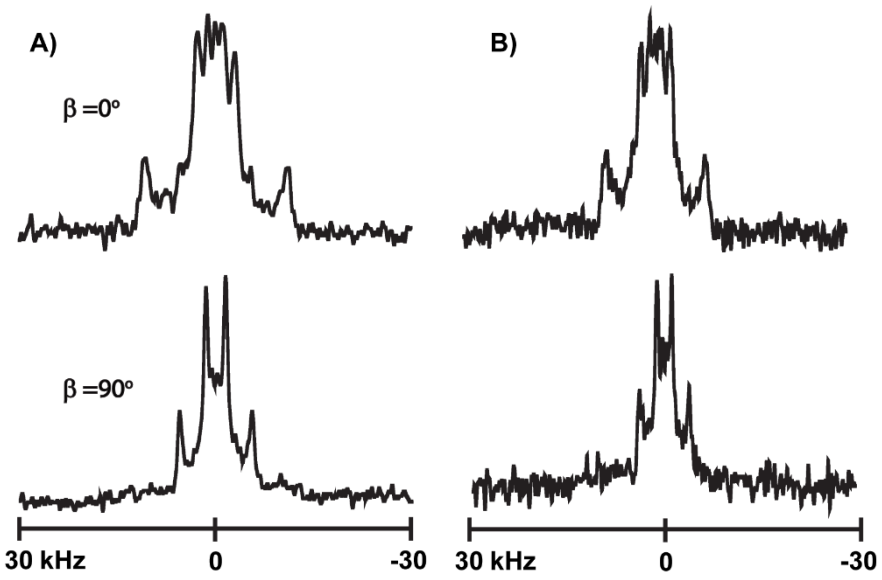

Figure 2: ^{2}H NMR spectra of labeled alanines A7(50%) and A9 (100%) of H^{5}GWALP23 (A) and A7(50%) and A17(100%) of Y^{5}GWALP23 (B) in DOPC lipid bilayer. For the H^{5}GWALP23 peptides, samples were hydrated with acetate buffers of pH 4. Spectra for both $\beta = 90^{o}$ and $\beta = 0^{o}$ sample orientations are shown

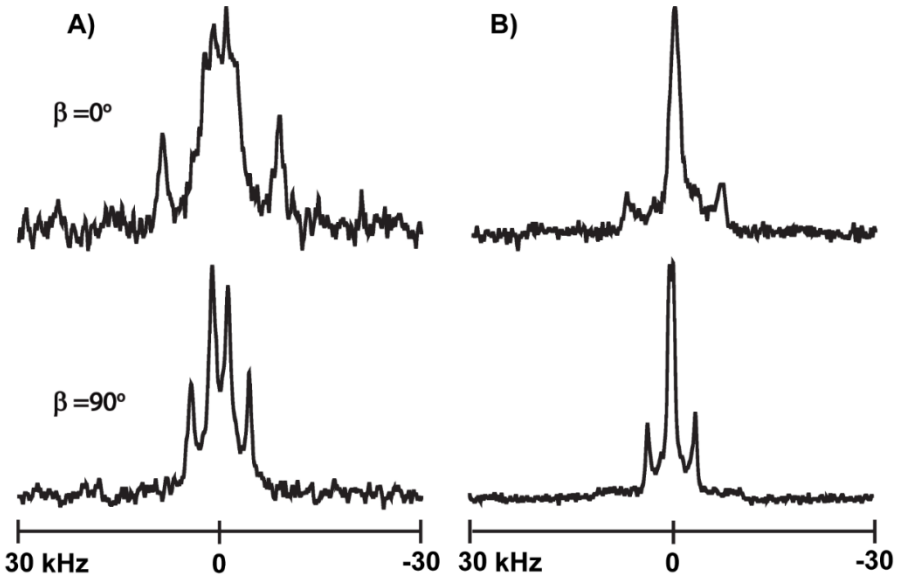

Figure 3: ^{2}H NMR spectra of labeled alanines A7(50%) and A9 (100%) of H^{19}GWALP23 (A) and A7(50%) and A17(100%) of Y^{19}GWALP23 (B) in DOPC lipid bilayer. For the H^{19}GWALP23 peptides, samples were hydrated with acetate buffers of pH 4. Spectra for both β =90^{o} and β =0^{o} sample orientations are shown

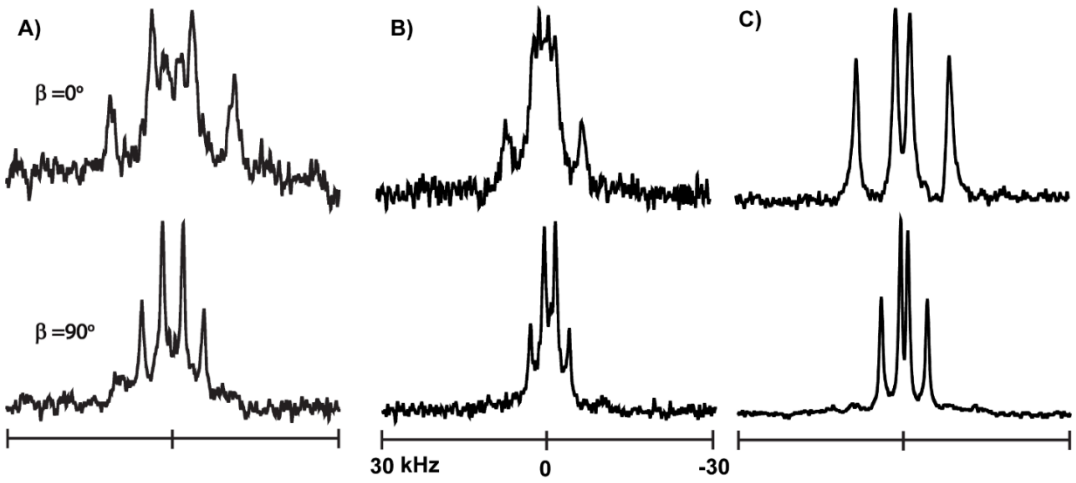

Figure 4: ^{2}H NMR spectra of labeled alanines A7(50%) and A9 (100%) of GH^{5,19}ALP23 (A) and A7(50%) and A17(100%) of GY^{5,19}ALP23 (B) and GW^{5,19}ALP23 (C) in DOPC lipid bilayer. For the histidine peptide, samples were hydrated with acetate buffers of pH 4. Spectra for both $\beta = 90^{o}$ and $\beta = 0^{o}$ sample orientations are shown

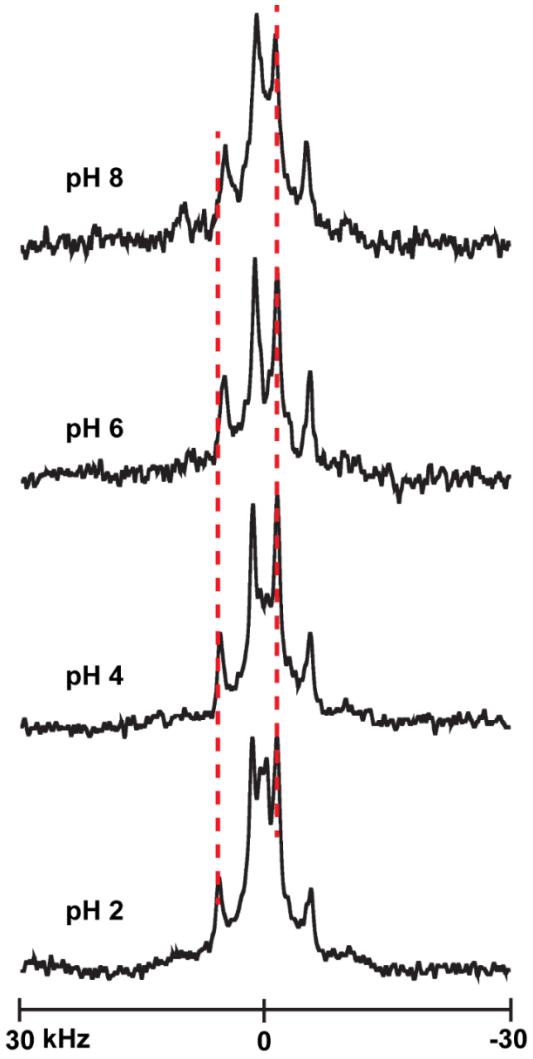

Figure 5: Selected ^{2}H NMR spectra to show the titration of H^{5}GWALP23 in DOPC lipid bilayer. Sample orientation is $\beta = 90^{o}$ for each spectrum and temperature is $50^{o}C$

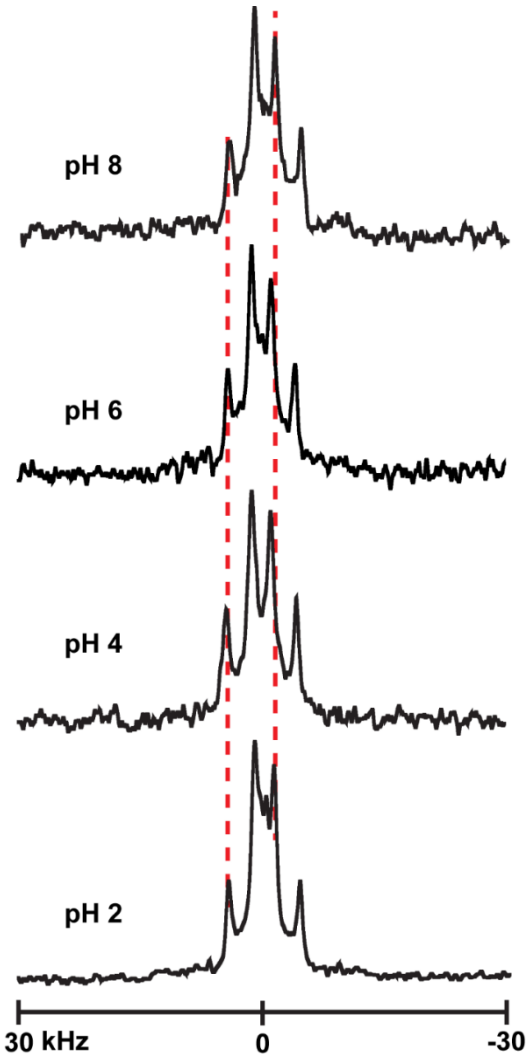

Figure 6: Selected ^{2}H NMR spectra to show the titration of H^{19}GWALP23 in DOPC lipid bilayer. Sample orientation is $\beta = 90^{o}$ for each spectrum shown and temperature is $50^{o}C$

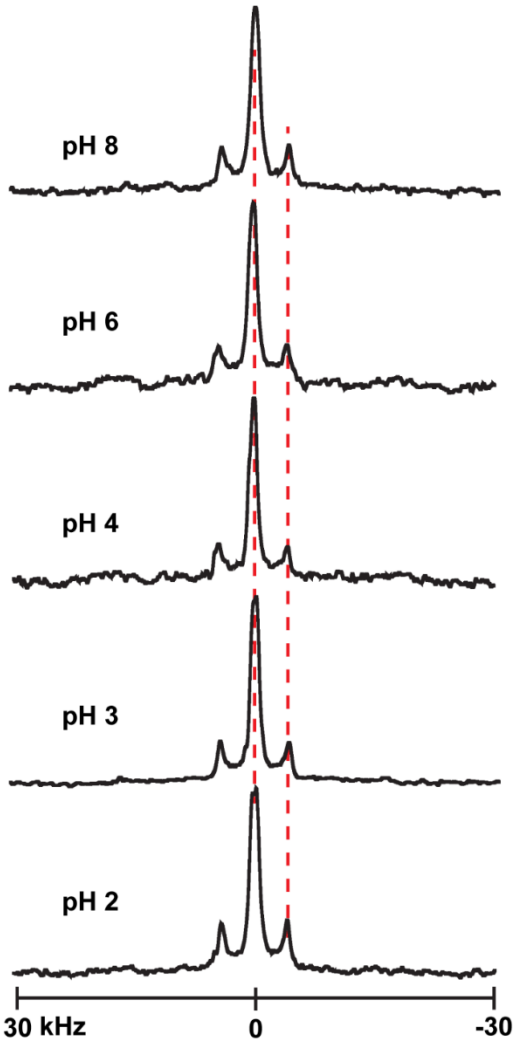

Figure 7: Selected ^{2}H NMR spectra to show the titration of $GH^{5,19}ALP23$ in DOPC lipid bilayer. Sample orientation is $\beta = 90^{o}$ and temperature is $50^{o}C$.

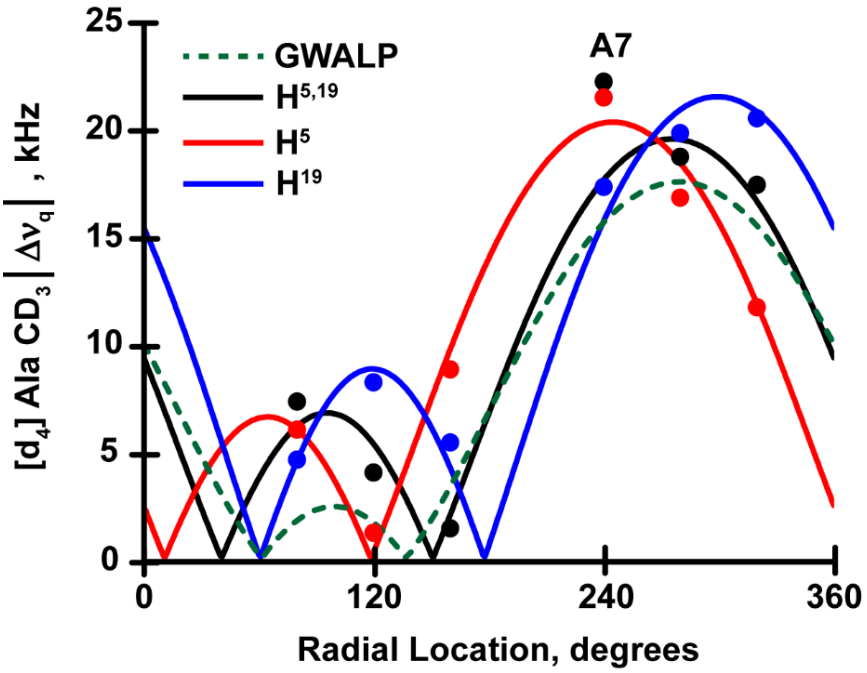

Figure 8: Quadrupolar wave analysis for oriented H^{5}GWALP (red), H^{19}GWALP (blue) and $GH^{5,19}$ALP23 (black) peptides in DOPC lipid bilayer. The analysis for host peptide $GW^{5,19}$ALP23 in the same lipid membrane id shown as dotted green plot.

3.11 **Supporting Figures**

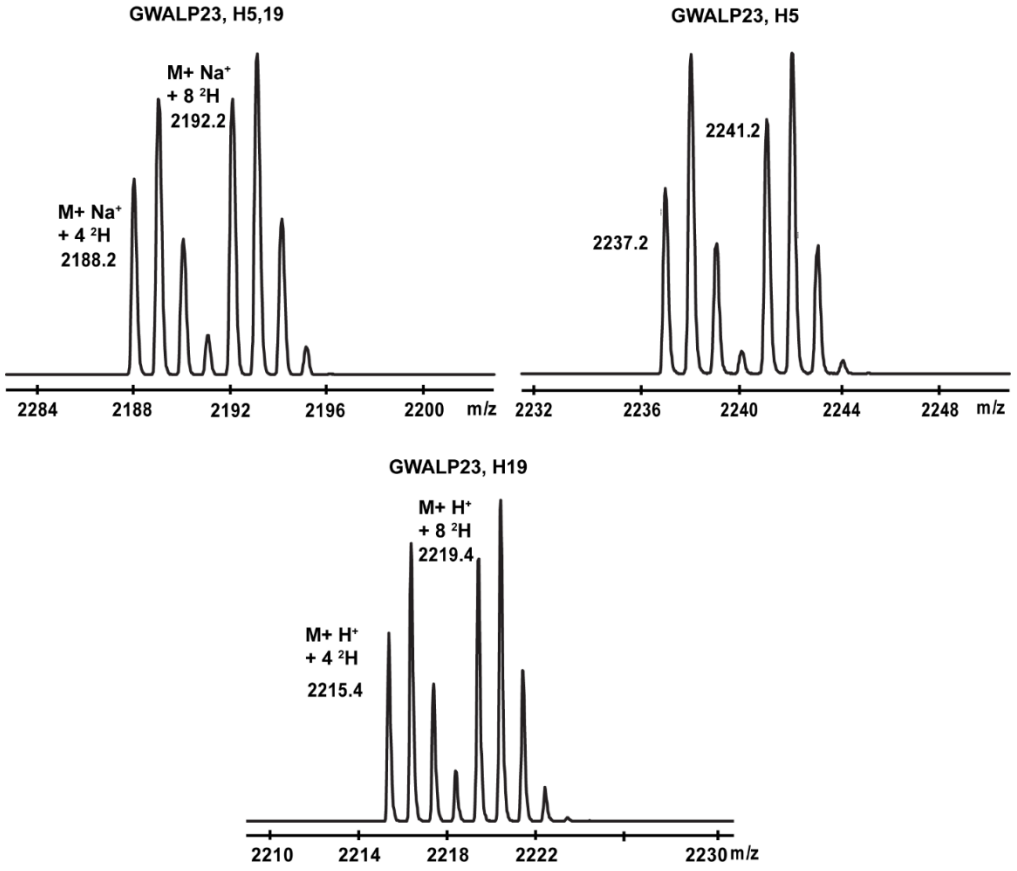

Figure S1: MALDI mass spectrum of synthesized $GH^{5,19}ALP$; $H^{5}GWALP$ and $H^{19}GWALP$

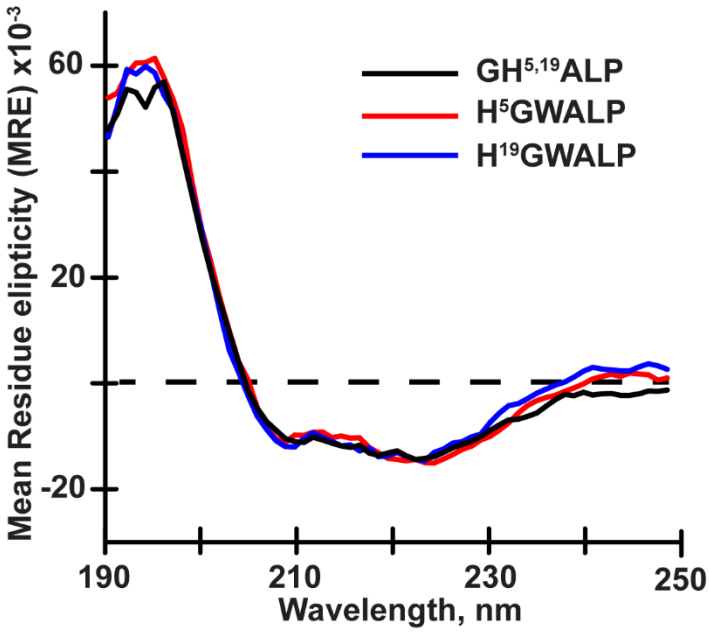

Figure S2: Circular Dichroism spectra of H^{5}GWALP23, H^{19}GWALP23 and $GH^{5,19}$ALP23 in DOPC lipid vesicles

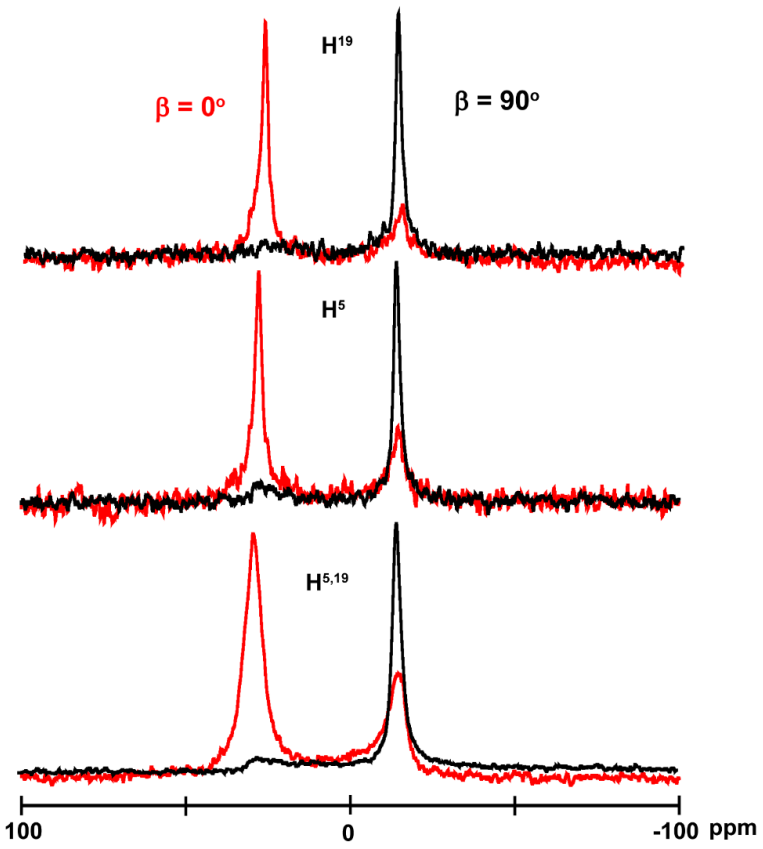

Figure S3: 31P NMR spectra of GWALP23 like peptides with tryptophan to histidine replacements in single or multiple positions. Spectra shown are in DOPC lipid bilayers.

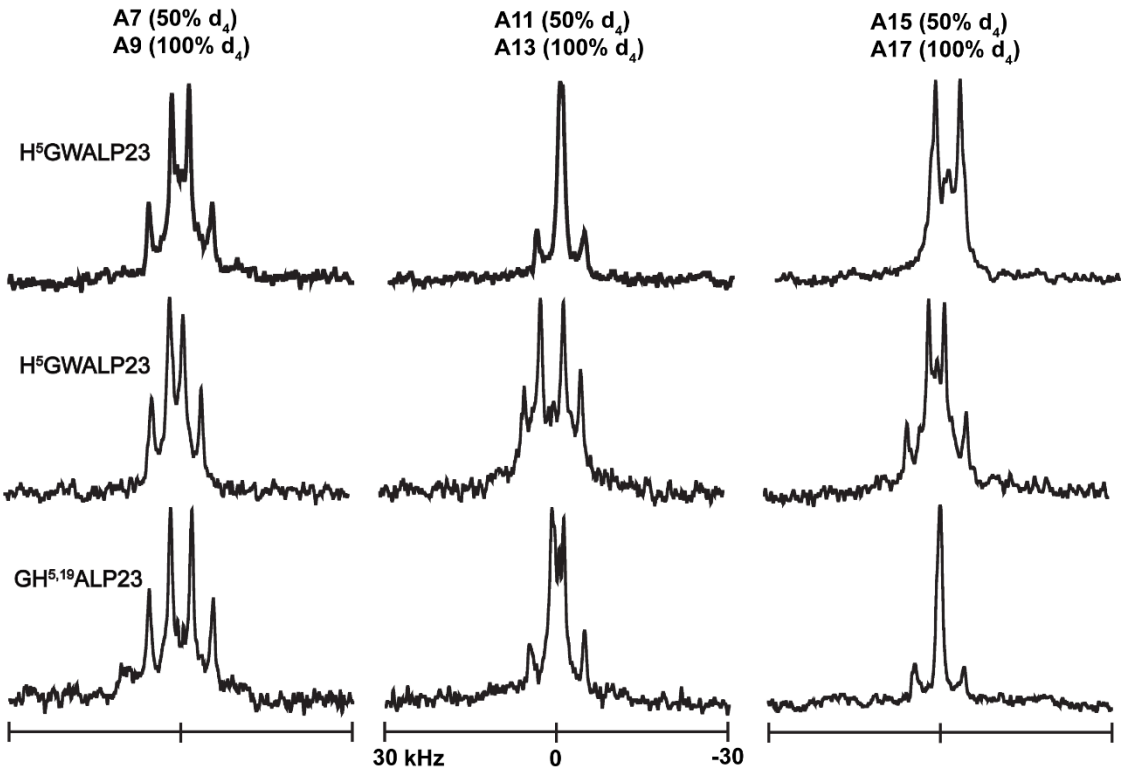

Figure S4: ^{2}H NMR spectra of labeled core alanines of H^{5}GWALP23, H^{19}GWALP23 and GH^{5,19}ALP23 in DOPC lipid bilayers. Spectra for sample orientation $\beta=90^{o}$ are shown

4. Chapter 4: Examination of pH Dependency and Orientation Differences of Membrane Spanning Alpha Helices Carrying a Single or Pair of Buried Histidine Residues

4.1 Abstract

Despite being scarce, polar amino acids within the helical core of a transmembrane sequence play essential roles in the function of many membrane proteins. To examine the interactions of such polar residues with lipid bilayer membranes, the peptide framework of GWALP23 (acetyl-GGALWLALALALALALALWLAGA-amide) is a useful tool. In this context, I have examined the orientation, dynamics and pH dependence of peptides having buried single or pairs of histidine residues. First, two residues from the hydrophobic core of the transmembrane GWALP23 helix, residues L8 and L16, were substituted by histidines, to yield the GWALP-$H^{8,16}$ peptide, acetyl-GGALWLAH^{8}ALALALAH^{16}ALWLAGA-amide. The ^{2}H-NMR spectra of ^{2}H-labeled core alanine residues for GWALP23-$H^{8,16}$ show, interestingly, no titration dependency from pH 2-8, yet a bilayer thickness-dependent orientation difference. The helix is found to adopt a transmembrane orientation in thin bilayers of DLPC, a combination of transmembrane and surface orientations in DMPC, and then a complete transition to a surface bound orientation in the thicker DPoPC and DOPC lipid bilayers. However, in the surface orientations, alanine A7 no longer fits within the core helix. To further analyze the effects of individual histidine residues, peptides with only H8 were examined. It is observed that although the helix with only H8 does not encounter any multiple orientations in DMPC similar to -$H^{8,16}$, the multi-state behavior now switched to bilayers of DOPC. Moreover, the single histidine residue H8 of GWALP23-H^{8} is also sensitive to pH and produces broad and overlapped signals when the pH is high. Two titration points for the deprotonation of H8 ranging from 3.3 to 3.9 are calculated in two different lipid bilayers of DLPC and DMPC. These results along with previous

studies with different locations of histidine residues suggest that hydrophobic thickness is a first determinant and pH a second determinant for the helical orientation when the His residues are incorporated into the hydrophobic region of a lipid bilayer.

4.2 **Introduction**

Many important functional roles such as pH sensing, ligand binding and metal transport in the transmembrane domains of membrane proteins are served by histidine [1-3]. The unique structural characteristics of histidine that combine properties of both polar and aromatic residues as well as its participation in a variety of intermolecular interactions make histidine a highly versatile amino acid [4-5]. Indeed, the histidine side chain engages in several aromatic interactions with neighboring residues which help to stabilize proteins [4, 6-8]. The crucial role of His residues for the activation [9] and selectivity [10]of the M2 proton channel of influenza A is well established. The pH dependency of the histidine imidazole side chain is equally important for functions of a variety of membrane proteins. For example, the protonation of some histidine residues in Diphtheria Toxin triggers the conformational changes of the T domain [11-12] that is necessary for catalysis. The electrostatic repulsion between protonated states of two histidine residues, H257 and H223, initiates the initial conformational change [13]. In case of prion proteins (PrP), whose misfolding is believed to be the cause of a group of rare and fatal neurodegenerative diseases [14], the protonation of some important histidine residues destabilizes the proteins [15]. Given the functional importance of these histidine residues, relatively little is known about the effect of this particular amino acid on protein or model peptide behavior when incorporated within the lipid bilayer.

To explore the influence of particular histidine residues on transmembrane peptide behavior, especially when located within the hydrophobic region of membranes, I utilized the well-studied model peptide framework of GWALP23 (acetyl-GGALW[LA]$_6$LWAGA-amide). Many sequence variants of this host peptide have been reported previously, and those results revealed some very important insights regarding the identities and locations of specific amino acids in the general protein-lipid interactions as determinants of the individual peptide orientations. For example, the presence of more than two interfacial Trp or Tyr residues tends to increase the extent of the motional averaging dramatically [16-17], while only two interfacial tryptophans reduces dynamic averaging [18]. Moreover, the presence of a charged residue, whether lysine[19] or arginine, [20-21] located within the central region of the helix, reveal dramatic effects when examined using this model system.

The advantages of GWALP23 framework are not limited to studies of the influence of specific amino acid residues upon the overall behavior of the peptide helix. GWALP23 (or its closely related analog having Tyr5 instead of Trp5) has also been employed to reveal the pKa values of several membrane-embedded charged residues including histidine [22], glutamic acid [23], lysine [19]and arginine [19, 21] in the lipid membrane environment. In many of the studies, these charged residues are located close to the center of the transmembrane helix sequence and found to titrate with pKa values lower than the aqueous pKa when the side chain is cationic. For example, a lipid-exposed lysine side chain located close to the center of a DOPC bilayer membrane exhibits a pKa of about 6.5 at 37^{o}C [19], while the pKa of histidine at the same location is about 4.3 [22]. In each case, the pKa value is lowered by 2-4 pH units. Nevertheless, the arginine side chain is observed not to titrate [19, 21], and the Arg guanidinium group would prefer to exit the lipid bilayer rather than to deprotonate [20]. In the case of histidine, which is of particular interest

of this work, the imidazole side chain has also shown pH sensitivity in the GWALP23 framework. When located at the center of the helix, the protonation of residue H12 drives the helix toward the membrane surface, whereas residue H14 responses only with some modifications in the helix tilt angle [22].Nonetheless , in each case the pKa values of the histidine side chains were successfully measured. [22]

To further analyze the significance of the histidine side chain and its ionization behavior with respect to protein-lipid interactions, I have incorporated a pair of histidine residues at positions 8 and 16 in the hydrophobic core of GWALP23, but not adjacent to each other and not at the center of the helix. Rather, the two His residues are partially buried and equidistance from the center of the peptide sequence. Residues H8 and H16 are also closer to each other than the previous double histidine mutants of GWALP23 reported in previous two chapters. It is of interest to note that positions 8 and 16 were previously studied with incorporated arginine residues [24]. Therefore, I aim to compare the changes in the helix orientation induced by the double arginine as opposed to double histidine replacements at positions 8 and 16 in GWALP23. Additionally, for better understanding of the behavior of GWALP23-$H^{8,16}$, a second peptide with only one histidine at position 8, naming GWALP23-H^{8} is also characterized and compared with previous results for GWALP23-H^{16} [25]. Analysis of these related peptides provides deeper understanding of the principal effects of a single or pair of buried histidine residues as well as their ionization properties for the interaction of an α-helix with lipid bilayer membranes.

4.3 **Materials and Methods**

The designed peptides were synthesized on a model 433A solid-phase peptide synthesizer (Applied Biosystems) from Life Technologies (Foster City, CA) using a modified FastMoc™

chemistry on a 0.1-mmol scale, with extended times for deprotection or coupling where needed. Prior to synthesis, commercial L-alanine-d4 (Cambridge Isotope Laboratories) was Fmoc-protected using Fmoc-ON-succinimide as described [26-27]. Other N-fmoc amino acids and rink amide resins were purchased from NovaBiochem (San Diego, Ca), Anaspec (Fremont, CA) and Bachem (Torrence, CA). Histidine and tryptophan side chains were additionally protected with trityl and t-butoxycarbonyl protecting groups. For each peptide synthesis, typically two deuterium-labeled alanines with 50% and 100% isotope abundance were used to enable subsequent distinguishing and assigning the ^{2}H NMR signals of labeled alanines based on relative intensities.

Synthesized peptides were cleaved from resin using a cleavage cocktail of 85:5:5:5 mixture of trifluoroacetic acid:phenol:triisopropylsilane:water at 22 °C for 2 h. After filtering off the resin support and precipitation of free peptides, purification of crude peptides was performed be means of reversed-phase HPLC. A Zorbax SB-C8 column (9.4 × 250 mm) packed with 3.5 μm octyl-silica from Agilent Technologies was used for purification. Following the purification step, the purified peptides were quantified using UV-Vis spectroscopy to measure the absorbance of Trp residues present in the peptide sequence at 280 nm [28]. MALDI-TOF analysis was used for to verify the peptide molecular mass.

Oriented samples for solid-state NMR experiments were prepared mechanically using glass slides with 1:60 peptide:lipid (mol:mol) ratio. The DLPC, DMPC, DpoPC and DOPC lipids from Avanti Polar Lipids (Alabaster, AL) were used as synthetic lipids to form the membrane. Peptide-lipid mixtures were hydrated following the procedure described previously [29] with buffers made from ^{2}H-depleted water (Cambridge Isotope Laboratories)

Solid-state NMR spectra for ^{31}P nuclei (for confirming the alignment of phosphate head groups in lipid bilayers) and ^{2}H nuclei (for analysis of peptide orientations and dynamics based on ^{2}H-labeled alanines in the peptide) were recorded using a Bruker Avance 300 spectrometer (Billerica, MA). The ^{31}P NMR spectra were recorded in a Doty 8 mm wide line probe (Doty Scientific Inc., Columbia, SC) with broadband ^{1}H decoupling on a Bruker Avance 300 spectrometer at both $\beta=0°$ (bilayer normal parallel to magnetic field) and $\beta=90°$ (bilayer normal perpendicular to magnetic field) macroscopic sample orientations. Before Fourier transformation, an exponential weighting function with 100 Hz line broadening was applied. The chemical shift was referenced externally to 85% phosphoric acid at 0 ppm.

The ^{2}H NMR spectra were recorded at 50 °C with macroscopic sample orientations of $\beta=90°$ and $\beta=0°$ A quadrupolar echo pulse sequence [30] was employed with full phase cycling, a pulse length of 3.2 μs, echo delay of 105 μs and a 120-ms recycle delay. Between 0.7 and one million free induction decays were accumulated during each ^{2}H experiment. Fourier transformation was accomplished after applying an exponential weighting function with 100 Hz line broadening.

Samples for circular dichroism spectroscopy were prepared by forming small lipid vesicles incorporating 0.0626 μmol peptide and 3.75 μmol lipid (1/60 peptide:lipid) using ultrasonication in unbuffered water. The peptide concentrations were determined by UV-Vis spectroscopy using a molar extinction coefficient of $\varepsilon_{280}=5600\ M^{-1}cm^{-1}Trp^{-1}$. An average of ten scans was recorded on a Jasco J-1500 spectropolarimeter, using a 1 mm cell path length, 1.0 nm bandwidth, 0.1 nm slit and a scan speed of 20 nm/min.

Helix orientation and dynamics were analyzed using two methods, a semi-static Geometric Analysis of Labeled Alanines ("GALA") [29] and a modified Gaussian approach [16, 31] for fitting the ^{2}H NMR signals from the CβD3 groups of Ala-d4 residues. The GALA method uses the quadrupolar splitting values from ^{2}H-NMR spectra and fits a principal order parameter Szz, an average tilt magnitude τ_0 and the direction of tilt also known as azimuthal rotation (ρ), while maintain an $\varepsilon_{//}$ angle between the alanine Cα−Cβ bond vector and the helix axis fixed at 59.4° [29]. The modified Gaussian approach involves three variable parameters, an average helix tilt τ_0, mean azimuthal rotation ρ_0 and rotational slippage $\sigma\rho$, with fixed values for Szz and $\sigma\tau$ (helix wobble) following [31]. In the case of two completely different orientations, $\sigma\tau$ is maintained constant with different values. For transmembrane orientations it is maintained at 10^0 while for surface orientation an $\sigma\tau$ of 25^o or 35^o is used in order to reduce the complexity with respect to $\sigma\rho$, as has been validated previously [24].

4.4 **Results**

The desired peptides listed in Table 1 and shown in Figure 1 were successfully synthesized and characterized with MALDI-TOF mass spectrometry for confirmation of the successful synthesis and extent of isotope labeling. Indeed, the mass spectra of GWALP23-H^{8,16} and GWALP23-H^8 shown in Figure S1confirm the expected isotopic mass distributions for labeled peptides with full or partial deuteration of two alanines. CD spectroscopy yields spectra characteristic of α-helices for both peptides in DLPC, DMPC and DOPC lipid vesicles, with a distinct minimum at 208 nm and a broad shoulder around 222 nm (Figure S2). The alignment of lipid molecules in the bilayers with the peptides has been assessed and confirmed by means of ^{31}P NMR spectroscopy (Figure S3, S4, S5).

GWALP23-H^{8,16}

^{2}H NMR in bilayers formed by shorter DLPC and longer DOPC lipids

Solid-state ^{2}H NMR spectra of the ^{2}H-labeled alanines in the peptide containing H8 and H16 and incorporated into mechanically oriented glass plate samples produce distinct signals for each side-chain methyl group of alanine residues 7, 9, 11, 13, 15 and 17 in DLPC and DOPC lipid bilayers (Figure 2A and 2D). The quadrupolar splittings ($|\Delta\nu_q|$) of this -H^{8,16}peptide are different, but well-defined, when comparing the magnitudes in DLPC with those observed in DOPC lipid bilayers. The displayed quadrupolar splitting range of GWALP23-H^{8,16} is 8-34 kHz in DLPC and 1-24 kHz in DOPC, indicating some possible changes in orientations of -H$^{8.16}$ peptide in lipid membranes of two different thicknesses (Table 2). Notably, the $|\Delta\nu_q|$ for alanine residues next to H8 and H16 i.e. A7, A9, A15 and A17 produce sharp and distinct resonances for the incorporated ^{2}H labels. Further analysis by the semi-static GALA method using measured $|\Delta\nu_q|$ values reveals that in DLPC and DOPC membranes, although the peptide is stable and has a single orientation in both lipids, these orientations are quite different from each other (Table 3, Figure 4A, black line and 4B, blue line). In DLPC, the helix of GWALP23-H^{8,16} resides in the membrane as a transmembrane helix with a tilt angle (τ_0) of ~25^{o}. Interestingly in the case of DOPC lipid membranes, where the peptide experiences negative hydrophobic mismatch, the quadrupolar wave plot shown as blue in Figure 4B indicates a surface bound orientation for the peptide helix. The variables calculated using GALA methods also provide proof for the surface orientation with a tilt (τ_0) of ~87.3^{o} (Table 3), meaning that the helix axis is essentially perpendicular to the bilayer. Furthermore, residue A7 fails to fit in the quadrupolar wave plot for the surface helix (Figure 4B) and deviates by about 5.4 kHz. This deviation suggests that residue

A7 misses the helical geometry and thereby is possibly unraveled from the surface-bound core helix.

To confirm these results, I employed a modified Gaussian analysis, described previously [16, 31]. This analysis further agrees with the results found for GWALP23-$H^{8,16}$ in DLPC and DOPC membranes, by showing similar values of τ_0 and ρ_0 as those derived from the GALA analysis (Table 3). Importantly, the surface orientation with respect to DOPC bilayers is confirmed by the modified Gaussian analysis. The rotational slippage $\sigma\rho$ remains always low, although it is even lower for the surface orientation (Table 3).

One very interesting aspect is, this lipid-dependent transition of GWALP23-$H^{8,16}$ helix orientation from transmembrane to surface bound was previously observed for related GWALP23 peptide with similar mutations, GWALP23-$R^{8,16}$ [24]. This peptide had arginine residues at positions 8 and 16, where I have incorporated the histidines for GWALP23-$H^{8,16}$. Notably, the -$R^{8,16}$ peptide helix displayed a transition from transmembrane to surface bound orientation when the helix was moved from 16-carbon acyl-chain DpoPC bilayers to 18-carbon acyl-chain DOPC bialyers. In that case the transition of orientation initiated in DOPC, indicated by multiple resonances in the NMR spectra, and was continued in the 20-carbon acyl-chain bilayers of DeiPC [24]. This means when a helix experiences two completely different orientations in bilayers of different thickness, it may be expected to display multiple orientations in bilayers that are of intermediate thickness compared to the other two. In the case of GWALP23-$H^{8,16}$, with alteration of orientations from DLPC to DOPC, it may be possible to observe multi-state behavior of this peptide in either DMPC or DpoPC, since each of these lipids has thickness

intermediate to DLPC and DOPC. Therefore, I investigated the orientations of GWALP23-H^{8,16} helix in DMPC and DpoPC bilayers as well (described in next section).

^{2}H NMR in intermediate-thickness DMPC and DpoPC lipid bilayers

In contrast to the well-defined ^{2}H quadrupolar splittings observed in the spectra from helices of GWALP23-H^{8,16} in the DLPC and DOPC bilayers, in DMPC, with nearly equal hydrophobic length of the bilayer and the core helix, it is observed that the ^{2}H NMR spectra from the labeled core alanines of GWALP23-H^{8,16} are poorly resolved and display multiple resonances for each alanine residue (Figure 2B). These multiple low-intensity broad peaks for GWALP23-H^{8,16} suggest two or more states for this peptide with respect to the lipid bilayer membrane, in slow exchange on the NMR time scale. By measuring the quadrupolar splitting for each signal, one deduces two distinct sets of these magnitudes for the set of alanine labels. One set of quadrupolar splittings matches closely with the signals observed in DLPC, while the other overlaps closely with the signals from DOPC (Table 2). Now due to a low signal to noise ratio, we could not resolve the quadrupolar splitting values for A15 and A17 in DMPC. Therefore, I have performed semi-static GALA analysis using only the signals from alanines 7, 9, 11 and 13.

Results obtained from the analysis using the GALA method reveal two orientations of the GWALP23-H^{8,16} helix in DMPC membranes, one being a transmembrane orientation with a tilt (τ_0) of ~22^o, slightly lower than the tilt in DLPC, while the other orientation is surface bound similar to that found on the surface of DOPC membranes (Figure 4A and 4B, Table 3). The azimuthal rotation (ρ_0) for the helix in the surface orientation remains remarkably identical to the orientation on DOPC membranes. For the transmembrane orientation, the helix azimuthal rotation (ρ_0) is slightly different than in DLPC, reflecting the difference in hydrophobic thickness

between DMPC and DLPC. Since the signal intensity for transmembrane orientation predominates (although nottremendously) over that for the surface orientation, we note that more than half of the peptide helix population adopts the transmembrane orientation in DMPC, while a significant minority population leaves the membrane and embraces a surface orientation.

For comparison with results in the 14-carbon and 18-carbon acyl-chain DMPC and DOPC bilayers, we have performed NMR experiments with oriented samples in oriented 16-carbon acyl-chain DpoPC bilayers. From the ^{2}H NMR spectra of helices in this 16 carbon unsaturated DpoPC lipid environment, it is evident that GWALP23-H^{8,16} exhibits a major set of distinct pairs of signals for the CD_3 methyl side chains of all six core alanines (Figure 2C), with quadrupolar splittings almost identical to those observed for DOPC experiments (Table 2). Nevertheless, the spectral quality is not as well resolved as for the DOPC spectra, although the resonances are prominent and overlap closely with the DOPC signals (Figure 2C). Interestingly, there are some additional signals with very low intensity, whose quadrupolar splitting values are similar those from the transmembrane helix in DMPC and DLPC. The minor peaks indicate the existence of a minor membrane-embedded population in DpoPC. Further orientational analysis confirms that the major orientation of GWALP23-H^{8,16} on DpoPC bilayers is surface bound, as shown by the quadrupolar wave plot in Figure 4B, with identical τ_0 and ρ_0 values as the surface population on DOPC membranes. Modified Gaussian analysis shows agreement with the semi-static analysis results (Table 3).

Titration of H8 and H16

Solid-state NMR can be used to determine the pH dependence of the properties of the GWALP23-H^{8,16} helix by monitoring the changes in the quadrupolar splitting of any of the core

alanine residues. The results will reflect the titration of either or both of the ionizable residues H8 and H16 in the helix. To address pH dependence, oriented samples of GWALP23-$H^{8,16}$ with ^{2}H-labeles at A11 and A13 were prepared in bilayers of DOPC under both acidic and basic conditions. Figure 3 shows the spectra in DOPC lipid membranes hydrated with buffers having pH from 2 to 8. Quadrupolar splittings and overall spectral quality remain universally unchanged over this pH range (Figure 3), indicating no change in the orientation of the GWALP23-$H^{8,16}$ peptide helix, whether or not the ionization of histidine side chains changes over this range of pH. I have also attempted these experiments in DLPC and DMPC lipid membranes where, once again, no noticeable changes are observed observed in either membrane. In DMPC the peptide continues to display multiple signals irrespective of pH, with almost no changes in the positions of peaks or signal intensity. These results involving no pH dependency in the peptide orientations are consistent with two other double histidine peptides GWALP23-$H^{12,16}$ and GWALP23-$H^{12,14}$ [25] studied previously, where the histidines are partially buried in the hydrophobic membrane, in similar fashion to GWALP23-$H^{8,16}$.

GWALP23-H^{8}

To examine whether one particular histidine residue is causing the bilayer thickness dependent orientation variation in GWALP23-$H^{8,16}$, I have removed H16 from the sequence of GWALP23-$H^{8,16}$ and incorporated a leucine at position 16. This produces a single histidine mutant of the parent GWALP23 peptide, namely GWALP23-H^{8}. Now, the other mutation with histidine residue at position 16 (GWALP23-H^{16}) was previously studied [25] and in this study the results from GWALP23-H^{8} will be compared with -H^{16} as well as -$H^{8,16}$ to analyze whether H8 or H16 or both are affecting the transmembrane to surface orientation transition of the GWALP23-$H^{8,16}$ helix in lipid membranes.

^{2}H NMR in shorter DLPC and DMPC

The ^{2}H NMR spectra for the aligned samples of GWALP23-H^{8} reveal well-defined signals and distinct quadrupolar splittings of core alanine residues in lipid bilayers of two different thicknesses (C12:0-C14:0). DLPC and DMPC (Figure 6). Now these results are quite dramatic because in DMPC the -H^{8,16} helix displays multiple resonances for the alanine residues, while when only H8 is present the multiple signals are completely absent. Rather the peptide exhibits signals for a single predominant tilted transmembrane orientation in each lipid (Figure 6). More interestingly, these signals change with pH from the acidic to basic range, which will be discussed later. The quadrupolar splitting magnitudes $|\Delta\nu_q|$ of GWALP23-H^{8} range from 2 kHz to 24 kHz in DLPC and 1.5 kHz to 23 kHz in DMPC (pH 2 in each case), which are significantly smaller ranges than those for the GWALP23-H^{8,16}, even in the case of the major signals in DMPC membranes (Table 2). These observations of the GWALP23-H^{8} $|\Delta\nu_q|$ ranges suggest a lower tilt compared to GWALP23-H^{8,16} in the same bilayer membranes. Therefore, residue H8 seems to have a large effect on peptide helix properties.

The combined analysis using semi-static and gaussian approaches reveals in DLPC and DMPC lipid bilayers, the addition of H8 decreases the helix tilt remarkably especially in DLPC (Figure 10). The GWALP23-H^{8} helix adopts tilt angles ranging from 10-12^{0} in DLPC and DMPC (Table 3) which in each case is only about half of the tilt magnitude observed for the helix having both H8 and H16. Moreover, the helix of GWALP23-H^{8} loses the sensitivity of tilt angle relative to bilayer thickness, indicated by the approximately same tilt angles in two different lipids (Table 3). The azimuthal rotation (ρ) ranges from 150-160^{0} in the two bilayers and differs by about 30^{0} when compared to the double histidine counterpart. Conversely when compared with the parent GWALP23 peptide, there is considerable change in the azimuthal rotation (Table

3). The observed azimuthal rotation for GWALP23 in DLPC to DMPC bilayers varies from 305^0 to 311^0, whereas in the case GWALP-H^8 the rotations are 160^0 and 156^0 respectively. The modified Gaussian analysis shows further agreement, with similar values of τ_0 and ρ_0, while maintain a moderate rotational slippage $\sigma\rho$ of about 40^0.

^{2}H NMR in longer and unsaturated DOPC lipid membranes

In the case of GWALP23-H^8, as the acyl chain length and bilayer lipid thickness increase from DLPC to DOPC, there is a drastic decrease in spectral quality. The spectra are characterized by poor signal-to-noise ratio where individual quadrupolar splittings are no longer distinguishable (Figure 7); rather the multiple overlapped signals give rise to broad peaks for each labeled alanine. This means that the GWALP23-H^8 peptide does experience multi-state behavior that may be similar to that of GWALP23-$H^{8,16}$, but interestingly in a thicker membrane. Due to a high noise level in the spectra of the DOPC samples that complicates the individual assignment of quadrupolar splittings, the $|\Delta\nu_q|$ magnitudes listed in Table 2 for the DOPC experiments are approximate. For the same reason, the GALA quadrupolar wave plot for GWALP23-H^8 in DOPC cannot be analyzed at this time.

Titration of H8

Because the sequence of GWALP-H^8 contains no ionizable residue other than H8, it provides an opportunity to observe any change, involving either spectral quality or quadrupolar splittings, that is directly linked to the ionization state of the H8 side chain. Changes in the ^{2}H NMR spectra therefore might enable calculation of the titration point of H8 in the membrane environment. The ^{2}H NMR spectra of GWALP23-H^8 under pH conditions from acidic to basic are shown in Figure 8 and supplementary Figure S6. In DLPC, although the spectral quality

remains unchanged from pH 2 to pH 8, the methyl ^{2}H quadrupolar splittings of A11 and A13 decrease from 6 kHz to 3.5 kHz and from 12 kHz to 10 kHz, respectively (Table 4). Using the $|\Delta\nu_q|$ values over a pH range from 2 to 8, titration curves are obtained for A11 and A13 in DLPC (Figure 9A), both showing midpoints at pH ~ 3.9, which indicates the pKa of H8 imidazole ring side chain in DLPC.

In DMPC, there are some additional spectral changes, including changes in the quadrupolar splittings. When the peptide is in acidic pH environment, i.e. from pH 2 to pH 4, the signals from the ^{2}H-alanine labels of GWALP-H^8 are well resolved with noticeable movement of the peaks for labeled A11 and A13, resulting from changes in quadrupolar splitting values. As the sample pH is raised incrementally from 4 to 8, there is then a progressive decrease in spectral quality leading to overlapping of the primary peaks (Figure 8). To confirm these dramatic changes between pH 2 and pH 8, samples with other ^{2}H-labeled core alanines were also hydrated with pH 8 buffer, and similar poorly resolved spectra were observed at pH 8 in each case (Figure 6B, rightmost panel). These results confirm the deprotonation of H8 side chain in DMPC when the pH is in the basic range. Plotting the $|\Delta\nu_q|$ values of A11 and A13 versus pH in DMPC, a pKa of 3.3 is predicted for the H8 imidazole ring in DMPC bilayers (Figure 9B), which is similar although slightly lower than that observed in DLPC.

I attempted also similar pH experiments in DOPC lipid membranes, with an aim to improve the spectral quality, but no change is observed. The GWALP23-H^8 peptide continues to display weak resonances and possibly remains multi-state or perhaps somewhat aggregated irrespective of the pH (Figure S6).

As the quadrupolar splittings for GWALP23-H^8 change with pH in DLPC and DMPC membranes, it is also reasonable that the orientation of the helix may change with pH. The GALA analysis results of GWALP23-H^8 at pH 2 and pH 8 are listed in Table 3 and the quadrupolar wave plots are shown in Figure 10. The GWALP23-H^8 helix in DLPC is found to decrease its tilt by 3^o with no significant change in the azimuthal rotation when the pH is raised from 2 to 8 (see Table 3 and Figure 10). In DMPC, because of the overlapping of signals, the number of quadrupolar splittings that could be measured was insufficient for determination of the change in helix orientation with pH.

4.5 **Discussion**

In this study, I have addressed the question of how the relative positions and number of histidine residues present within the central hydrophobic region of a lipid-bilayer membrane affects the orientation and dynamics of a transmembrane helix. I have used a α-helical model transmembrane helix GWALP23 as the initial host into which the "guest" histidine residue/s were then introduced singly or as a pair, to determine the properties and influence of this aromatic and potentially positively charged residue in a hydrophobic lipid bilayer. The effects of the His residue/s will be considered and compared with the baseline properties of the host peptide helix, as well as with the influence of some other similar mutations performed previously.

GWALP23-$H^{8,16}$

In the modifications of GWALP23 with histidines studied here, the His residues are located at positions 8 and 16, with their α-carbons are about 12 Å apart from each other. A previous study with mutations involving arginine residues at the same positions showed some

very interesting results [24]. Because of the potential "snorkeling" of arginine guanidinium side chains, the distance between R8 and R16 can increase and provide access of the side chains to the membrane-water interface. As a result, the peptide helix with R8 and R16 adopts transmembrane orientations in thinner membranes such as DLPC and DMPC, while having a transition state in the thicker DOPC bilayer, where the major orientation is surface bound and the minor orientation is transmembrane. However, the minor transmembrane orientation is completely absent when the peptide is transferred to DeiPC, a bilayer with 20-carbon acyl chains that is even thicker than DOPC [24]. These results support the snorkeling behavior of arginine side chains, which were introduced by others in earlier studies [32-33].Similar snorkeling of lysine residue was also studied [34]. Here, I have investigated whether histidine, another potentially positively charged residue but with less steric flexibility than Lys or Arg, has similar ability to confer a bilayer thickness dependence to a transmembrane helix. Although the snorkeling effect may allow positively charged residues to place near the negatively-charged phospholipid head groups [32 34 35], the situation could be more complicated because the histidine side chain has a ring and not a flexible chain. Histidine furthermore can titrate with a pKa that typically is close to physiological pH. For these reasons, my analysis involved experiments with different pH environments ranging from acidic to basic, pH 2 to 8, to investigate how histidine behaves when its side chain titrates from positive to neutral.

The results from the ^{2}H NMR spectroscopy of GWALP23-H^{8,16} reveal similar orientation transitions in bilayer membranes that depend solely on the thicknesses of bilayers. GWALP23-H^{8,16} exhibits a tilted transmembrane orientation in DLPC lipid membrane with a tilt angle of 25^{0}, which is slightly higher compared to GWALP23. With arginines present at the same positions, the tilt of the GWALP23-R^{8,16} helix peptide (τ) is even higher (29^{0}) [24]. Thus, the

observed magnitude of τ is possibly tuned by the length of the positively-charged side chains of residues 8 and 16. Since the arginine side chain is longer than the histidine side chain, the R8 and R16 side chains stretch more to position the guanidine groups closer to the interface than is possible for the imidazole rings of H8 and H16, which may cause the 4^0 change in the overall tilt angle. Moreover, the aromaticity of histidine may also have some role to play here, rendering the side chain somewhat compatible with the hydrophobic region of the bilayer. In DMPC, this hydrophobic region increases by 4 Å and hence H8 and H16 may fail to snorkel to the membrane-water interface. While some of the subtle details are unknown, the combined effects eventually lead to multiple orientations for the GWALP23-$H^{8,16}$ helix with respect to DMPC lipid bilayers. Although the major population remains oriented as a transmembrane helix, a significant fraction of the GWALP23-$H^{8,16}$ helix population goes to the surface of DMPC bilayers (Figure 5). Interestingly in the case of the arginine cousin, a similar transition happens in DOPC membranes as opposed to DMPC membranes [24]. Due to the length of arginine side chain the GWALP23-$R^{8,16}$ peptide apparently is able to preserve its membrane spanning orientation in DMPC, while histidines with shorter side chains fail to do so in the same membrane. Notably, when the helix of GWALP23-$H^{8,16}$ is moved to the comparatively thicker DpoPC or DOPC bilayers, the surface orientation dominates as the major population of the peptide (Figures 4 and 5). (Note: the thicknesses of DLPC, DMPC and DOPC at 25^0 C are 20.8, 24.8 and 26.2 Å [36-37].)

Two other GWALP23 family peptide with pairs of histidine residues (with $H^{12,14}$ and $H^{12,16}$) displayed such surface-bound orientations in DOPC. In each case, due to a failure to accommodate both histidine residues within the bilayer, the helices leave the membranes and prefer to sit close to the interface [25] These peptides too exhibited transmembrane orientations in the thinner DLPC bilayer. All of these results involving histidine residues tested in present work

as well as previous works suggest that, histidine may to a small extent extend or "snorkel" its side chain, although to a lesser extent than lysine or arginine.

To test the effect of histidine ionization states in the two different orientations experienced by GWALP23-H^{8,16}, I have done experiments with labeled A7 and A9 of this peptide at acidic and basic pH. Having an aqueous pKa value near physiological pH (6.5), histidine imidazole side chains tend to protonate at low pH and thus carry a positive charge, which is necessary for the "snorkeling" of Lys and Arg side chains to reach toward the interface. At high pH, with the deprotonation of imidazole rings, the His side chain loses the positive charge and that may result in some conformational changes. Since in the hydrophobic region of a lipid bilayer, the pKa of a histidine chain is expected to be lower, in my experiments I have maintained the pH range from 2 to 8, with an aim to observe any spectral change within this range in DLPC, DMPC and DOPC lipid bilayers. Interestingly, no changes in spectral quality or quadrupolar splittings are observed in any of the lipid membranes when the peptide helix is placed in lipid environments with different pH (Figure 3). Although the spectra for the helix in DLPC at pH 2 are broader compared to the other pH values, that result does not seem to change the overall peptide conformation or helix orientation. The helix persists as transmembrane in DLPC, multi-state in DMPC and surface-bound in DOPC. Now these results are not very surprising because it has been found previously that pairs of buried histidine residues lose the pH response, whereas a single isolated histidine is very sensitive to pH when present alone [25]. Therefore, in the case of GWALP23-H^{8,16}, it is likely that the peptide prefers to maintain the same orientation irrespective of pH, even though the side chains may or may not be titrating. An alternative yet unlikely explanation could be that the imidazole rings preserve their positive

charge up to pH 8, to help the peptide helix adopt a modest orientation. Nevertheless, a plausible reason for such behavior would remain obscure.

GWALP23,H^8

The results for GWALP23-H^8 help us to understand the behavior observed for GWALP-$H^{8,16}$. Similar to the double histidine counterpart, this peptide too exhibits multiple broad resonances of ^{2}H-labels present in the core alanines, but not in the same lipid membranes. My findings in DLPC and DMPC bilayers include well resolved ^{2}H-NMR resonances for the helix with the buried H8 residue, which interestingly change with pH (discussed later). The GALA analysis of GWALP23-H^8 indicates a transmembrane orientation but distinct from that of GWALP23-$H^{8,16}$ in DLPC as well as DMPC bilayers. This new orientation corresponds to a tilt value about 50% lower than that of the double histidine -$H^{8,16}$ peptide and also lower than the parent peptide GWALP23 helix (Table 3). As discussed earlier, in DLPC the tilt (τ) of GWALP23-$H^{8,16}$ is ~25^0, large enough for the H8 and H16 side chains to reach the surface. When H16 is removed from the helix, however, this tilt angle decreases to ~12^0 in DLPC. In addition, the helix with only H8 also loses the sensitivity of tilt angle to bilayer thickness and adopts about same amount of tilt in DMPC (Table 3). However, in the case of DMPC, the orientation of GWALP23-H^8 is comparable to that of GWALP23, as their tilt angles are similar. Comparing the azimuthal rotation ρ, the GWALP23-H^8 helix changes its rotation by about 40^0 when compared to GWALP23-$H^{8,16}$, but this change is quite large compared to the helix with leucine at position 8. This may mean that the introduction of H8 alters the helix rotation angle largely to reposition the Trp side chains. This alteration in rotation also allows the side-chain snorkeling of H8. Thereby the combination of helix rotation and tilt could permit the H8

imidazole group to interact with the interfacial region and allow the helix to retain a transmembrane orientation despite having a positively charged side chain in the bilayer-spanning hydrophobic region. However, this well-defined transmembrane orientation is disrupted when the H8 imidazole ring loses its charge (discussed later).

In DOPC, the behavior of GWALP23-H^{8} is strikingly different. In this thicker bilayer, the spectra observed for each core alanines of GWALP23-H^{8} peptide are poorly resolved, broad and overlapped with each other, indeed similar to the spectra of GWALP23-$H^{8,16}$ in DMPC. Due to the low signal to noise ratio, the individual quadrupolar splittings are obscured and I have reported the approximate values of quadrupolar splittings n Table 2. For the same reason, it was not possible to assign these values with respect to particular alanines and therefore GALA analysis of the helix orientation was not feasible for GWALP23-H^{8} in DOPC. It is likely that two populations of this helix are present in DOPC, as was seen for GWALP23-$H^{8,16}$ in DMPC. To assess whether GWALP23-H^{8} adopts a single orientation in a membrane thicker than DOPC, I performed some experiments the longer DeiPC lipid (C20:1, data not shown). But interestingly the peptide continued to display multiple resonances, meaning the orientation transition is not yet complete and the peptide seems to struggle to move to a single orientation. With the presence of two histidine side chains, this transition is comparatively easier for the GWALP23-$H^{8,16}$ helix; seemingly, its larger tilt angle helps to provide greater access to the interfacial region and later supports an exit from the bilayer. But with H16 removed, the adjusted tilt angle in thinner lipids significantly decreases to orient H8 and apparently fails to adjust when the bilayer thickness increases.

The extreme effects of residue H8 on the overall behavior of the peptide helix raises questions about the impact of H16. What happens if only H16 is present? Surprisingly, H16 itself

has no effect on transitioning the helix from one orientation to another [25], whether in DOPC or thinner lipid bilayers. The GWALP23-H[16] peptide is transmembrane in bilayers from DLPC to DOPC, with relatively low tilt angles and no evidence for multi-states orientation in these bilayers of varying thickness. These results suggest the multi-state behavior shown by GWALP23-H[8,16] is mostly influenced by H8, although in a different lipid membrane than the transition membrane when H8 is alone in GWALP23-H[8].

Ionization of H8

In addition to lipid bilayer thickness, GWALP23-H[8] is also sensitive to pH and responds when the pH of the bilayer environment varies. As previously observed for the some other GWALP23 mutations with a single histidine such as H[12], H[14 22] orH[16 25], changes in the peptide helix behavior as a function of pH are observed also for the GWALP23-H[8] peptide, especially in DLPC and DMPC lipid bilayers. In the case of DOPC, the changes with pH are complicated due to the multiple signals (Figure S6). The response to pH is nevertheless straightforward and more prominent in DLPC and DMPC bilayers At low pH, this peptide shows well resolved NMR spectra in both DLPC and DMPC lipid bilayers. These spectra reveal minor yet measurable changes in the core ^{2}H-alanine quadrupolar splittings in DLPC when H8 is introduced (Figure S6). A significant reduction in the ^{2}H NMR spectra quality is nevertheless observed at pH higher than 4 in DMPC bilayers. In each of these lipid membranes, titration points are observed, near pH 4 in the thinner DLPC and near pH 3 in the somewhat thicker lipid DMPC. These low pKa values of a buried histidine residue show general agreement with those observed previously for GWALP23-H[12], GWALP23-H[14] and GWALP23-H[16], in the vicinity of pH 2.5, 4 and 3.5, respectively [22, 25]. The results therefore suggest that the pKa of the His side chain may vary somewhat (as expected) depending on the depth of burial of the imidazole ring, which also is

observed for soluble proteins. [38] Among all these mutants studied so far, the depth of burial of H12 is highest and that probably is the reason that H12 exhibits the lowest pKa compared to the others.

The shift of pKa for the histidine imidazole ring in membrane environments is indeed biologically relevant. For example, a pKa value of < 2.3 was found for a buried histidine residue H149 in xylanase [38]. On the other hand, for H72 in bovine tyrosine phosphatase the pKa is close to 9 [39]. Even in the M2 ion channel of influenza A protein, the functionally important histidine residue H37 generates two different pKa values as the folded protein changes its conformation [40]. Another good example of such behavior is observed for membrane insertion peptides such as pHLIP, which transitions from a membrane-inserted state to a surface orientation depending on ionization of an Asp residue. Introduction of a histidine residue at the opposite face of the helix shifts the pKa to a lower value (~ 4.7) which in turn influences the pKa of the Asp residue and therefore stabilizes a membrane-inserted state within the 3.1−6.8 pH range [41]. Our results which reveal varying pKa values for histidine that also affect the multi-state properties, response to lipid thickness, and stability of a transmembrane state, are consistent with these studies of larger membrane protein systems.

In summary, I have aimed to elucidate further the histidine side chain ionization properties and influence on helix properties when buried within the hydrophobic core of lipid bilayer membranes. The influence of two buried histidine residues essentially equidistant from the two ends of an α-helix is also addressed. My findings suggest a minor extent of snorkeling behavior of histidine side chains that in line with previous observations for arginine and lysine.

In addition, the observed prominent effect of H8 over H16 for the properties of GWALP23-$H^{8,16}$ peptide is also revealed.

4.6 **Acknowledgments**

This work was supported in part by grants from the National Science Foundation and the Arkansas Biosciences Institute. The NMR facility was supported by NIH grant GM103429. Mass spectrometry of peptides were performed at the State Wide Mass Spectrometry Facility at the University of Arkansas

4.7 **References**

1. Stewart, A. K.; Kurschat, C. E.; Burns, D.; Banger, N.; Vaughan-Jones, R. D.; Alper, S. L., Transmembrane domain histidines contribute to regulation of AE2-mediated anion exchange by pH. *Am. J. Physiol., Cell Physiol.* **2007,** *292* (2), C909-C918.

2. Rehwald, M.; Neuschäfer-Rube, F.; de Vries, C.; Püschel, G. P., Possible role for ligand binding of histidine 81 in the second transmembrane domain of the rat prostaglandin F2α receptor. *FEBS Lett.* **1999,** *443* (3), 357-362.

3. Larson, C. A.; Adams, P. L.; Blair, B. G.; Safaei, R.; Howell, S. B., The role of the methionines and histidines in the transmembrane domain of mammalian copper transporter 1 in the cellular accumulation of cisplatin. *Mol Pharmacol* **2010,** *78* (3), 333-339.

4. Loewenthal, R.; Sancho, J.; Fersht, A. R., Histidine-aromatic interactions in barnase: Elevation of histidine pKa and contribution to protein stability. *J. Mol. Biol.* **1992,** *224* (3), 759-770.

5. Cauët, E.; Rooman, M.; Wintjens, R.; Liévin, J.; Biot, C., Histidine−Aromatic Interactions in Proteins and Protein−Ligand Complexes: Quantum Chemical Study of X-ray and Model Structures. *J. Chem. Theory Comput.* **2005,** *1* (3), 472-483.

6. Jasanoff, A.; Weiss, M. A., Aromatic-histidine interactions in the zinc finger motif: Structural inequivalence of phenylalanine and tyrosine in the hydrophobic core. *Biochemistry* **1993,** *32* (6), 1423-1432.

7. Fernández-Recio, J.; Vázquez, A.; Civera, C.; Sevilla, P.; Sancho, J., The Tryptophan/Histidine interaction in α-helices *J. Mol. Biol.* **1997,** *267* (1), 184-197.

8. Bhattacharyya, R.; Saha, R. P.; Samanta, U.; Chakrabarti, P., Geometry of Interaction of the Histidine Ring with Other Planar and Basic Residues. *J. Proteome Res.* **2003,** *2* (3), 255-263.

9. Hu, F.; Schmidt-Rohr, K.; Hong, M., NMR Detection of pH-Dependent Histidine–Water Proton Exchange Reveals the Conduction Mechanism of a Transmembrane Proton Channel. *J. Am. Chem. Soc.* **2012,** *134* (8), 3703-3713.

10. Venkataraman, P.; Lamb, R. A.; Pinto, L. H., Chemical Rescue of Histidine Selectivity Filter Mutants of the M2 Ion Channel of Influenza A Virus. *J. Biol. Chem.* **2005,** *280* (22), 21463-21472.

11. Ladokhin, A. S., pH-triggered conformational switching along the membrane insertion pathway of the diphtheria toxin T-domain. *Toxins* **2013,** *5* (8), 1362-1380.

12. Perier, A.; Chassaing, A.; Raffestin, S.; Pichard, S.; Masella, M.; Ménez, A.; Forge, V.; Chenal, A.; Gillet, D., Concerted Protonation of Key Histidines Triggers Membrane

Interaction of the Diphtheria Toxin T Domain. *J. Biol. Chem.* **2007,** *282* (33), 24239-24245.

13. Kurnikov, I. V.; Kyrychenko, A.; Flores-Canales, J. C.; Rodnin, M. V.; Simakov, N.; Vargas-Uribe, M.; Posokhov, Y. O.; Kurnikova, M.; Ladokhin, A. S., pH-triggered conformational switching of the diphtheria toxin T-domain: the roles of N-terminal histidines. *J. Mol. Biol.* **2013,** *425* (15), 2752-2764.

14. Prusiner, S. B., Prions. *Proc. Natl. Acad. Sci. U.S.A.* **1998,** *95* (23), 13363.

15. Malevanets, A.; Chong, P. A.; Hansen, D. F.; Rizk, P.; Sun, Y.; Lin, H.; Muhandiram, R.; Chakrabartty, A.; Kay, L. E.; Forman-Kay, J. D.; Wodak, S. J., Interplay of buried histidine protonation and protein stability in prion misfolding. *Sci. Rep.* **2017,** *7* (1), 882.

16. Grage, S. L.; Strandberg, E.; Wadhwani, P.; Esteban-Martin, S.; Salgado, J.; Ulrich, A. S., Comparative analysis of the orientation of transmembrane peptides using solid-state ^{2}H and ^{15}N NMR: Mobility matters. *Eur. Biophys. J. Biophy.* **2012,** *41* (5), 475-482.

17. Gleason, N. J.; Vostrikov, V. V.; Greathouse, D. V.; Grant, C. V.; Opella, S. J.; Koeppe, R. E., II, Tyrosine replacing tryptophan as an anchor in GWALP peptides. *Biochemistry* **2012,** *51* (10), 2044-2053.

18. Vostrikov, V. V.; Grant, C. V.; Opella, S. J.; Koeppe, R. E., II, On the combined analysis of ^{2}H and ^{15}N/^{1}H solid-state NMR data for determination of transmembrane peptide orientation and dynamics. *Biophys. J.* **2011,** *101* (12), 2939-2947.

19. Gleason, N. J.; Vostrikov, V. V.; Greathouse, D. V.; Koeppe, R. E., Buried lysine, but not arginine, titrates and alters transmembrane helix tilt. *Proc. Natl. Acad. Sci. U.S.A.* **2013,** *110* (5), 1692.

20. Vostrikov, V. V.; Hall, B. A.; Greathouse, D. V.; Koeppe, R. E.; Sansom, M. S. P., Changes in Transmembrane Helix Alignment by Arginine Residues Revealed by Solid-State NMR Experiments and Coarse-Grained MD Simulations. *J. Am. Chem. Soc.* **2010,** *132* (16), 5803-5811.

21. Thibado, J. K.; Martfeld, A. N.; Greathouse, D. V.; Koeppe, R. E., Influence of High pH and Cholesterol on Single Arginine-Containing Transmembrane Peptide Helices. *Biochemistry* **2016,** *55* (45), 6337-6343.

22. Martfeld, A. N.; Greathouse, D. V.; Koeppe, R. E., Ionization Properties of Histidine Residues in the Lipid Bilayer Membrane Environment. *J. Biol. Chem.* **2016,** *291* (36), 19146-19156.

23. Rajagopalan, V.; Greathouse, D. V.; Koeppe, R. E., Influence of glutamic acid residues and pH on the properties of transmembrane helices. *Biochim. Biophys. Acta Biomembr* **2017,** *1859* (3), 484-492.

24. Lipinski, K.; McKay, M. J.; Afrose, F.; Martfeld, A. N.; Koeppe Ii, R. E.; Greathouse, D. V., Influence of Lipid Saturation, Hydrophobic Length and Cholesterol on Double-Arginine-Containing Helical Peptides in Bilayer Membranes. *ChemBioChem* **2019,** *0* (0).

25. Henderson, A. N., Influence of Histidine Residues, pH and Charge Interactions on Membrane-Spanning Peptides. **2017**.

26. Kortenaar, P. B. W.; Dijk, B. G.; Peeters, J. M.; Raagen, B. J.; Adams, P. J.; Tesser, G. I., Rapid and efficient method for the preparation of Fmoc-amino acids starting from 9-fluorenylmethanol. *Int. J. Pept. Prot. Res.* **1986,** *27*, 398-400.

27. Greathouse, D. V.; Koeppe, R. E., II; Providence, L. L.; Shobana, S.; Andersen, O. S., Design and characterization of gramicidin channels. *Methods Enzymol.* **1999,** *294*, 525-550.

28. Pace, C. N.; Vajdos, F.; Fee, L.; Grimsley, G.; Gray, T., How to measure and predict the molar absorption coefficient of a protein. *Protein Sci* **1995,** *4* (11), 2411-2423.

29. van der Wel, P. C. A.; Strandberg, E.; Killian, J. A.; Koeppe, R. E., II, Geometry and intrinsic tilt of a tryptophan-anchored transmembrane alpha-helix determined by ^{2}H NMR. *Biophys. J.* **2002,** *83*, 1479-1488.

30. Davis, J. H.; Jeffrey, K. R.; Valic, M. I.; Bloom, M.; Higgs, T. P., Quadrupolar echo deuteron magnetic resonance spectroscopy in ordered hydrocarbon chains. *Chem. Phys. Lett.* **1976,** *42*, 390-394.

31. Sparks, K. A.; Gleason, N. J.; Gist, R.; Langston, R.; Greathouse, D. V.; Koeppe, R. E., II, Comparisons of Interfacial Phe, Tyr, and Trp Residues as Determinants of Orientation and Dynamics for GWALP Transmembrane Peptides. *Biochemistry* **2014,** *53* (22), 3637-3645.

32. Strandberg, E.; Morein, S.; Rijkers, D. T. S.; Liskamp, R. M. J.; van der Wel, P. C. A.; Killian, J. A., Lipid dependence of membrane anchoring properties and snorkeling behavior of aromatic and charged residues in transmembrane peptides. *Biochemistry* **2002,** *41* (23), 7190-7198.

33. Öjemalm, K.; Higuchi, T.; Lara, P.; Lindahl, E.; Suga, H.; von Heijne, G., Energetics of side-chain snorkeling in transmembrane helices probed by nonproteinogenic amino acids. *Proc. Natl. Acad. Sci. U.S.A.* **2016,** *113* (38), 10559.

34. Strandberg, E.; Killian, J. A., Snorkeling of lysine side chains in transmembrane helices: how easy can it get? *FEBS Lett.* **2003,** *544* (1-3), 69-73.

35. Krishnakumar, S. S.; London, E., The control of transmembrane helix transverse position in membranes by hydrophilic residues. *J. Mol. Biol.* **2007,** *374* (5), 1251-1269.

36. Kučerka, N.; Nieh, M.-P.; Katsaras, J., Fluid phase lipid areas and bilayer thicknesses of commonly used phosphatidylcholines as a function of temperature. *Biochim. Biophys. Acta Biomembr* **2011,** *1808* (11), 2761-2771.

37. Pan, J.; Tristram-Nagle, S.; Kucerka, N.; Nagle, J. F., Temperature dependence of structure, bending rigidity, and bilayer interactions of dioleoylphosphatidylcholine bilayers. *Biophys J* **2008,** *94* (1), 117-124.

38. Plesniak, L. A.; Connelly, G. P.; Wakarchuk, W. W.; McIntosh, L. P., Characterization of a buried neutral histidine residue in Bacillus circulans xylanase: NMR assignments, pH titration, and hydrogen exchange. *Protein Sci* **1996,** *5* (11), 2319-2328.

39. Tishmack, P. A.; Bashford, D.; Harms, E.; Van Etten, R. L., Use of 1H NMR Spectroscopy and Computer Simulations To Analyze Histidine pKa Changes in a Protein Tyrosine Phosphatase: Experimental and Theoretical Determination of Electrostatic Properties in a Small Protein. *Biochemistry* **1997,** *36* (39), 11984-11994.

40. Colvin, M. T.; Andreas, L. B.; Chou, J. J.; Griffin, R. G., Proton association constants of His 37 in the Influenza-A M218-60 dimer-of-dimers. *Biochemistry* **2014,** *53* (38), 5987-5994.

41. Vila-Viçosa, D.; Silva, T. F. D.; Slaybaugh, G.; Reshetnyak, Y. K.; Andreev, O. A.; Machuqueiro, M., Membrane-Induced p K(a) Shifts in wt-pHLIP and Its L16H Variant. *J. Chem. Theory Comput.* **2018,** *14* (6), 3289-3297.

42. Vostrikov, V. V.; Daily, A. E.; Greathouse, D. V.; Koeppe, R. E., II, Charged or aromatic anchor residue dependence of transmembrane peptide tilt. *J. Biol. Chem.* **2010,** *285* (41), 31723-31730.

43. DeLano, W. L., The PyMOL Molecular Graphics System. *Delano Scientific, San Carlos, CA* **2002**.

4.8 **Tables**

Table 1: Sequence of buried single and paired histidine and arginine mutants of GWALP23 peptides

Name of peptide	**Sequence**	**Reference**
GWALP23	acetyl-GGAL**W**LALALALALALAL**W**LAGA-amide	[42]
GWALP23, $H^{8,16}$	acetyl-GGAL**W**LA**H**^{8}ALALALA**H**^{16}AL**W**LAGA-amide	This work
GWALP23, H^{8}	acetyl-GGAL**W**LA**H**^{8}ALALALALAL**W**LAGA-amide	This work
GWALP23, H^{16}	acetyl-GGAL**W**LALALALALA**H**^{16}AL**W**LAGA-amide	[25]
GWALP23, $R^{8,16}$	acetyl-GGAL**W**LAR^{8}ALALALAR^{16}AL**W**LAGA-amide	[24]

Table 2: ^{2}H-NMR quadrupolar splitting magnitudes of labeled core alanines of GWALP23 family peptides with single and double histidine substitution

Peptide	**Lipid**	**pH**	**[d4] Ala CD_3 quadrupolar splittings[a]**					
			A7	**A9**	**A11**	**A13**	**A15**	**A17**
GWALP23	DLPC		26.4	25.5	26.9	14.6	20.7	3.4
	DMPC		21.9	8.9	20.9	3.8	17.6	2.9
	DOPC		16.6	1.7	16.7	1.5	15.4	2.6
$H^{8,16}$	DLPC	4	33.7	33.7	30.2	29.8	8.4	18.5
	DMPC[b] (major)		28.4	29.2	24.6	25.8	--	--
	DMPC (minor)		24	24	16.2	1.8	--	--
	DpoPC		24.1	24.0	16.1	1.7	13.7	29.0
	DOPC		22.3	23.8	16.0	1.4	13.4	31.2
H^{8}	DLPC	2	2.2	22.2	11.7	24.0	10.7	21.1
		8	2.3	16.1	7.5	19.7	2.2	15.2
	DMPC	2	1.4	20.7	10.7	23.0	8.3	16.8
		8[c]	1.0, 12.5		3.0, 13.9		1.8, 8.7	
	DOPC	8[c]	2.2, 20.0, 6.8, 13.8		10.6, 23.4, 19.8, 7.0		6.4, 15.8, 1.8, 11.8	

[a] Values reported here are for $\beta = 0^{o}$ sample orientations.

[b] The signals from labeled alanines of GWALP23-$H^{8,16}$ in DMPC display multiple broad and overlapped signals. To address the $\Delta\nu_q$ values we have reported here the average values of overlapped signals. The assignments for A15 and A17 in DMPC were not possible to retrieve due to a poor signal to noise ratio.

[c] Since multiple weak and overlapped signals are observed for each double-labeled sample, it was not possible to report the exact $|\Delta\nu_q|$ values for GWALP23-H^{8} in DMPC or DOPC lipids at pH 8.

Table 3: Semi-static GALA and Modified Gaussian analysis results for GWALP23-$H^{8,16}$ and GWALP23-H^{8} helices in lipid bilayers.

Peptide	**Lipid**	**pH**	**Semi-static**				**Modified Gaussian**					**Ref**
			τ_0	**ρ_0**	**S_{zz}**	**RMSD**	**τ_0**	**ρ_0**	**σ_τ**	**σ_ρ**	**RMSD**	
GWALP23	DLPC	-	20.7°	305°	0.66	0.71	23°	304°	33	15 °	0.7	[42]
	DMPC		9.0°	311°	0.89	1.06	13°	308	42	10	1.19	
	DOPC		6.0°	323°	0.87	0.57	9°	321°	48	9 °	0.7	
$H^{8,16}$	DLPC	4	25.0°	122°	0.82	1.06	29	122	10	28	0.94	This work
	DMPC (major)		21.7°	116°	0.8	1.15						
	DMPC (minor)		87°	31°	0.57	0.76						
	DpoPC		87.3°	32°	0.54	0.76	84	28	35	16	1.45	
	DOPC		87.6°	32°	0.55	0.82	83	28	35	16	1.18	
H^{8}	DLPC	2	11.7°	160°	0.85	0.23	15°	160°	10°	38°	0.48	This work
		8	8.7 °	148 °	0.77	1.20	8	144	10	0	1.03	
	DMPC	2	10.7°	156 °	0.81	0.90	14	156	10	42	0.98	
		8[b]	-	-	-	-	-	-	-	-	-	
	DOPC	8[b]	-	-	-	-	-	-	-	-	-	

[a] The GWALP23 samples were unbuffered at neutral pH.

[b] Since the individual quadrupolar splitting values for GWALP23-H^{8} in DMPC at pH 8 and in DOPC were not possible to retrieve, GALA analysis was not performed for these two cases

Table 4: Trends for the quadrupolar splitting magnitudes ($|\Delta\nu_q|$) with pH for labeled alanine A11 and A13 CD_3 groups in GWALP23-H[8]

Lipid(s)	**pH / $\Delta\nu_q$ (in kHz)[a]**					
		2.0	3.0	4.0	6.0	8.0
DLPC	A11	6.0	-	4.5	3.4	3.7
	A13	11.9	-	10.9	10	9.6
DMPC	A11	5.1	3.9	1.7	1.5	1.5
	A13	11.4	9.8	7.0	6.2	6.5

[a] sample orientation for $\beta = 90^0$ is reported

4.9 **Figure legends.**

Figure 1: Models to illustrate positions of histidine residues introduced within the helix of GWALP23 and the orientations of two peptides in DLPC lipid bilayers, drawn using Pymol [43]

Figure 2: ^{2}H NMR spectra of labeled alanines in the GWALP23-H^{8,16} core helix in DLPC, DMPC, DpoPC and DOPC lipid bilayers hydrated with 20 mM buffer at pH 4. Sample orientation is $\beta = 90^{o}$, 1:60 peptide:lipid at 50^{o}C. The numbers indicate the identities of the ^{2}H-Ala residues.

Figure 3: Selected ^{2}H NMR spectra of GWALP23-H^{8,16} labeled alanines A11 and A13 in the core helix in DLPC (A), DMPC (B) and DOPC (C) lipid bilayers hydrated with 20mM buffer at the indicated pH. Sample orientation is $\beta = 90^{o}$, 1:60 peptide:lipid at 50^{o}C

Figure 4: Quadrupolar wave analysis depicting two different orientations of GWALP23-H^{8,16} peptide in DLPC, DMPC, DpoPC and DOPC lipid membranes obtained by GALA method [29]. Panel A shows the plots for transmembrane orientations with $\tau_0 = 25^0$ in DLPC (solid black) and with $\tau_0 = 22^0$ for major population in DMPC (solid green). In panel B each plot represents surface orientation with tilt angles of ~ 87^0 for minor population in DMPC (dashed green) and major populations in DpoPC (solid red) and DOPC (solid blue) lipids. Detailed results are listed in Table 3 and the orientation transitions are represented in Figure 5.

Figure 5: Models to illustrate the transition of GWALP23-H^{8,16} from its tilted transmembrane orientation (in DLPC) to a primary orientation at the surface of DOPC bilayer membranes. In the bilayer of intermediate thickness, DMPC, the major population of the helix adopts a transmembrane orientation with slightly smaller tilt than in DLPC, shown in the center panel. The minor population in DMPC has a surface bound orientation (not shown) similar to that in DOPC (right panel).

Figure 6: ^{2}H NMR spectra of labeled alanines in the GWALP23-H^{8} core helix in DLPC (A) and DMPC (B) lipids at pH 2 and 8. Sample orientation is $\beta = 90^{o}$, 1:60 peptide:lipid at 50^{o}C The changes in quadrupolar splittings in DLPC and spectral quality in DMPC indicate the response of the helix to the change in ionization state of histidine H8

Figure 7: ^{2}H NMR spectra of labeled alanines in the GWALP23-H^{8} core helix in DOPC lipid bilayers. Multiple peaks are observed for each labeled alanine. Sample orientation is $\beta = 90^{o}$, 1:60 peptide:lipid at 50^{o}C

Figure 8: Selected ^{2}H NMR spectra for deuterated alanines A11 and A13 of GWALP23-H^{8} in DMPC hydrated with 20 mM buffer at the indicated pH values. Sample orientation is $\beta = 90^{o}$, 1:60 peptide:lipid at 50^{o}C

Figure 9: Plots indicating the titration points of H8 present in GWALP23-H^{8} in DLPC (A) and. DMPC (B) bilayers. The pH dependence of the $\Delta\nu_q$ values for the CD_3 groups of Ala11 and Ala13 are shown as black and red respectively. The curves indicate slightly different pKa values of 3.9 in DLPC and 3.3 in DMPC lipid bilayers (blue dashed lines).

Figure 10: Quadrupolar wave plots for the helix of GWALP23-H^{8} in (A) DLPC at pH 2 and pH 8, and (B) DMPC at pH 2.

4.10 **Figures**

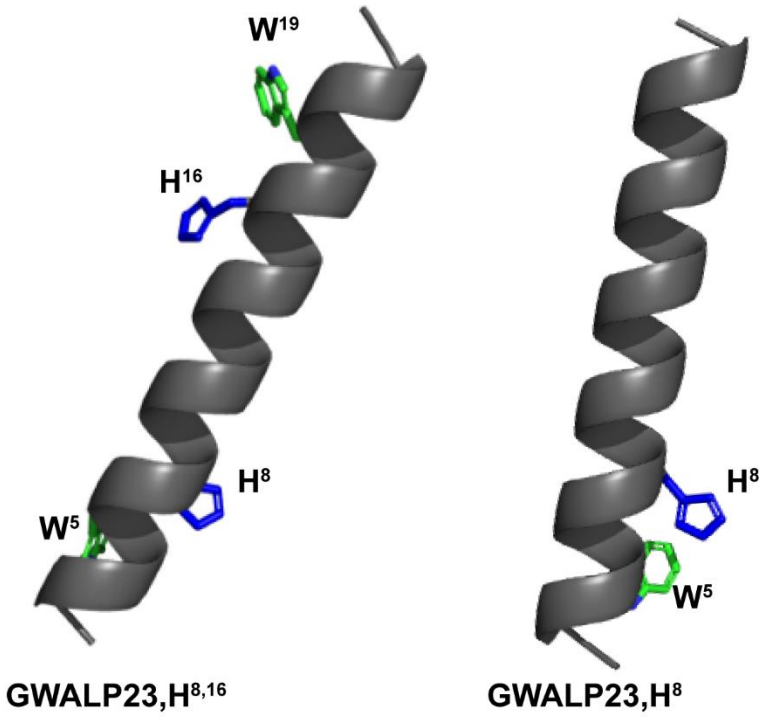

Figure 1: Models to illustrate positions of histidine residues introduced within the helix of GWALP23 and the orientations of two peptides in DLPC lipid bilayers, drawn using Pymol [43].

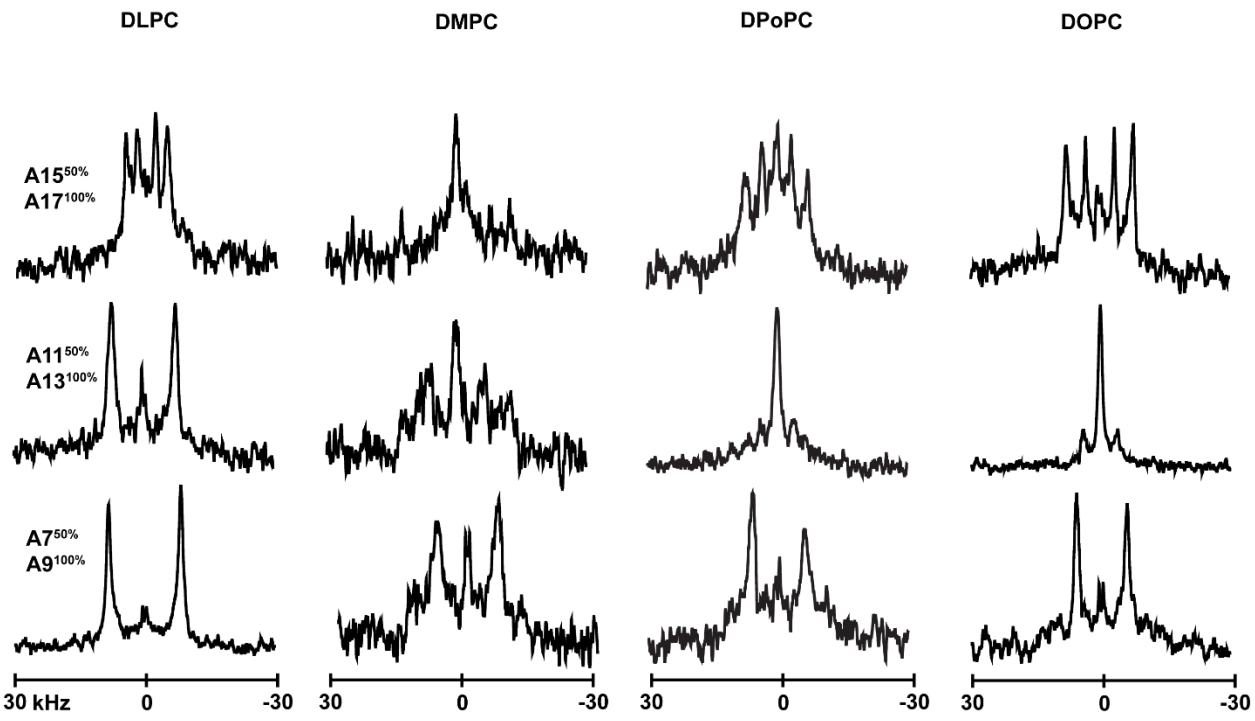

Figure 2: ^{2}H NMR spectra of labeled alanines in the GWALP23-H^{8,16} core helix in DLPC, DMPC, DPoPC and DOPC lipid bilayers hydrated with 20 mM buffer at pH 4. Sample orientation is $\beta = 90^{o}$, 1:60 peptide:lipid at 50^{o}C. The numbers indicate the identities of the ^{2}H-Ala residues.

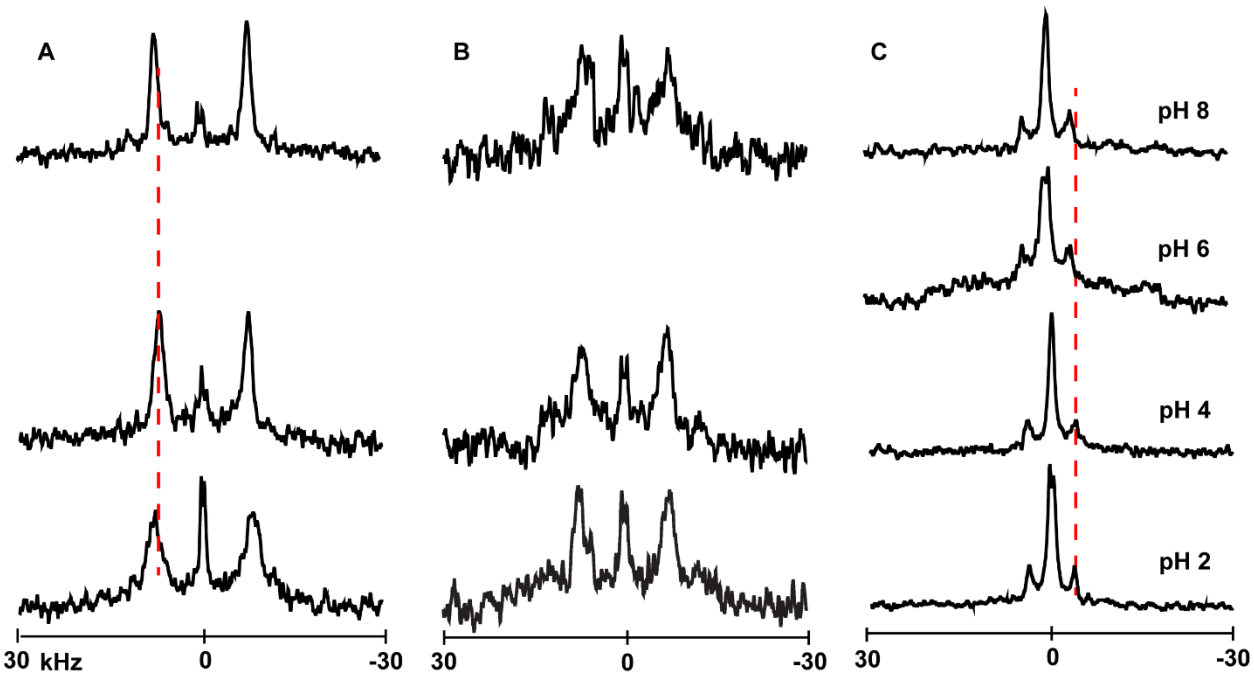

Figure 3: Selected ^{2}H NMR spectra of GWALP23-$H^{8,16}$ labeled alanines A11 and A13 in the core helix in DLPC (A), DMPC (B) and DOPC (C) lipid bilayers hydrated with 20mM buffer at the indicated pH. Sample orientation is $\beta = 90^{o}$, 1:60 peptide:lipid at $50^{o}C$

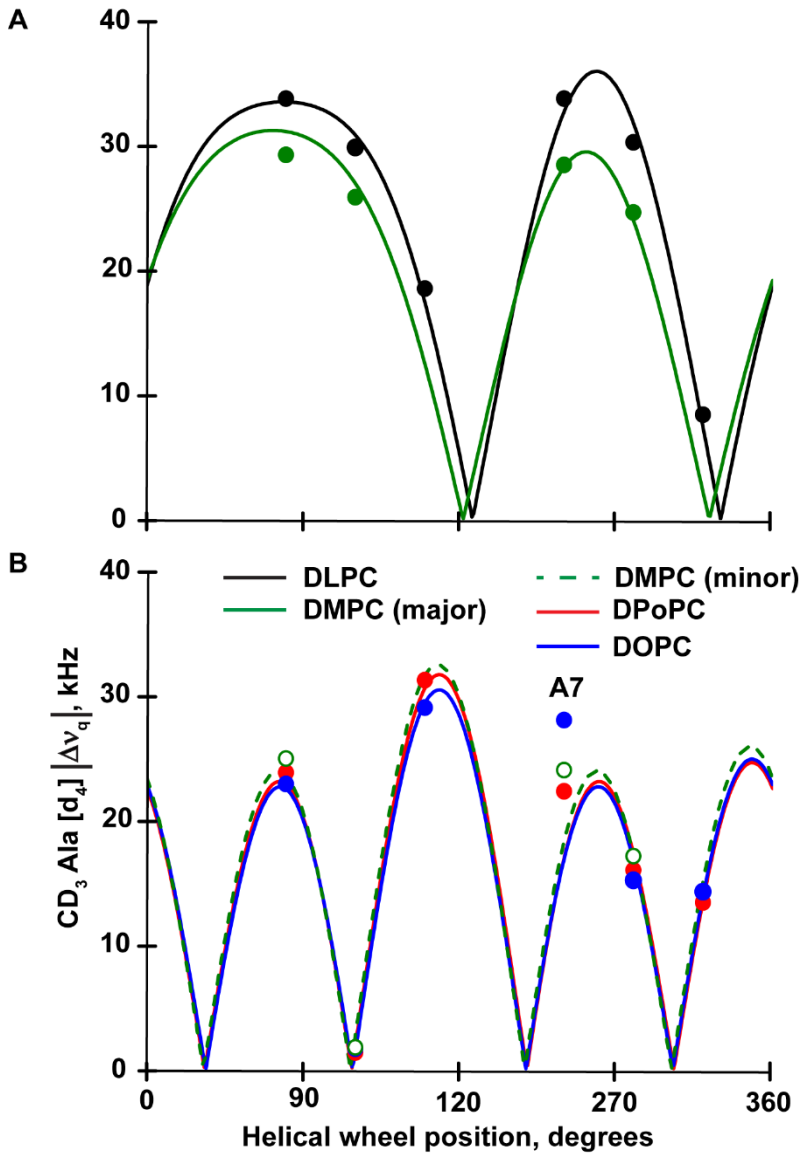

Figure 4: Quadrupolar wave analysis depicting two different orientations of GWALP23-H[8,16] peptide in DLPC, DMPC, DPoPC and DOPC lipid membranes obtained by GALA method [29]. Panel A shows the plots for transmembrane orientations with $\tau_0 = 25^0$ in DLPC (solid black) and with $\tau_0 = 22^0$ for major population in DMPC (solid green). In panel B each plot represents surface orientation with tilt angles of ~ 87^0 for minor population in DMPC (dashed green) and major populations in DpoPC (solid red) and DOPC (solid blue) lipids. Detailed results are listed in Table 3 and the orientation transitions are represented in Figure 5.

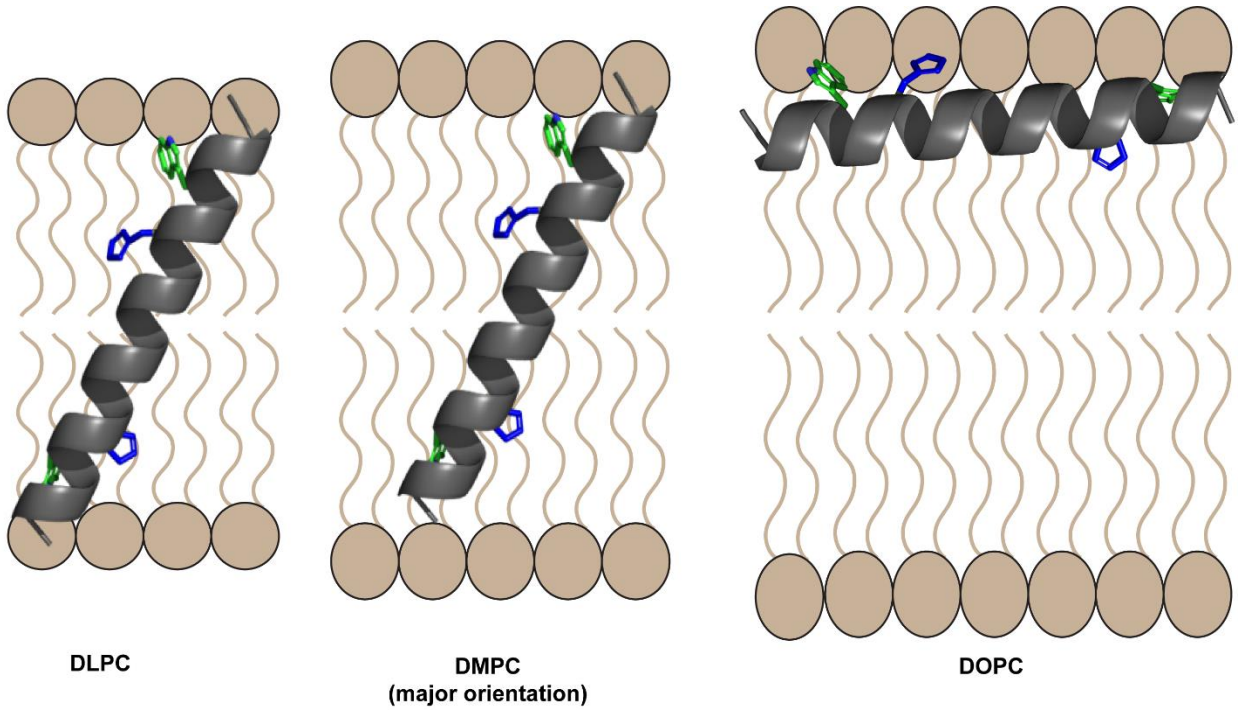

Figure 5: Models to illustrate the transition of GWALP23-H[8,16] from its tilted transmembrane orientation (in DLPC) to a primary orientation at the surface of DOPC bilayer membranes. In the bilayer of intermediate thickness, DMPC, the major population of the helix adopts a transmembrane orientation with slightly smaller tilt than in DLPC, shown in the center panel. The minor population in DMPC has a surface bound orientation (not shown) similar to that in DOPC (right panel).

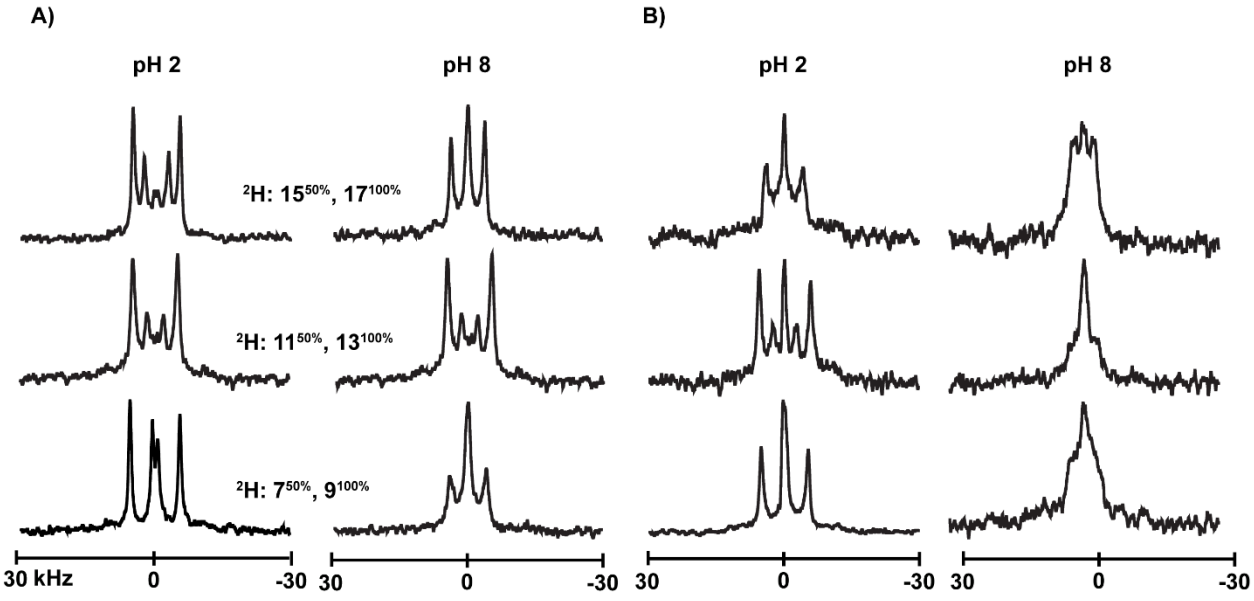

Figure 6: ^{2}H NMR spectra of labeled alanines in the GWALP23-H^8 core helix in DLPC (A) and DMPC (B) lipids at pH 2 and 8. Sample orientation is $\beta = 90^o$, 1:60 peptide:lipid at 50^{o}C The changes in quadrupolar splittings in DLPC and spectral quality in DMPC indicate the response of the helix to the change in ionization state of histidine H8.

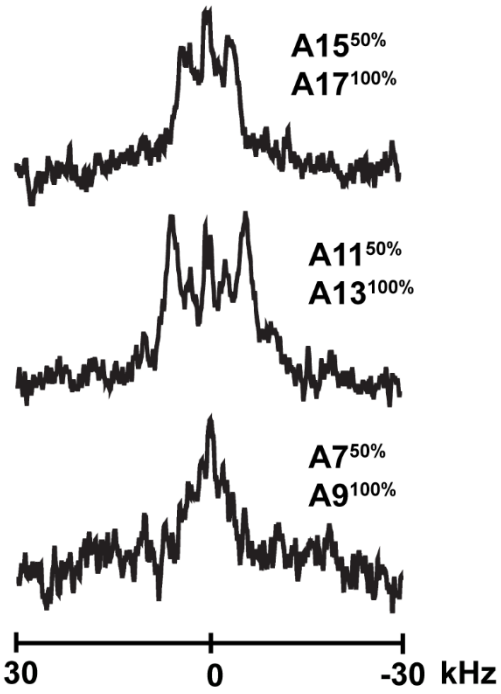

Figure 7: ^{2}H NMR spectra of labeled alanines in the GWALP23-H^{8} core helix in DOPC lipid bilayers. Multiple peaks are observed for each labeled alanine. Sample orientation is $\beta = 90^{o}$, 1:60 peptide:lipid at $50^{o}C$.

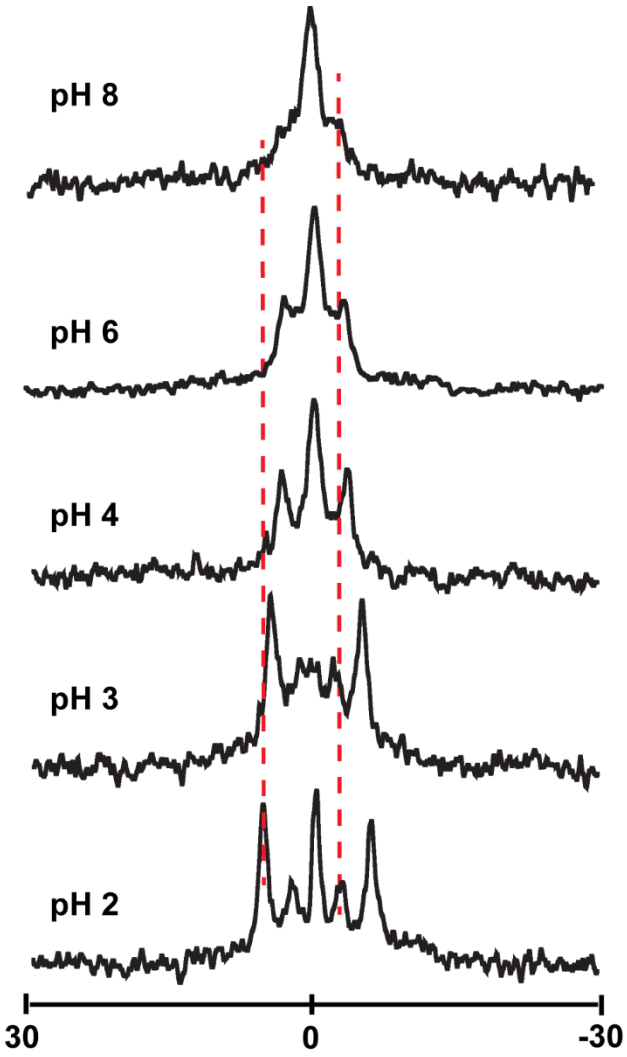

Figure 8: Selected ^{2}H NMR spectra for deuterated alanines A11 and A13 of GWALP23-H^{8} in DMPC hydrated with 20 mM buffer at the indicated pH values. Sample orientation is $\beta = 90^{o}$, 1:60 peptide:lipid at $50^{o}C$

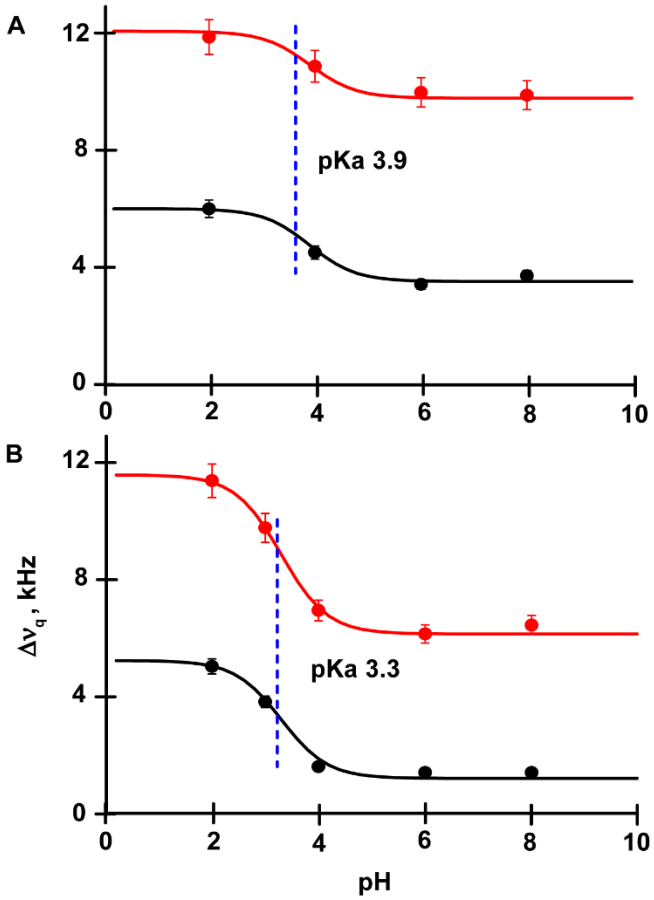

Figure 9: Plots indicating the titration points of H8 present in GWALP23-H^8 in DLPC (A) and. DMPC (B) bilayers. The pH dependence of the $\Delta\nu_q$ values for the CD_3 groups of Ala11 and Ala13 are shown as black and red respectively. The curves indicate slightly different pKa values of 3.9 in DLPC and 3.3 in DMPC lipid bilayers (blue dashed lines).

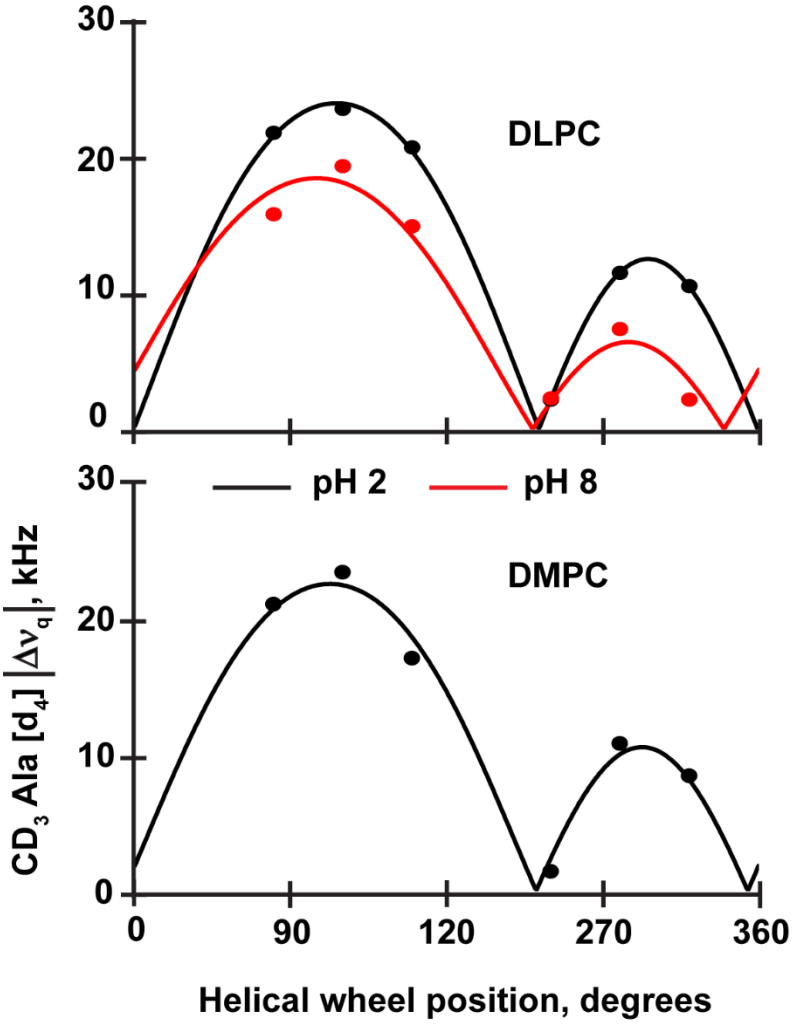

Figure 10: Quadrupolar wave plots for the helix of GWALP23-H^8 in (A) DLPC at pH 2 and pH 8, and (B) DMPC at pH 2.

4.11 **Supporting Figures**

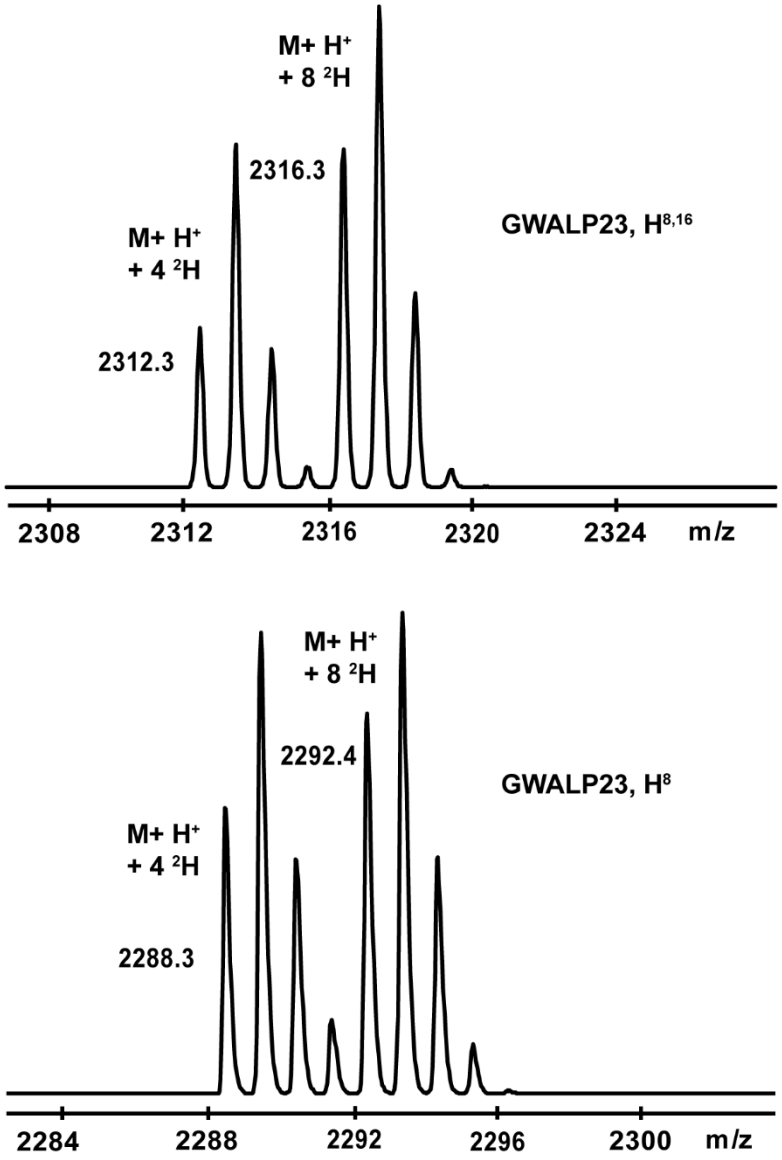

Figure S1: MALDI-Mass spectra of GWALP23-$H^{8,16}$ and GWALP23-H^{8} showing the isotope distributions in the synthetic peptides. Successive peaks within each envelope (representing the molecules with 4 deuterons or with 8 deuterons) differ by ± 1 atomic mass unit due to the statistical distribution of naturally abundant ^{13}C (1.1% natural abundance).

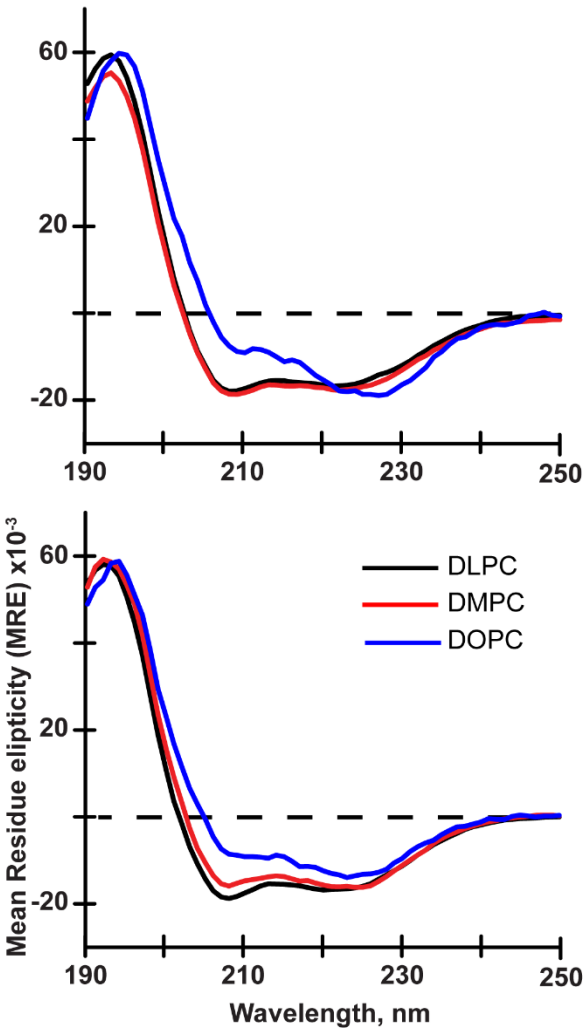

Figure S2: Circular Dichroism spectra of GWALP23-H[8,16] (A) and GWALP23-H[8] (B) in DLPC, DMPC and DOPC lipid vesicles

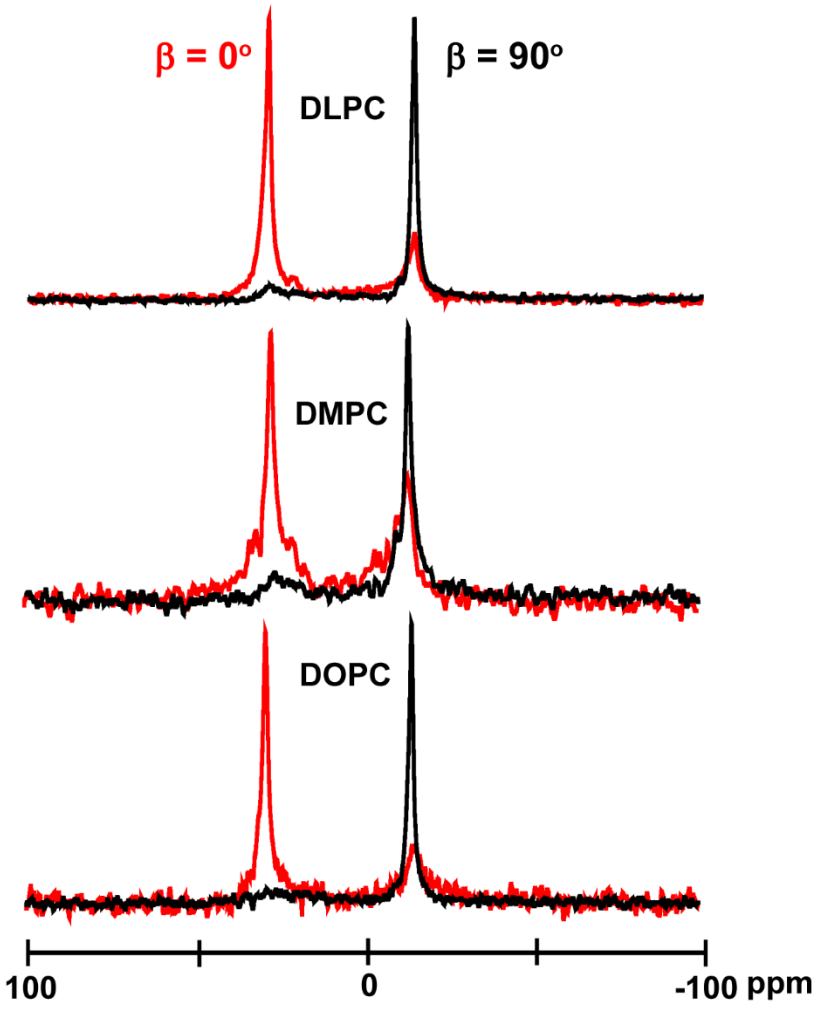

Figure S3: ^{31}P NMR spectra of GWALP23-H^{8,16} in DLPC, DMPC and DOPC lipid bilayers

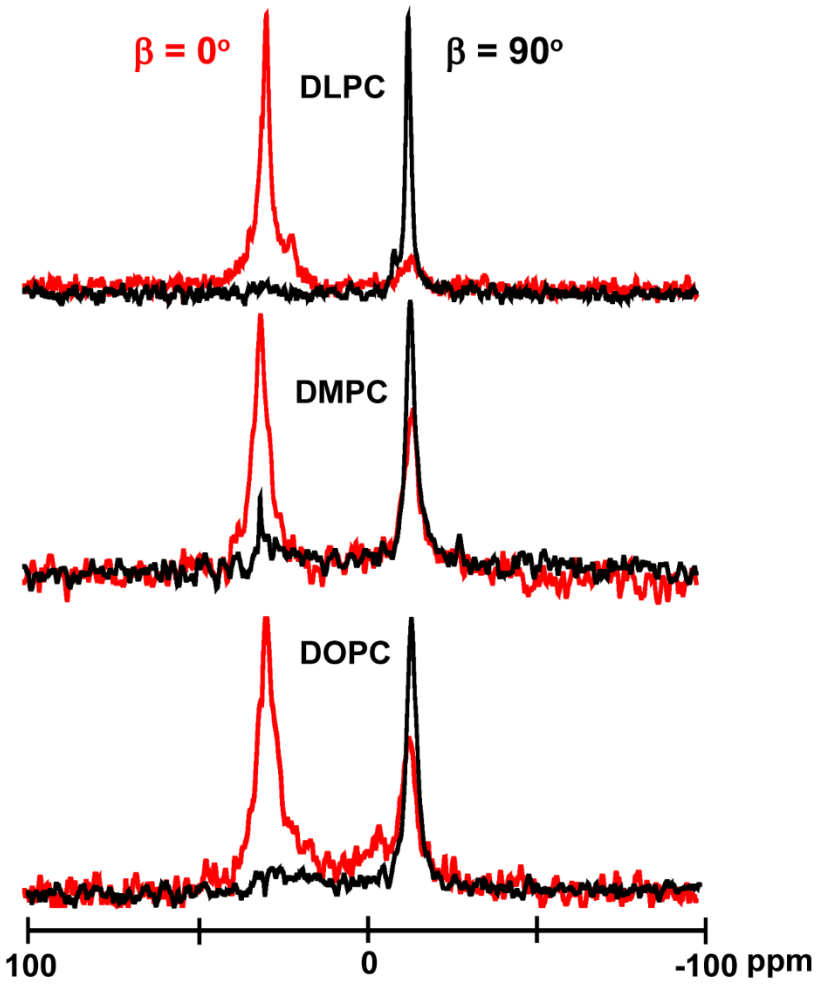

Figure S4: ^{31}P NMR spectra of GWALP23-H^{8} in DLPC, DMPC and DOPC lipid bilayers at pH 8

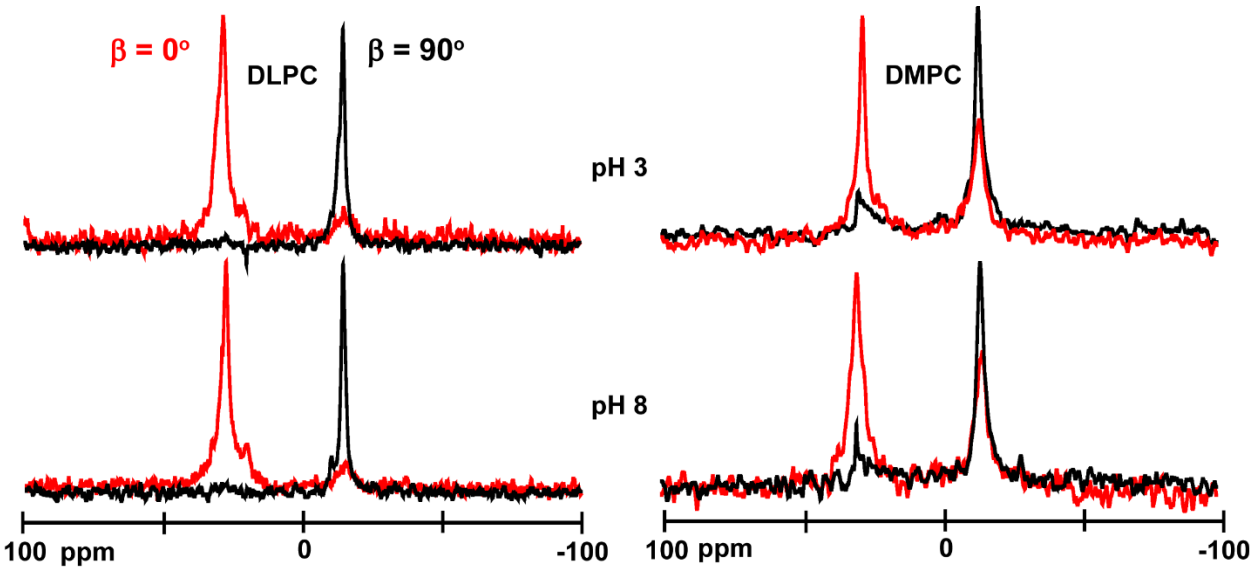

Figure S5: ^{31}P NMR spectra of GWALP23-H^{8} in DLPC and DMPC lipid bilayers at pH 3 and pH 8

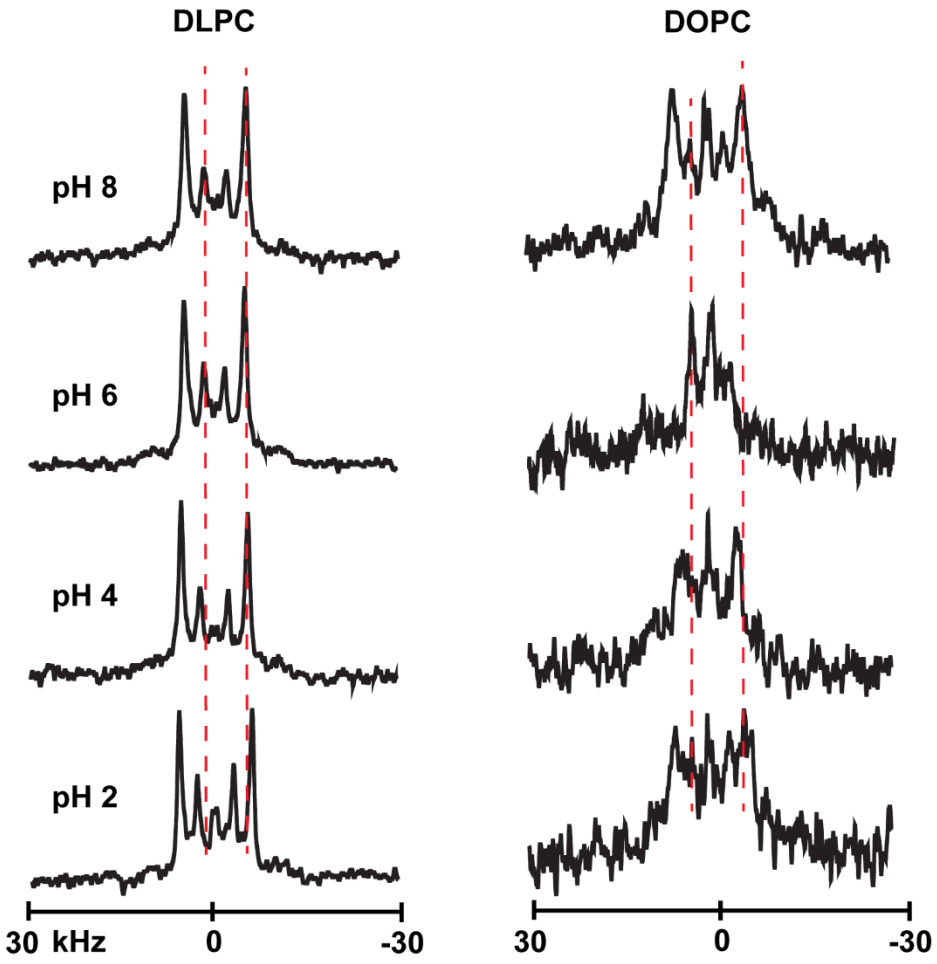

Figure S6: Selected ^{2}H NMR spectra for deuterated A11 and A13 of GWALP23-H^{8} in DMPC and DOPC lipid bilayers hydrated with 20mM buffer at indicated pH. Sample orientation is $\beta = 90^{o}$, 1:60 of peptide: lipid at $50^{o}C$

5. Chapter 5: Transmembrane Helix Integrity Versus Fraying to Expose Hydrogen Bonds at a Membrane-Water Interface

A revised version was published in F. Afrose, M. J. McKay, A. Mortazavi, V. S. Kumar, D.V. Greathouse and R.E. Koeppe 2nd. Transmembrane Helix Integrity versus Fraying to Expose Hydrogen Bonds at a Membrane-Water Interface *Biochemistry* 2019, 58, 6, 633-645

5.1 Abstract

Transmembrane helices dominate the landscape for the membrane-spanning domains of many membrane proteins. Often flanked by interfacial aromatic amino acids, these transmembrane helices also contain loops and inter-helix segments, which could help in stabilizing a transmembrane orientation. By using ^{2}H-NMR spectroscopy to monitor bilayer incorporated model GWALP23 family peptides, we address systematically the issue of helix fraying in relation to the dynamics and orientation of closely similar individual transmembrane helices. Adjacent to a core transmembrane helix, we inserted both aromatic (Phe, Trp, Tyr, His) and non-aromatic residues (Ala, Gly) into positions 4 and 5, to examine the side chain dependency of the transmembrane orientation, helix dynamics and helix integrity (extent and location of unraveling). Incorporation of ^{2}H-alanine labels in terminal alanines enables one to assess the helicity of the core sequence and the peptide termini. For most of the peptides under consideration, we observed substantial unwinding involving at least 3 residues at both ends. For the unique case of histidine at positions 4 and 5, an extended N-terminal unwinding was observed up to residue 7. For further investigation regarding the onset of fraying, we employed

$A^{4,5}$GWALP23 with ^{2}H labels at residues 4 and 5 and found that the number of terminal residues involved in the unwinding is dependent on bilayer thicknesses and helps to govern the helix dynamics. The combined results enable us to compare and to contrast the extent of fraying for each of the related helices, as reflected by the deviation of experimental ^{2}H quadrupolar splitting magnitudes of juxta-terminal alanines A3 and A21 from those represented by an ideal helix geometry.

5.2 **Introduction**

Transmembrane alpha-helices constitute a major structural motif for many biologically important integral membrane proteins including, for example, the seven-helix G-protein coupled receptors [1-2] and a wide variety of single-span membrane proteins [3-5]. The helices often terminate at or near the lipid membrane-water interface, yet the molecular interactions responsible for helix continuation, segment looping or helix termination are not well understood. Computational approaches to transmembrane helices sometimes presume an uninterrupted helical secondary structure [6 7-8] which is not necessarily validated. Some segments may loop naturally to join consecutive helices of a multi-helix membrane protein [9-12], while other transmembrane helices may extend beyond the membrane surface [13-14]. Well controlled experiments with appropriate model peptide-lipid systems can help to address some of the considerations for helix folding and protein-lipid interactions.

In this work, I address the unwinding of helix terminals at a membrane/water interface, which we hypothesize may be a general property for many individual and bundled polypeptide helices that span lipid-bilayer membranes. As a choice of model system, we employ here the GWALP family of transmembrane peptide helices, which like the parent WALP peptides [15] have

proven useful for elucidating fundamental principles. In particular, a second-generation peptide GWALP23, acetyl-GGALW(LA)$_6$LWLAGA-amide, [16-17] exhibits favorable properties, including a well-defined tilted transmembrane orientation [16] wherein the tilt of the GWALP23 helix scales with the bilayer thickness [17]. The helix furthermore undergoes only modest dynamic averaging about a principal transmembrane orientation [18-19]. Interestingly, nevertheless, the presence of more than two interfacial Trp or Tyr residues, flanking the central helix, tends to increase dramatically the extent of the motional averaging [18-20].

Comparisons among several derivatives of GWALP23, namely similar transmembrane helices with different numbers or locations of interfacial Trp, Tyr or Phe residues [21-22], have suggested that factors other than interfacial aromatic residues might help to determine particular orientations for neutral transmembrane helices. Experiments with deuterium labels on residues A3 and A21, separated by 18 residues or five turns on a "perfect" α-helix [23], revealed the fraying of helix terminals for acetyl-GGAAA(LA)$_6$LWLAGA-amide and acetyl-GGAFF(LA)$_6$LWLAGA-amide in bilayer membranes [24] (Figure 1). Is helix fraying therefore a general feature that is commonly observed for transmembrane helices? Do particular combinations of side chains govern the location and the extent of helix unwinding? To address these questions, we have examined the influence of residues 4 and 5 for the core helix integrity and unwinding of N- and C-terminals of a series of GWALP23-like transmembrane peptides. In particular, we have compared the influence of small side chains, G^4G^5 and A^4A^5, and aromatic side chains, F^4F^5, Y^4Y^5, W^4W^5 and H^4H^5 (Table 1), for important properties such as the helix orientation, dynamic averaging and terminal fraying in bilayer membranes of DOPC, DMPC and DLPC. The results give insight into the molecular interactions of protein domains that are in direct contact with lipids in bilayer membranes.

5.3 **Materials and methods**

Peptides were synthesized on a model 433A solid-phase peptide synthesizer (Applied Biosystems) from Life Technologies (Foster City, CA) using a modified FastMoc™ chemistry on a 0.1-mmol scale, with extended times for deprotection or coupling where needed. N-fmoc amino acids were purchased from NovaBiochem (San Diego, Ca), Anaspec (Fremont, CA) and Bachem (Torrence, CA), including histidine and tryptophan whose side chains were additionally protected with trityl and t-butoxycarbonyl protecting groups, respectively. Prior to peptide synthesis, commercial L-alanine-d4, from Cambridge Isotope Laboratories was manually derivatized with an N-terminal Fmoc protecting group, as described previously [25-26], with monitoring by ^{1}H-NMR spectroscopy to confirm successful synthesis of Fmoc-Ala-d4. Typically, each peptide was synthesized with two deuterium-labeled alanines at 50% and 100% isotope abundance levels, to distinguish and assign the ^{2}H NMR signals based on relative intensities.

Peptides with His-trityl and Trp-butoxycarbonyl were deprotected and cleaved from Rink amide resin (NovaBiochem) using a cleavage cocktail containing trifluoroacetic acid (TFA): phenol:triisopropylsilane:water in a 85:5:5:5 ratio at 22 °C for two h, to release a peptide with a neutral amidated C-terminal. After filtering the free peptide solution from resin support, peptides were precipitated with a cold 50:50 methyl-t-butyl-ether:hexane (0 °C, 30 m) mixture and collected by centrifugation. To remove traces of TFA, multiple steps of washing (with MtBE:hexane) and lyophilization (from 1:1 acetonitrile:water) were performed. Crude peptides were purified by means of reversed-phase HPLC, using a 9.4 × 250 mm Zorbax SB-C8 column packed with 3.5 μm octyl-silica (Agilent Technologies, Santa Clara, CA), eluted with a gradient of 95-99% ($W^{4,5}$ peptide), 88-92% ($H^{4,5}$ peptide) or 94-98% ($G^{4,5}$ peptide) methanol in water

containing 0.1% TFA (v/v). Purified peptides were quantified by measuring the absorbance at 280 nm based on a molar extinction coefficient of 5600 M^{-1} cm^{-1} Trp^{-1} in the peptide sequence [27]. MALDI-TOF analysis was used for to verify the peptide molecular mass.

Mechanically oriented samples for solid-state NMR experiments were prepared with 1:60 peptide:lipid (mol:mol) ratio, using DLPC, DMPC and DOPC lipids (Avanti Polar Lipids, Alabaster, AL). Peptide-lipid mixtures were hydrated with ^{2}H-depleted water (Cambridge Isotope Laboratories) to achieve 45% w/w hydration following the procedure described previously [28]. Solid-state NMR spectra for ^{31}P nuclei (for confirming the alignment of phosphate head groups in lipid bilayers) and ^{2}H nuclei (for analysis of peptide orientations and dynamics based on ^{2}H-labeled alanines in the peptide) were recorded using a Bruker Avance 300 spectrometer (Billerica, MA).

The ^{31}P NMR spectra were recorded in a Doty 8 mm wideline probe (Doty Scientific Inc., Columbia, SC) with broadband ^{1}H decoupling on a Bruker Avance 300 spectrometer at both $\beta=0°$ (bilayer normal parallel to magnetic field) and $\beta=90°$ (bilayer normal perpendicular to magnetic field) macroscopic sample orientations. Measurements were performed at 50° C using the zgpg pulse program, a 6 μs 90° pulse, and a recycle delay time of 5 s. Before Fourier transformation, an exponential weighting function with 100 Hz line broadening was applied. The chemical shift was referenced externally to 85% phosphoric acid at 0 ppm.

The ^{2}H NMR spectra were recorded at 50 °C with macroscopic sample orientations of $\beta=90°$ (bilayer normal perpendicular to magnetic field) and $\beta=0°$ (bilayer normal parallel to magnetic field). A quadrupolar echo pulse sequence [29] was employed with full phase cycling, a pulse length of 3.2 μs, echo delay of 105 μs and a 120-ms recycle delay. Between 0.7 and one

million free induction decays were accumulated during each ^{2}H experiment. Fourier transformation was accomplished after applying an exponential weighting function with 100 Hz line broadening.

Circular dichorism measurements were performed on peptides incorporated into small unilamellar vesicles of lipids (1:60, peptide: lipid), obtained by ultrasonication treatment. Peptide concentrations were in 100 μM range, determined by UV-Vis spectroscopy. Spectra were recorded in a Jasco J-1500 spectropolarimeter, using a 1 mm cell path length, 1.0 nm bandwidth, 0.1 nm slit and a 20 nm/min scan rate. An average of six scans typically were recorded to enhance signal to noise ratio

Helix integrity, end fraying, orientation and dynamics were analyzed using two methods, a semi-static geometric analysis of labeled alanines ("GALA") [28] and a modified Gaussian approach [22, 30] for fitting the ^{2}H NMR signals from the CβD3 groups of Ala-d4 residues. The GALA method fits a principal order parameter Szz, an average tilt magnitude τ_0 of the helix axis with respect to the bilayer normal and azimuthal rotation τ_0 about the helix axis, while maintaining an $\varepsilon_{\parallel}$ angle between the alanine Cα−Cβ bond vector and the helix axis fixed at 59.4° [28]. The modified Gaussian approach also involves three variable parameters, an average helix tilt τ_0, mean azimuthal rotation ρ_0 and rotational slippage $\sigma\rho$, while maintaining fixed values for Szz (principal order parameter) and $\sigma\tau$ (helix wobble) that were held constant at 0.88 and 10°, respectively, following [22]. The helix integrity, or lack thereof, was assessed by observations of alanine side-chain CD3 $|\Delta\nu_q|$ values that deviated from the quadrupolar wave plot for the core helix, following [24].

For the $A^{4,5}$GWALP23 helix, a full Gaussian analysis [31] was performed using eight data points, quadrupolar splittings for deuterated alanines 4, 5, 7, 9, 11, 13, 15 and 17. For this analysis, the search increments were 0-90° for τ_0, 0-360° for ρ_0, 0-40° for $\sigma\tau$ and 0-120° for $\sigma\rho$. Then the best fits for each of the variables τ_0, ρ_0, $\sigma\rho$ and $\sigma\tau$ were determined.

5.4 **Results**

Favored by $(Leu\text{-}Ala)_6$ repeats, synthetic model peptides of the GWALP23 family adopt primarily transmembrane alpha-helical secondary structures within the hydrophobic region of a lipid bilayer, which may be further stabilized by two flanking tryptophan residues. In the modified peptides under consideration here, the L^4W^5 sequence of GWALP23 is replaced by neutral Gly or Ala, or by aromatic residues that may be neutral, polar or amphipathic, resulting in $G^{4,5}$, $A^{4,5}$, $F^{4,5}$, $H^{4,5}$, $Y^{4,5}$ and $W^{4,5}$GWALP23 peptides (Table 1). After synthesizing and purifying the peptides, their molecular masses and ^{2}H labeling patterns were confirmed by MALDI-TOF mass spectrometry (Figure S1 of the Supporting Information). The helicity of peptides was checked using circular dichorism (CD) spectroscopy in DLPC, DMPC and DOPC lipid bilayers. The CD spectra generally show double minima near 208 nm and 222 nm, which are characteristic features for alpha-helical structure (Figure S2 of the Supporting Information). (The situation may be complicated by the Trp residues in $W^{4,5}$GWALP23, for which the ratio $\varepsilon 222/\varepsilon 208$ in DOPC is about 1.1 instead of the more usual observation of about 0.9.) In the macroscopically oriented samples, the peptide-lipid mixtures are well aligned in bilayers, as indicated by the ^{31}P NMR spectra for the lipid head groups in the $\beta = 0°$ and $\beta = 90°$ sample orientations (Figure S3 of the Supporting Information).

To evaluate the helix orientations, as well as the helix integrity in more detail, we recorded ^{2}H NMR spectra of d_4-labeled alanine residues of $G^{4,5}$, $H^{4,5}$ and $W^{4,5}$GWALP23 in DLPC, DMPC and DOPC bilayer-incorporated samples, for comparison with previously reported spectra for the other related peptides. The ^{2}H quadrupolar splitting magnitudes ($|\Delta\nu q|$) from methyl side chain (CD_3) groups of six core alanines provide required data for estimating the preferred tilted and averaged orientations of the core transmembrane helical segments with respect to a bilayer normal in an applied magnetic field [28, 32]. The data for the core Ala residues also allow estimates and comparisons of the global helix dynamics using semi-static [28, 32] and modified Gaussian methods [22, 30].

Glycine and alanine comparisons.

In the design of GWALP23 [16-17], W^5 was presented as an "anchoring" interfacial Trp residue to help stabilize a well-defined tilted transmembrane orientation for the core helix. Nevertheless, it was found that the $A^{4,5}$ derivative of GWALP23, without W^5, exhibits also a well-defined transmembrane orientation for its core helix, with only a small extent of dynamic averaging [24]. Now, having removed the #4 and #5 side chains altogether, we observe and report similar properties for $G^{4,5}$GWALP23 as for $A^{4,5}$GWALP23 (Figure 2). Indeed, the ^{2}H NMR spectra for the core alanines 7, 9, 11, 13, 15 and 17 are quite similar for $G^{4,5}$GWALP23 and $A^{4,5}$GWALP23 (Figure 2; Figure S4 of the Supporting Information). The maximal quadrupolar splitting magnitudes, those that eventually define the amplitudes of the quadrupolar wave plots (see below), are only slightly smaller with G4 and G5, compared to A4 and A5 (Table 2), indicating a similarly low extent of dynamic averaging for $G^{4,5}$GWALP23 and $A^{4,5}$GWALP23. For example, $A^{4,5}$ produced wide ranges of $|\Delta\nu_q|$ magnitudes, from 6.5 to 23.2 kHz in DLPC, 6-21 kHz in DMPC and 0.5-18.6 in DOPC (Table 2), resulting in a relatively similar orientation

and dynamics to GWALP23 [24]. For $G^{4,5}$ the $|\Delta\nu_q|$ values extend from 1.4-19 kHz in DLPC, 7.0-20 kHz in DMPC and 1-17 kHz in DOPC (Table 2). The scope, defined by the tilted helix, appears equivalent when the helices are in DMPC or DOPC bilayers, while in DLPC the quadrupolar splittings of $G^{4,5}$ are slightly lower compared to $A^{4,5}$ (Table 2). While similar, the detailed results could be indicative of slight changes in helix tilt, dynamics or unwinding (see below) for $G^{4,5}$GWALP23 compared to $A^{4,5}$GWALP23 in DLPC, with quite similar helix properties in DMPC and DOPC.

For evaluation of the tilt angles, the observed quadrupolar splittings were subjected initially to a semi-static GALA analysis [28, 32], a technique that uses an α-helical geometry and a principal order parameter S_{zz} as an estimate for a relative extent of overall helix motion. Based on the ^{2}H NMR quadrupolar splittings, this method finds the lowest RMSD values using three variables, S_{zz}, the mean helix tilt (τ_0) and azimuthal rotation (ρ_0). Additionally, helix dynamics were further analyzed using a modified Gaussian analysis [22, 30] that employs also a three-parameter fit, with variables being τ_0, ρ_0 and $\sigma\rho$, the rotational "slippage" about the helix axis. To maintain an equivalent "playing" field (with three parameters), the modified Gaussian method maintains fixed estimated values of S_{zz} and $\sigma\tau$, the helix "wobble" [22]. The results and corresponding r.m.s.d. values obtained from the GALA and Gaussian analysis methods are listed in Table 3. The theoretical quadrupolar wave plots of $|\Delta\nu_q|$ versus the alanine Cα radial location, corresponding to the best fits for τ_0, ρ_0 and S_{zz} or $\sigma\rho$, are presented in Figure 3, overlaid with the experimental data. In general, Figure 3 indicates that the overall results for the $G^{4,5}$GWALP23 helix are quite similar to those for the parent GWALP23 peptide helix that has L^4,W^5 instead G^4,G^5. Remarkably, the helices with G^4,G^5, A^4,A^5, or L^4,W^5, show analogous characteristics in each of the lipid bilayer membranes.

Notably, the small tilt angles observed for $G^{4,5}$GWALP23 in DMPC and DOPC (about 8° and 6° respectively) are nearly identical to those found previously [17] for the GWALP23 helix (Table 3). Results from the semi-static GALA method reveal nevertheless a distinctly smaller apparent tilt in DLPC bilayers for the $G^{4,5}$ peptide helix, albeit with a similar azimuthal rotation angle ρ_0, when compared to the parent GWALP23 helix (Figure 3). Indeed, $G^{4,5}$GWALP23 exhibits a helix tilt angle that appears about 10^o lower than that observed for GWALP23, $A^{4,5}$GWALP23 or $F^{4,5}$GWALP23 in DLPC (Table 3). The modified Gaussian analysis furthermore shows general agreement with the results from semi-static method for the helix orientation and dynamics (Table 3). Notably, the value of $\sigma\rho$, which is a key indicator for high levels of dynamic averaging [18, 20, 30], remains modest (near 40°) in each of the DLPC, DMPC and DOPC bilayers membranes (Table 3). Importantly, the $\sigma\rho$ values for $G^{4,5}$GWALP23 are essentially indistinguishable from those for GWALP23 in each of the lipid membranes. After considering the aromatic residues, we will further compare the helix orientations (see below). As is typical for transmembrane helices that exhibit only moderate dynamic averaging [18], the fitted values for the helix tilt and azimuthal rotation from the GALA and Gaussian analytical methods tend to agree (Table 3).

Aromatic residue comparisons.

In similar fashion, we compare the influence of different aromatic residues at positions 4 and 5 in derivatives of GWALP23, relating now $H^{4,5}$ and $W^{4,5}$ with previous results for $F^{4,5}$GWALP23 [22] and $Y^{4,5}$GWALP23 [20-21]. Compared to the parent GWALP23, $W^{4,5}$GWALP23 contains an extra tryptophan, W^4 in place of L^4. As the third polar aromatic residue in the sequence, W^4 might have been expected to confer excessive dynamic averaging and a dramatic

narrowing of the range of quadrupolar splittings for the deuterated core alanines, as observed previously for $Y^{4,5}$GWALP23 [20-21]. Notably, nevertheless, $W^{4,5}$GWALP23, with adjacent tryptophans at positions 4 and 5, displays wide ranges of quadrupolar splittings for the core alanine side chains when the helix is dispersed in lipid bilayers (3-22 kHz for DLPC, 2-18 kHz for DMPC and 1-15 kHz for DOPC). The ^{2}H NMR spectral results (Figure 4, Figure S6 of the Supporting Information) contrast not only with those for $Y^{4,5}$GWALP23 but also with results for other WALP family analogues carrying four tryptophans, namely $W^{2,3,17,18}$ALP19, $W^{2,3,21,22}$ALP23 and $W^{2,5}W^{19,22,}$ALP23 which show splitting ranges that span less than 15 kHz in all cases [17, 28, 32-34]. Indeed, the results for $W^{4,5}$GWALP23 are more similar to those for $F^{4,5}$GWALP23 [22, 24] than for $Y^{4,5}$GWALP23 [20-21]; see Figure 4 and Table 2.

On the other hand, $H^{4,5}$GWALP23 is found to behave differently than $W^{4,5}$GWALP23, with an apparent membrane thickness dependence of the observed range of core alanine quadrupolar splittings (Table 2; Figure 4; Figure S5 of the Supporting Information). The range is quite wide (1-18 kHz) in DLPC, moderate (2.5-14.5 kHz) in DMPC and narrow (5.5-11 kHz) in DOPC bilayers. Interestingly, the $|\Delta\nu_q|$ values and ranges of $H^{4,5}$GWALP23 in DMPC and DOPC bilayer are very similar to those observed for the highly dynamic $Y^{4,5}$GWALP23. These results signify the possibility of $H^{4,5}$GWALP23 exhibiting comparably high levels of dynamic averaging to those of $Y^{4,5}$GWALP23 in lipid-bilayer membranes.

Indeed, when a pair of histidine residues is introduced in positions 4 and 5, keeping the single Trp residue (W^{19}) near the C-terminus, $H^{4,5}$GWALP23 is found to behave quite differently from GWALP23 or $G^{4,5}$GWALP23. The semi-static GALA and Gaussian fits show some similarities with the orientational and motional properties of $Y^{4,5}$GWALP23, yet also some differences. $H^{4,5}$GWALP23 indeed is seen to be highly dynamic, showing $\sigma\rho$ values that range

from about 57° in DLPC to 114° in DOPC (Table 3). In DOPC bilayer membranes, $H^{4,5}$GWALP23 and $Y^{4,5}$GWALP23 show similar properties, where each helix displays a small tilt angle ($\tau_0 \sim 6°$) and similar mean azimuthal rotation (ρ_0 from -8° to 8°), with a very large rotational slippage ($\sigma\rho > 70°$; Table 3). The properties of $H^{4,5}$GWALP23 and $Y^{4,5}$GWALP23 diverge in the thinner DMPC and DLPC lipid membranes. Reflecting again the high extent of dynamic averaging, the best fits for ρ_0 now differ between the two helices and differ also from the ρ_0 observed for each in DOPC (Table 3). Interestingly, $H^{4,5}$GWALP23 displays the same mean azimuthal rotation in DMPC as DLPC, but $Y^{4,5}$GWALP23 does not. With the exception of $Y^{4,5}$GWALP23 in DMPC, the values of $\sigma\rho$ are uniformly large for these two helices (Table 3). Curiously, $Y^{4,5}$GWALP23 exhibits extensive dynamic averaging in DLPC although it can be fitted with very little dynamic averaging in DMPC (see Discussion). We note also that residue A21 of $Y^{4,5}$GWALP23 fits with the core helix in DMPC (see below).

As a new feature, the ^2H $|\Delta\nu_q|$ magnitude for deuterated A7, near the beginning of the core helix of $H^{4,5}$GWALP23, fails to fit the core helix backbone geometry in bilayers of DOPC or DMPC. In these lipid membranes, therefore, the core helix of $H^{4,5}$GWALP23 extends only from about residue 9 to 19, resulting in a longer unwound N-terminal up to about residue 8 (Figure 5A). We will address residue 7 further below when we consider the more generalized unwinding of the N- and C-terminals. At present, this type of core helix unwinding at A7 is unique for $H^{4,5}$ as we do not observe such results for other $X^{4,5}$ analogues, including the highly dynamic $Y^{4,5}$GWALP23.

As noted above, a similar analogue, containing tryptophans at positions 4 and 5, shows very different results. $W^{4,5}$GWALP23, unlike the $Y^{4,5}$ and $H^{4,5}$ peptides, does not exhibit the high

dynamic averaging and gives quadrupolar wave fits for tilt and azimuthal rotation similar to those for GWALP23 (Figure 5B). The modified Gaussian analysis reveals low to moderate $\sigma\rho$ values that increase only slightly with lipid bilayer thickness (Table 3). The overall trends are very similar for the helix properties of $W^{4,5}$GWALP23 and GWALP23, for the DLPC, DMPC and DOPC bilayer membranes. It seems that W4 is tolerated equally as well as L4. (Actually, the $\sigma\rho$ values for $W^{4,5}$GWALP23 are even slightly lower than for the already well oriented GWALP23 helix.) The azimuthal rotation ρ_0 for $W^{4,5}$GWALP23 changes by about 12° from DLPC to DMPC and 20° from DMPC to DOPC (Table 3), which is a slightly larger lipid dependence for helix rotation than observed for GWALP23 (about 5^o and 10^o respectively). Taken together, these results indicate that the helix properties do not vary significantly when L4 is changed to W5 in the GWALP23 framework.

Helix terminal fraying.

Additional important considerations are the length and integrity of the core transmembrane helix. The data for the CD_3 groups of juxta-terminal alanines A3 and A21 serve to define the helical integrity near the peptide ends [24]. Occasionally, we find that residue A7 or A17 may deviate from the core helix geometry.

To test the unwinding of helix terminals, we labeled alanines 3 and 21 of the $G^{4,5}$, $Y^{4,5}$, $W^{4,5}$ and $H^{4,5}$ derivatives of GWALP23 with deuterium. The ^{2}H NMR spectra for alanines 3 and 21 of these peptides are shown in Figure 6. The spectra display distinct and sharp peaks for the CD_3 side chains of alanines 3 and 21. Typically, the $|\Delta\nu_q|$ magnitudes (Figure 3, Table 2) are different for residues 3 and 21, indicating unwinding of one or both helix ends [24]. Occasionally, as observed for $G^{4,5}$- and $H^{4,5}$GWALP23 in DLPC, residues A3 and A21 display the same $|\Delta\nu_q|$

value. A coincidence of $|\Delta\nu_q|$ values for A3 and A21 could indicate that the helix is intact from residue 3 through residue 21 or, alternatively, both residues 3 and 21 could deviate from the core helix (see below).

When the $|\Delta\nu_q|$ values for A3 and A21 are visualized next to the quadrupolar wave plots for the core transmembrane helix (Figure 3), it is evident that residues 3 and 21 deviate from the core $G^{4,5}$GWALP23 helix in each of the DLPC, DMPC and DOPC lipid membranes. The results for $G^{4,5}$GWALP23 are similar to those observed previously for $A^{4,5}$GWALP23 and $F^{4,5}$GWALP23 [24]. The closest approach of residue 3 or 21 to the $G^{4,5}$GWALP23 core helix involves residue A3 in DLPC, where the $|\Delta\nu_q|$ deviation is only 1.5 kHz (Figure 3). Residue A3 fits the GWALP23 helix in DOPC but not in DMPC or DLPC (Figure 4), while reside A21 is consistently off of both core helices in each of the lipid membranes.

Considering $H^{4,5}$GWALP23 and $W^{4,5}$GWALP23 (Figure 4), we find that residue A7 deviates from the core helix of $H^{4,5}$GWALP23 in all three lipid membranes, effectively shortening the core helix of $H^{4,5}$GWALP23. Residue A21 also deviates, so the core helix of $H^{4,5}$GWALP23 extends, at most, from residue 8-20 (yet is verified only between residues 9-17). Residue 3 of $H^{4,5}$GWALP23 does not change its orientation much when the lipid membrane is changed (Figure 5), as the A3 $|\Delta\nu_q|$ values are nearly identical in DLPC, DMPC and DOPC membranes (Table 2). The orientation of residue 3 of $H^{4,5}$GWALP23 indeed is probably dictated by peptide bond/lipid interactions without relation to any helix (since the core helix is already unraveled at residue 7). One notes that the similar $|\Delta\nu_q|$ values for A3 of $H^{4,5}$GWALP23 are fortuitously close to the core helix in DMPC, probably a coincidence. The core helix of $W^{4,5}$GWALP23 is intact between residues 7-17, with residues 3 and 21 unwound (Figure 5), very similar to the situation observed with $F^{4,5}$GWALP23 and $A^{4,5}$GWALP23 [24].

Within the context of the helix dynamics and helix end fraying, we compare again the helix orientations based on contour plots for best-fit values of helix tilt τ and azimuthal rotation ρ (Figure 7). These contour plots confirm the conclusions from the GALA wave plots in Figures 3 and 5. One notes that the transmembrane helices with residues F4F5, W4W5 or A4A5 display a helix tilt that increases systematically when the host bilayer becomes thinner (Figure 7). These helices whose tilt angle scales with the bilayer thickness also display limited dynamic averaging (with $\sigma\rho$ generally < 50°; Table 3). By contrast, the helices with residues Y4Y5 or H4H5 display extensive dynamic averaging (with $\sigma\rho$ generally > 70°; Table 3) and an "apparent" helix tilt angle that is obscured by the dynamic averaging and therefore appears to depend little on the bilayer thickness (Figure 7). A revised analysis (Table 3), with $\sigma\tau$ set to 5, indicates a high value of $\sigma\rho$ also for $Y^{4,5}$GWALP23 in DMPC. Somewhat curiously, the helix $G^{4,5}$GWALP23 shows only modest dynamic averaging (Table 3) yet also a tilt angle that varies little with the bilayer thickness (Figure 7). With one particular helix, additionaly ^{2}H labels enabled us to examine more closely the N-terminal unraveling of the core helix.

Sequence position for the onset of fraying.

Because we have seen a number of transmembrane helical peptides undergo unwinding, regardless of the lipid thickness, we decided to investigate the onset of the unwinding for a particular case from the N-terminal end. With the exception of $H^{4,5}$GWALP23, residue A7 is part of the core helix for each of the transmembrane peptides listed in Table 1. For the case of $H^{4,5}$GWALP23, with A7 not part of a helix (Figure 5), the core helix must begin after residue 7, as the sequence of the first six residues would be too short to form a helix. With data points available for residues A7 and A3, to expand the analysis, we have deuterated and investigated

alanines 4 and 5 of $A^{4,5}$GWALP23. Our previous study on $A^{4,5}$GWALP23 [24] suggested that this peptide, despite its lack of an aromatic or charged flanking residue, N-terminal to the core helix, aligns well in the lipid bilayers with typical rapid reorientation about the bilayer normal [15] yet little additional dynamic averaging.

Alanines A4 and A5 provide a particular opportunity for the use of deuterium labels to investigate the onset of helix fraying. Figure 8 shows the ^{2}H NMR signals from A4 (50% d_4) and A5 (100% d_4) of $A^{4,5}$GWALP23. The respective $|\Delta\nu_q|$ values are listed in Table 2. Notably, the results for the onset of helix unraveling are lipid dependent for both boundaries of the core helix. When viewing the ^{2}H $|\Delta\nu_q|$ magnitudes of the A4 and A5 side chains alongside the quadrupolar wave plot for the core helix from the six central alanines of $A^{4,5}$GWALP23, one observes that A4 and A5 deviate from helix geometry in DLPC bilayers, but are included with or very close to the core helix in DMPC and DOPC (Figure 8). The core helix is nevertheless longer in DOPC bilayers because, remarkably, residue A17 deviates from the core helix in DMPC! These results imply that both terminal segments of the tilted transmembrane helix of $A^{4,5}$GWALP23 respond to the lipid membrane thickness. The transmembrane helix is frayed from residues 1-5 in DLPC but only from residues 1-3 in DOPC or DMPC; yet the C-terminal segment is further frayed back to residue 17 in DMPC. In the other bilayers of DLPC and DOPC, the C-terminal is unraveled from at least residues 21-23, perhaps farther, with further information not available at this time.

Refining the analysis of helix dynamics

The differential fraying of the terminals of $A^{4,5}$GWALP23 in different bilayer membranes raised questions about the dynamics of the core helix. At the same time, the access to data points

for deuterated A4 and A5 enabled a full Gaussian analysis of the dynamic averaging for the core helix (residues 4-17 or 4-16) in DOPC and DMPC, using the quadrupolar splitting magnitudes for seven or eight alanines. The best-fit preferred ranges of RMSD as functions of $\sigma\tau$ and $\sigma\rho$ (Figure 10) reveal now a much larger preferred value (72°) for $\sigma\rho$ and a much larger allowed range for ($\sigma\tau$, $\sigma\rho$) for the more "perfect" core helix in DOPC bilayer membranes (lowest panel of Figure 10). These results suggest a correlation for the helix of $A^{4,5}$GWALP23 being less frayed and showing more dynamic averaging in DOPC. The longer core helix would have shorter exposed "stakes" on the ends which in turn could lead to more dynamic averaging.

5.5 **Discussion**

Key results shown above indicate that the helix integrity or extent and location of terminal unraveling of a transmembrane helix can relate to the primary protein structure at the membrane interface, the membrane thickness and the dynamic properties of the helix. Cause and effect can sometimes propagate in either direction, as for example, changes to particular interfacial residues or the bilayer thickness may influence the helix fraying, which in turn could influence the dynamics of the core helix. Interactions between side chains and lipid head groups also could influence the molecular dynamics and the extent of helix unwinding. We will focus first on helix to non-helix transitions as a general feature at lipid membrane interfaces for model peptides and membrane proteins. We will then address the interplay among particular interfacial residues, lipid bilayer thickness, and the core helix length, boundaries, wobble and rotational dynamics.

Interfacial helix unwinding as a general feature.

With now a large set of peptides from the GWALP23 family, one observes a core transmembrane helix that is tilted in lipid-bilayer membranes. Yet the helix geometry of the central core does not extend to the terminals of the 23-residue sequence. Instead, residues 3 and 21 consistently are observed to deviate from the core helix configuration. The terminal unraveling was first suggested for GWALP23 in DMPC bilayers [17] and then was observed for the single-Trp helices of $F^{4,5}$GWALP23 and $A^{4,5}$GWALP23 in bilayers of DLPC, DMPC and DOPC [24]. By comparison, an amphipathic 14-residue helical peptide, $(KIAGKIA)_2$-amide, is found to unravel at its N-terminus when bound to the surface of DOPC or DMPC bilayers; yet the helix spans residues 4-14 all the way to the C-terminus [35].

In this work, we extend the observations for a larger number of related 23-residue membrane-spanning helices and observe, as a general feature, that both the N-terminal and C-terminal tend to unwind from the core helix at the membrane interfaces. Occasionally, the unraveling is less extensive near the C-terminal than near the N-terminal, a result which may couple to increased rotational dynamics for the core helix. The detailed dependence upon the identities of residues 4 and 5 will be discussed below. Next, we address examples of the relevance of helix conformational transitions for membrane protein function.

Helix fraying and structural plasticity indeed may have functional relevance in a variety of membrane proteins. Consider, for example, NsaS, an intramembrane histidine kinase that helps *S. aureus* adapt to a variety of environmental stimuli.[7] A marginally stable interfacial α-helical coiled-coil linker adopts a variety of conformations during antibiotic induced signaling. The structural plasticity of the linker region, similar to ones found in a number of signal

transduction proteins, may provide soft coupling between the transmembrane and signaling domains.[7]

Another example involves alpha-synuclein (αS), a small highly conserved protein linked to Parkinson's disease that localizes to presynaptic vesicles [36]. An N-terminal lipid-binding domain of αS can interconvert between helix and disordered conformations, depending on the membrane environment. Conversion from extended to broken helix has been proposed to enable αS to bridge between two closely apposed membranes. Similar behavior is observed in apolipoproteins with common sequence and structural features. Reorganization between membrane-bound extended and broken helices is thought to be important for normal protein function and may play a role aggregation and toxicity[37] N-terminal acetylation, present in native αS, was found to decrease helix fraying and increase affinity for vesicles with physiological anionic lipid content.[38]

Partial fraying of a membrane proximal region of gp41 may play a role in the fusion of HIV to target cell membranes.[39] Unwinding of a transmembrane coiled-coil of a heterodimeric integrin receptor was found to release a constraint on the ectodomains, enabling ligand-induced conformational changes [40]. The unwinding of a C-terminal α-helix could be important for regulating the function of Switch-associated protein-70 at a membrane surface.[41] Helix unwinding may help cytoskeletal spectrin proteins to regulate cell deformation. [42]. The influenza A matrix protein 2 may adjust its length by partially unwinding a helix and forming loop structures.[43] These and other examples illustrate the need for better understanding of biophysical features that govern the continuity and unraveling of protein helices in lipid membranes.

Influence of Positions 4 and 5 on Tilt and Dynamics.

Residues 4 and 5 influence the helix properties differently in different membrane environments. The parent helix of GWALP23 with residues L4 and W5 is moderately dynamic with modest values of σ_ρ while adopting a tilt τ_0 that adjusts to the lipid thickness without a need to modify its azimuthal rotation.[17] Replacing L4 with W4 interestingly does not increase the predicted σ_ρ. The presence of W4,5 maintains similar orientations and lipid dependent trends to those of GWALP23 with L4W5. Competing hydrogen bonding interactions at the membrane interface sometimes result in increased dynamic averaging about ρ_0, much like the behavior observed for $Y^{4,5}$GWALP23 [22] and the original WALP peptides with four interfacial Trp residues.[18] Notably, the dynamic averaging about ρ_0 is much less extensive for $W^{4,5}$GWALP23 than for $Y^{4,5}$GWALP23. As previously discussed,[20, 22] Y4 and Y5 individually are well tolerated in the transmembrane environment. The combination of the Y4 and Y5 side chains, nevertheless, gives rise to much more "slippage" about the helix axis (dynamic averaging; higher $\sigma\rho$) than is observed with W4,5 in all three lipid membranes. (We note also in the case of Y4,5 a trade-off between $\sigma\tau$ and $\sigma\rho$. The modified Gaussian predicts a much higher $\sigma\rho$ of 124° instead of 18° in DMPC if $\sigma\tau$ is 5° instead of 10° (Table 3).[44]) Similar highly dynamic behavior is also seen with $H^{4,5}$GWALP23.

The case with H4 and H5 is intermediate. Although the peptide helix with H4 and H5 prefers the same average rotation in the two shorter lipids, the rotational slippage indicated by $\sigma\rho$ is much higher in DMPC. The helix further adjusts its rotation by increasing $\sigma\rho$ in the thicker DOPC bilayers (Table 3). Competition for positioning with the polar head groups is likely for the two imidazole side chains. The situation is more straightforward with the nonpolar F4 and

F5 side chains. While maintaining aromaticity, the side chain hydrogen bonding capability is removed at these positions in F4,5. This change lowers the dynamics and is well tolerated in all three bilayer membranes as $F^{4,5}$GWALP23 can adapt to hydrophobic mismatch by modulating its tilt alone. So why are two neighboring tryptophan residues W4 and W5 also so well tolerated in all three membranes, as opposed to the complications with H4,5 and Y4,5? The additional motion observed in the helices with Y4,5 and H4,5 may instead arise due to the need for individual side chains to compete with one another for favorable interactions with the polar head groups. F4 and F5 seem both to be content with "generalized" interfacial locations. The Trp side chains alternatively sample many complex interactions at the interface to adapt the indole ring structure to both the hydrophobic lipid tail and the polar head group environments.[45-46] We surmise that W4 and W5 may simultaneously be able to find appropriate orientations at the interface and form stable interactions with the lipid head groups, e.g. through indole hydrogen bond formation. Such interactions would additionally explain the observed drop in $\sigma\rho$ compared to GWALP23 (Table 3), as the combined interactions of these Trp residues could limit azimuthal rotation of the helix.

Removing side chains L4 and W5 completely, as with G4 and G5, decreases the helix tilt in the thinnest bilayer, DLPC, by about 10° compared to the tilt of helices having L4W5 or A4,5 (Table 3). In fact, the tilt of the $G^{4,5}$GWALP23 helix remains essentially the same in all three lipid membranes, and the core helix instead seems instead to satisfy the demands of the bilayer by changes of 10°-30° in its azimuthal rotation. Furthermore, the helix dynamics with G4 and G5 are roughly the same as when W5 is present (in the GWALP23 helix). The lower than expected dynamic averaging and the low tilt angle in DLPC could also be explained by helix

unwinding, as the Gly residues are likely not part of the core helix. Exposed backbone carbonyl groups then would be able to reach out and form stable interactions at the lipid interface.

Replacing the side chains of L4W5 with methyl groups in the case of A4,5 (once again lacking an aromatic Trp residue) also retains helix properties similar to those of GWALP23. The major difference lies in the increased dynamic averaging when the peptide helix is incorporated into the thicker DOPC bilayer. In this environment, both A4 and A5 are part of a longer core helix that extends at least to residue 17 and as discussed above, the containment of the backbone carbonyl groups within the helix structure could make the helix more "slippery". In DLPC, the extent of dynamic motion is low when A4 and A5 are absent from the core helix. In DMPC, residue A17 is absent from the core helix, and the helix rotational slippage is in between the values observed in DOPC and DLPC. When the core helix of $A^{4,5}$Gwalp23 is shorter, in similar fashion to G4,5, some of the free backbone carbonyl groups would be able to help stabilize the helix dynamics. The methyl side chains may play a further role, as the best-fit $\sigma\rho$ is lower when A4 and A5 are unwound than when G4 and G5 are present.

Sequence and lipid dependence of the magnitude of deviation of residues 3 and 21 from the core helix.

Alanines 3 and 21 are separated by 18 residues and therefore would give identical ^{2}H NMR signals in cases where both reside within a continuous "perfect" α-helix.[23-24] However, residues A3 and A21 do not give identical ^{2}H quadrupolar splittings for any of the transmembrane helices (Table 1) considered here. Instead, the ^{2}H $|\Delta\nu q|$ magnitude of either A3 or A21 (or both) deviates from the value predicted by the quadrupolar wave plot for the core

helix in all cases (e.g., see figures 3, 5, 9). All of these transmembrane helices are partially unwound. What is the extent of the unraveling for the N-terminal and C-terminal of each helix?

To examine and compare the extent of unwinding and view any trends that may depend on the lipid environment or particular amino-acid side chains, we consider the deviation (in kHz) of experimental quadrupolar splitting values of A3 and A21 from the theoretical magnitudes that would fit the corresponding quadrupolar wave plot for the core helix of each particular transmembrane peptide. Thus, while we are unable to deduce a straightforward helix unwinding angle, one can nevertheless use the ^{2}H $|\Delta\nu_q|$ deviations to calculate the corresponding side-chain theta angle (θ) deviations from helix geometry for the A3 and A21 methyl groups in each individual peptide helix in each lipid membrane. Figure 11 shows these histograms for $X^{4,5}$ peptides carrying N-flanking side chains (N-terminal to the core helix) with no hydrogen bonding ability, namely $G^{4,5}$, $A^{4,5}$, $F^{4,5}$ and $L^{4}W^{5}$. Additional histograms for comparisons of different N-flanking aromatic side chains are shown in Figure S7 of the Supporting Information. In this section we will consider the trends with respect to lipid bilayer thickness and the sizes and identities of the residue 4 and 5 side chains. An interesting initial point is that the quadrupolar splitting magnitude for A3 is higher and that of A21 lower than the predicted value (based on the core helix geometry) in nearly all cases (with occasional exceptions that will be noted below). These features generate positive deviation of $|\Delta vq|$ for A3 and negative A21, which are displayed in the histograms in Figure 11 and Figure S7. The exact reason for these consequences is unknown. Nevertheless, these trends might indicate, generally, an opposite direction of fraying for each end.

Examining first the deviation of A3 in the parent GWALP23 helix (with $L^{4}W^{5}$ in Figure 11), we observe that the deviation of A3 from the core helix follows the actual tilted orientation

of the helix. The tilt of GWALP23 varies with the bilayer thickness, from about 23° in DLPC down to about 6° in DOPC [17] (Table 3). Residue A3 likewise shows smaller deviation when the helix is moved from thinner to thicker lipid, with the A3 side chain ^{2}H |Δνq| deviating about 7.4 kHz, 6.5 kHz and 0.5 kHz in DLPC, DMPC and DOPC, respectively, from theoretical values predicted by the core helix. The helix of F^{4,5}GWALP23 exhibits a similar difference between DLPC and DOPC, with a notably much higher deviation of A3 from the core helix in DMPC. But the G^{4,5}GWALP23 and A^{4,5}GWALP23 cousins, lacking aromatic residues 4 and 5, do not follow the same scenarios. Notably, in DLPC the experimental $|\Delta\nu_q|$ magnitude of A3 in the presence of G^{4,5} lies below the quadrupolar wave plot, giving rise to a negative deviation. The reason for this outcome is unknown, but the lower tilt of G^{4,5}GWALP23 in DLPC (Table 3), compared to other analogs, could be a factor to influence the direction of the helix unraveling. The A^{4,5} helix shows about the same extend of unwinding of residue A3 in all three lipids (Figure 11); the findings are notable since A4 and A5 deviate from helix geometry only in DLPC bilayers, but are included on the core helix in DOPC and are very close in DMPC (Figure 8).

Residue A21, in contrast to A3, shows negative deviation in all cases (Figure 11). With the exception of F^{4,5}GWALP23 in DLPC, the extent of deviation of A21 from the prediction of the core helix is essentially the same in each lipid membrane. The magnitude of the deviation of A21 in G^{4,5}Gwalp23 is in all cases slightly less than for the other helices (Figure 11).

For the N-flanking aromatic side chains 4 and 5, the W4,5 helix displays low motional averaging (σρ values) in all lipid environments (Table 3) and significant deviations of A3 and A21 from the predictions of the core helix (Figure S7 of the Supporting Information). The F4,5 helix also exhibits low motional averaging and, notably, the largest deviations of residue A21 from the core helix, especially in DLPC (Figure S7). By contrast, the Y4,5 helix undergoes very

extensive motional averaging (Table 3) and has A21 very close to the core helix, suggesting a longer core helix toward the C-terminal in each of the lipid membranes (Figure S7). Moving to other peptides, $H^{4,5}$ shows somewhat similar consequences, though the status of A3 is complicated by the fact the A7 already is away from the core helix (Figure 5). The highly dynamic peptides with $Y^{4,5}$ or $H^{4,5}$ display quite low extent of deviation at one or both ends, suggesting a longer core helix and again pointing toward a possible inverse link between helix dynamics and terminal residue deviation. A "competition" between polar aromatic residues 4 and 5 for hydrogens bonds with lipid head groups also could contribute to high levels of dynamic averaging.

Seeing that the deviations of terminal residues from a core transmembrane helix may be directed by side chain identities as well as lipid thickness, we have compared the influence of large and small nonpolar side chains (Figure 11). Comparing the terminal unraveling of helices bearing $G^{4,5}$, $A^{4,5}$ and $F^{4,5}$, the deviations of A21 and A3 from core helix geometry generally increase with the side chain size, although the trend is opposite for A3 in DOPC membranes (Figure 11). The largest deviations are seen for $F^{4,5}$GWALP23, with A3 deviating most from the core helix in DMPC, and A21 in DLPC (Figure 11).

A view of energetics at the interface.

The results with deuterium labels on A4 and A5 of $A^{4,5}$GWALP23 (Figures 8-9) reveal possible links involving helix fraying, interfacial interactions between unfettered peptide bonds and lipids, and a lessening of the dynamic averaging of the core helix around its principle orientation. The transmembrane helix of $A^{4,5}$GWALP23 has no charged residues with only W19 as an interfacial aromatic residue and, notably, only small side chains near the N-terminal. In

DOPC membranes, the core helix extends farther toward the terminals than in thinner membranes, with the ^{2}H quadrupolar splittings from A4 through A17 falling on the wave plot for the core helix in DOPC (Figure 9). At the same time, and possibly as a correlation, the rotational slippage, $\sigma\rho$ around the axis of the core helix, is much larger in DOPC than in DMPC or DLPC, when a full Gaussian analysis is considered (Table 3; Figure 10). We speculate that a full Gaussian analysis, if more data points were available, might reveal more dynamic averaging also for $G^{4,5}$GWALP23 in DOPC. The situation is more complicated for $Y^{4,5}$GWALP23, which is highly dynamic in each of the lipid systems. The results suggest that helix fraying may be less important for the dynamics when polar side chains (Y4 and Y5) are able themselves to interact directly with lipid head groups. Considerations of helix unraveling at membrane interfaces, nevertheless, could be significant for molecular dynamics simulations and representations of membrane proteins.

In summary, our systematic experiments with closely related transmembrane model peptide helices have enabled us to address specific questions concerning lipid-protein interactions, helix integrity and dynamics. The central findings are: (i) All of the transmembrane helices considered here are tilted in the bilayer membrane and are somewhat unraveled, by at least three residues, at each membrane interface. (ii) The extent of the N-terminal unraveling depends upon the lipid bilayer thickness and the identities of juxta-terminal side chains at positions 4 and 5. The size and polarity of the #4 and #5 side chains help to determine the length of the core helix and the onset of helix unwinding. (iii) The extent of the C-terminal unraveling has yet to be examined. (iv) In some cases (with more examples needed), the dynamic averaging of the transmembrane helix orientation may couple to the extent of helix fraying and

to the bilayer thickness. Some of these properties will be important for the plasticity and functioning of membrane proteins.

5.6 **Acknowledgement**

This work was supported in part by NSF MCB grant 1713242, and by the Arkansas Biosciences Institute. The peptide, NMR and mass spectrometry facilities were supported in part by NIH grant GM103429.

5.7 **References**

1. Hilger, D.; Masureel, M.; Kobilka, B. K., Structure and Dynamics of GPCR Signaling Complexes. *Nat. Struct. Mol. Biol.* **2018,** *25* (1), 4-12.

2. Vass, M.; Kooistra, A. J.; Yang, D.; Stevens, R. C.; Wang, M.-W.; de Graaf, C., Chemical Diversity in the G Protein-Coupled Receptor Superfamily. *Trends Pharmacol. Sci.* **2018,** *39* (5), 494-512.

3. Landolt-Marticorena, C.; Williams, K. A.; Deber, C. M.; Reithmeier, R. A., Non-Random Distribution of Amino Acids in the Transmembrane Segments of Human Type I Single Span Membrane Proteins. *J. Mol. Biol.* **1993,** *229* (3), 602-608.

4. Arkin, I. T.; Brunger, A. T., Statistical Analysis of Predicted Transmembrane Alpha-Helices. *Biochim. Biophys. Acta, Protein Struct. Mol. Enzymol.* **1998,** *1429* (1), 113-128.

5. Ulmschneider, M. B.; Sansom, M. S. P., Amino Acid Distributions in Integral Membrane Protein Structures. *Biochim Biophys Acta, Biomembr.* **2001,** *1512* (1), 1-14.

6. Reddy, T.; Manrique, S.; Buyan, A.; Hall, B. A.; Chetwynd, A.; Sansom, M. S. P., Primary and Secondary Dimer Interfaces of the Fibroblast Growth Factor Receptor 3 Transmembrane Domain: Characterization Via Multiscale Molecular Dynamics Simulations. *Biochemistry* **2014,** *53* (2), 323-332.

7. Bhate, M. P.; Lemmin, T.; Kuenze, G.; Mensa, B.; Ganguly, S.; Peters, J. M.; Schmidt, N.; Pelton, J. G.; Gross, C. A.; Meiler, J.; DeGrado, W. F., Structure and Function of the Transmembrane Domain of NsaS, an Antibiotic Sensing Histidine Kinase in *Staphylococcus Aureus*. *J. Am. Chem. Soc.* **2018,** *140* (24), 7471-7485.

8. Brown, M. C.; Abdine, A.; Chavez, J.; Schaffner, A.; Torres-Arancivia, C.; Lada, B.; JiJi, R. D.; Osman, R.; Cooley, J. W.; Ubarretxena-Belandia, I., Unwinding of the Substrate Transmembrane Helix In intramembrane Proteolysis. *Biophys. J.* **2018,** *114* (7), 1579-1589.

9. Bischoff, L.; Wickles, S.; Berninghausen, O.; van der Sluis, E. O.; Beckmann, R., Visualization of a Polytopic Membrane Protein During Secy-Mediated Membrane Insertion. *Nat. Commun* **2014,** *5*, 4103.

10. Nikiforovich, G. V.; Baranski, T. J., Structural Mechanisms of Constitutive Activation in the C5a Receptors with Mutations in the Extracellular Loops: Molecular Modeling Study. *Proteins* **2012,** *80* (1), 71-80.

11. Abrol, R.; Kim, S.-K.; Bray, J. K.; Griffith, A. R.; Goddard, W. A., Characterizing and Predicting the Functional and Conformational Diversity of Seven-Transmembrane Proteins. *Methods* **2011,** *55* (4), 405-414.

12. Yeagle, P. L.; Salloum, A.; Chopra, A.; Bhawsar, N.; Ali, L.; Kuzmanovski, G.; Alderfer, J. L.; Albert, A. D., Structures of the Intradiskal Loops and Amino Terminus of the G-Protein Receptor, Rhodopsin. *J. Pept. Res* **2000,** *55* (6), 455-465.

13. Bennett, J. S., Structure and Function of the Platelet Integrin Aiibβ3. *J. Clin. Invest* **2005,** *115* (12), 3363-3369.

14. Ma, Y. Q.; Qin, J.; Plow, E. F., Platelet Integrin Aiibβ3: Activation Mechanisms. *J. Thromb. Haemostasis* **2007,** *5* (7), 1345-1352.

15. Killian, J. A.; Salemink, I.; De Planque, M. R.; Lindblom, G.; Koeppe, R. E., II; Greathouse, D. V., Induction of Non-Bilayer Structures in Diacylphosphatidylcholine Model Membranes by Transmembrane α-Helical Peptides. Importance of Hydrophobic Mismatch and Proposed Role of Tryptophans. *Biochemistry* **1996,** *35*, 1037-1045.

16. Vostrikov, V. V.; Grant, C. V.; Daily, A. E.; Opella, S. J.; Koeppe, R. E., II, Comparison of "Polarization Inversion with Spin Exchange at Magic Angle" and "Geometric Analysis of Labeled Alanines" Methods for Transmembrane Helix Alignment. *J. Am. Chem. Soc.* **2008,** *130* (38), 12584-85.

17. Vostrikov, V. V.; Daily, A. E.; Greathouse, D. V.; Koeppe, R. E., II, Charged or Aromatic Anchor Residue Dependence of Transmembrane Peptide Tilt. *J. Biol. Chem.* **2010,** *285* (41), 31723-31730.

18. Vostrikov, V. V.; Grant, C. V.; Opella, S. J.; Koeppe, R. E., II, On the Combined Analysis of 2H and 15N/1H Solid-State NMR Data for Determination of Transmembrane Peptide Orientation and Dynamics. *Biophys. J.* **2011,** *101* (12), 2939-2947.

19. Grage, S. L.; Strandberg, E.; Wadhwani, P.; Esteban-Martin, S.; Salgado, J.; Ulrich, A. S., Comparative Analysis of the Orientation of Transmembrane Peptides Using Solid-State 2H and 15N NMR: Mobility Matters. *Eur Biophys J Biophy* **2012,** *41* (5), 475-482.

20. Gleason, N. J.; Vostrikov, V. V.; Greathouse, D. V.; Grant, C. V.; Opella, S. J.; Koeppe, R. E., II, Tyrosine Replacing Tryptophan as an Anchor in Gwalp Peptides. *Biochemistry* **2012,** *51* (10), 2044-2053.

21. Gleason, N. J.; Greathouse, D. V.; Grant, C. V.; Opella, S. J.; Koeppe, R. E., II, Single Tryptophan and Tyrosine Comparisons in the N-Terminal and C-Terminal Interface Regions of Transmembrane Gwalp Peptides. *J. Phys. Chem. B* **2013,** *117* (44), 13786-13794.

22. Sparks, K. A.; Gleason, N. J.; Gist, R.; Langston, R.; Greathouse, D. V.; Koeppe, R. E., II, Comparisons of Interfacial Phe, Tyr, and Trp Residues as Determinants of Orientation and Dynamics for Gwalp Transmembrane Peptides. *Biochemistry* **2014,** *53* (22), 3637-3645.

23. Pauling, L.; Corey, R. B.; Branson, H. R., The Structure of Proteins: Two Hydrogen-Bonded Helical Configurations of the Polypeptide Chain. *Proc. Natl. Acad. Sci. U. S. A.* **1951,** *37* (4), 205-211.

24. Mortazavi, A.; Rajagopalan, V.; Sparks, K. A.; Greathouse, D. V.; Koeppe, R. E., II, Juxta-Terminal Helix Unwinding as a Stabilizing Factor to Modulate the Dynamics of Transmembrane Helices. *ChemBioChem* **2016,** *17* (6), 462-465.

25. Kortenaar, P. B. W.; Dijk, B. G.; Peeters, J. M.; Raagen, B. J.; Adams, P. J.; Tesser, G. I., Rapid and Efficient Method for the Preparation of Fmoc-Amino Acids Starting from 9-Fluorenylmethanol. *Int. J. Pept. Prot. Res.* **1986,** *27*, 398-400.

26. Greathouse, D. V.; Koeppe, R. E., II; Providence, L. L.; Shobana, S.; Andersen, O. S., Design and Characterization of Gramicidin Channels. *Methods Enzymol.* **1999,** *294*, 525-550.

27. Pace, C. N.; Vajdos, F.; Fee, L.; Grimsley, G.; Gray, T., How to Measure and Predict the Molar Absorption Coefficient of a Protein. *Protein Sci* **1995,** *4* (11), 2411-2423.

28. van der Wel, P. C. A.; Strandberg, E.; Killian, J. A.; Koeppe, R. E., II, Geometry and Intrinsic Tilt of a Tryptophan-Anchored Transmembrane Alpha-Helix Determined by 2H NMR. *Biophys. J.* **2002,** *83*, 1479-1488.

29. Davis, J. H.; Jeffrey, K. R.; Valic, M. I.; Bloom, M.; Higgs, T. P., Quadrupolar Echo Deuteron Magnetic Resonance Spectroscopy in Ordered Hydrocarbon Chains. *Chem. Phys. Lett.* **1976,** *42*, 390-394.

30. Strandberg, E.; Esteban-Martin, S.; Ulrich, A. S.; Salgado, J., Hydrophobic Mismatch of Mobile Transmembrane Helices: Merging Theory and Experiments. *Biochim. Biophys. Acta.* **2012,** *1818*, 1242-1249.

31. Strandberg, E.; Esteban-Martín, S.; Salgado, J.; Ulrich, A. S., Orientation and Dynamics of Peptides in Membranes Calculated from 2H-NMR Data. *Biophys. J.* **2009,** *96* (8), 3223-3232.

32. Strandberg, E.; Özdirekcan, S.; Rijkers, D. T. S.; van der Wel, P. C. A.; Koeppe, R. E., II; Liskamp, R. M. J.; Killian, J. A., Tilt Angles of Transmembrane Model Peptides in Oriented and Non-Oriented Lipid Bilayers as Determined by 2H Solid-State NMR. *Biophys. J.* **2004,** *86*, 3709-3721.

33. Özdirekcan, S.; Etchebest, C.; Killian, J. A.; Fuchs, P. F. J., On the Orientation of a Designed Transmembrane Peptide: Toward the Right Tilt Angle? *J. Am. Chem. Soc.* **2007,** *129*, 15174-15181.

34. Esteban-Martín, S.; Salgado, J., The Dynamic Orientation of Membrane-Bound Peptides: Bridging Simulations and Experiments. *Biophys. J.* **2007,** *93*, 4278-4288.

35. Strandberg, E.; Grau-Campistany, A.; Wadhwani, P.; Bürck, J.; Rabanal, F.; Ulrich, A. S., Helix Fraying and Lipid-Dependent Structure of a Short Amphipathic Membrane-Bound Peptide Revealed by Solid-State NMR. *J. Phys. Chem. B* **2018,** *122* (23), 6236-6250.

36. Sung, Y.-H.; Eliezer, D., Structure and Dynamics of the Extended-Helix State of Alpha-Synuclein: Intrinsic Lability of the Linker Region. *Protein Sci.* **2018,** *27* (7), 1314-1324.

37. Georgieva, E. R.; Ramlall, T. F.; Borbat, P. P.; Freed, J. H.; Eliezer, D., The Lipid-Binding Domain of Wild Type and Mutant A-Synuclein: Compactness and Interconversion between the Broken and Extended Helix Forms. *J. Biol. Chem.* **2010,** *285* (36), 28261-28274.

38. Dikiy, I.; Eliezer, D., N-terminal Acetylation Stabilizes N-terminal Helicity in Lipid- and Micelle-Bound A-Synuclein and Increases Its Affinity for Physiological Membranes. *J. Biol. Chem.* **2014,** *289* (6), 3652-3665.

39. Louis, J. M.; Baber, J. L.; Ghirlando, R.; Aniana, A.; Bax, A.; Roche, J., Insights into the Conformation of the Membrane Proximal Regions Critical to the Trimerization of the HIV-1 Gp41 Ectodomain Bound to Dodecyl Phosphocholine Micelles. *PLoS ONE* **2016,** *11* (8), e0160597.

40. Yang, J.; Ma, Y.-Q.; Page, R. C.; Misra, S.; Plow, E. F.; Qin, J., Structure of an Integrin Aiibβ3 Transmembrane-Cytoplasmic Heterocomplex Provides Insight into Integrin Activation. *Proc. Natl. Acad. Sci. U. S. A.* **2009,** *106* (42), 17729-17734.

41. Tokuda, N.; Kawai, K.; Lee, Y.-H.; Ikegami, T.; Yamaguchi, S.; Yagisawa, H.; Fukui, Y.; Tuzi, S., Membrane-Induced Alteration of the Secondary Structure in the SWAP-70 Pleckstrin Homology Domain. *J. Biochemistry* **2012,** *151* (4), 391-401.

42. Takahashi, H.; Rico, F.; Chipot, C.; Scheuring, S., A-Helix Unwinding as Force Buffer in Spectrins. *ACS Nano* **2018,** *12* (3), 2719-2727.

43. Liu, Y.; Tan, J.; Zhang, J.; Li, C.; Luo, Y.; Ye, S., Influenza a M2 Transmembrane Domain Tunes Its Conformational Heterogeneity and Structural Plasticity in the Lipid Bilayer by Forming Loop Structures. *Chem. Commun.* **2018,** *54* (46), 5903-5906.

44. McKay, M. J.; Martfeld, A. N.; De Angelis, A. A.; Opella, S. J.; Greathouse, D. V.; Koeppe, R. E., Control of Transmembrane Helix Dynamics by Interfacial Tryptophan Residues. *Biophys. J.* **2018,** *114* (11), 2617-2629.

45. Yau, W.-M.; Wimley, W. C.; Gawrisch, K.; White, S. H., The Preference of Tryptophan for Membrane Interfaces. *Biochemistry* **1998,** *37* (42), 14713-14718.

46. Sun, H.; Greathouse, D. V.; Andersen, O. S.; Koeppe, R. E., The Preference of Tryptophan for Membrane Interfaces: Insights from N-methylation of Tryptophans in Gramicidin Channels. *J. Biol. Chem.* **2008,** *283* (32), 22233-22243.

47. DeLano, W. L., The Pymol Molecular Graphics System. *Delano Scientific, San Carlos, CA* **2002**.

5.8 **Tables**

Table 1. Sequences of $X^{4,5}$GWALP23 peptides[a]

Name	Sequence	Reference
GWALP23	Acetyl-GGALWLALALALALALALWLAGA-amide	[22]
$G^{4,5}$GWALP23	Acetyl-GGAG^{4}G^{5}LALALALALALALWLAGA-amide	This work
$A^{4,5}$GWALP23	Acetyl-GGAA^{4}A^{5}LALALALALALALWLAGA-amide	[24]
$F^{4,5}$GWALP23	Acetyl-GGAF^{4}F5LALALALALALALWLAGA-amide	[22]
$Y^{4,5}$GWALP23	Acetyl-GGAY^{4}Y^{5}LALALALALALALWLAGA-amide	[20]
$W^{4,5}$GWALP23	Acetyl-GGAW^{4}W^{5}LALALALALALALWLAGA-amide	This work
$H^{4,5}$GWALP23	Acetyl-GGAH^{4}H^{5}LALALALALALALWLAGA-amide	This work

[a]Abbreviations: “a” denotes “acetyl” and “e” denotes “ethanolamide.”

Table 2. Observed quadrupolar splitting magnitudes, $|\Delta\nu_q|$ in kHz, for d_4-labeled alanines of $X^{4,5}$GWALP23 peptides in DLPC, DMPC and DOPC bilayer membranes

		Deuterated (d_4) alanine location in sequence (helical wheel position, degrees)[a]									
$X^{4,5}$GWALP23	**Lipid**	**7 (240)**	**9 (80)**	**11 (280)**	**13 (120)**	**15 (320)**	**17 (160)**	**3 (200)**	**21 (200)**	**4 (300)**	**5 (40)**
L^4W^5	DLPC	26.4	25.5	26.9	14.6	20.7	3.4	27.5	12.8	--	--
	DMPC	21.9	8.9	20.9	3.8	17.6	2.9	10.8	3.2	--	--
	DOPC	16.6	1.7	16.7	1.5	15.4	2.6	10.4	2.7	--	--
$F^{4,5}$	DLPC	23.7	23.5	25.7	19.6	23.4	1.8	20.6	2.6	--	--
	DMPC	20.3	--	20.6	--	20.6	3.8	20.4	2.0	--	--
	DOPC	16.2	0.8	18.6	0.8	18.6	1.9	11.8	2.2	--	--
$A^{4,5}$	DLPC	23.2	19.0	23.6	11.7	18.7	6.6	22.3	10.2	18.6	16
	DMPC	20.4	10.8	20.6	9.0	18.8	7.1	19.6	6.3	18.1	5.2
	DOPC	15.4	4.0	18.6	5.2	16.4	0.5	14.4	1.8	18.6	2.0
$G^{4,5}$	DLPC	18.8	6.9	16.7	1.4	12.6	7.2	10.9	10.9	--	--
	DMPC	19	6.0	17.5	1.6	14.1	5.0	16.8	7.8	--	--
	DOPC	15.5	1.5	15.6	1.2	15.3	2.4	16.8	4.6	--	--
$H^{4,5}$	DLPC	17.9	1.1	13.3	3.5	9.4	9.8	11.3	11.6	--	--
	DMPC	14.5	2.4	11.2	4.8	8.3	8.5	11.9	8.4	--	--
	DOPC	11.1	6.5	9.1	6.1	10.1	5.6	11.4	5.4	--	--
$W^{4,5}$	DLPC	21.5	15.0	20.7	9.4	17.4	3.3	22.7	8.4	--	--
	DMPC	17.3	5.8	17.5	4.5	16.2	1.6	20.8	4.9	--	--
	DOPC	12.8	0.9	14.4	1.4	14.9	1.3	20.8	2.3	--	--
$Y^{4,5}$	DLPC	11.6	0.5	6.9	4.6	6.9	11.6	19.2	11.6	--	--
	DMPC	11.7	3.2	10.7	2.8	10.7	4.4	18.2	7.7	--	--
	DOPC	10.2	3.8	10.0	3.8	12.6	3.8	16.2	3.2	--	--

[a] Values are listed in kHz for the $\beta = 0^o$ sample orientation. Values not listed (--) were not recorded

Table 3. Semi-static GALA and modified Gaussian analysis of GWALP23 and related $X^{4,5}$ peptide helix orientations and dynamics in bilayer membranes[a]

Lipid	Peptide	GALA fit results				Modified Gaussian results[b]					Ref.
		τ_0	ρ_0	S_{zz}	RMSD	τ_0	ρ_0	$\sigma\rho$	$\sigma\tau$[b]	RMSD	
DLPC	L^4W^5	20.7°	305°	0.66	0.71	23°	304°	33	15°	0.7	[22]
	$F^{4,5}$	21.3°	317°	0.67	0.5	18°	314°	0°	15°	0.7	[22]
	$A^{4,5}$	17.7°	301°	0.68	0.6	17°	302°	26°	15°	0.5	[24]
	$G^{4,5}$	9.0°	293°	0.77	0.72	10°	296°	38°	10°	0.71	This work
	$H^{4,5}$	6.0°	280°	0.83	0.74	11°	279°	57°	10°	0.75	
	$W^{4,5}$	15.0°	307°	0.67	0.53	12°	309°	8°	10°	1.25	
	$Y^{4,5}$	5.3°	261°	0.65	1.6	14°	259°	>90°	20°	1.7	[20 22]
	$Y^{4,5}$					23°	259°	128°	5°	1.7	This work
DMPC	L^4W^5	9.0°	311°	0.89	1.06	13°	308°	42°	10°	1.19	This work
	$F^{4,5}$	11.3°	331°	0.8	1.3						
	$A^{4,5}$	11.1°	317°	0.76	0.6	11°	316°	14°	10°	0.5	[24]
	$*A^{4,5}$	12.3°	312°	0.72	1.05	15°	311°	39°	16°	1.0	This work
	$G^{4,5}$	8.0°	304°	0.80	0.64	11°	303°	47°	10°	0.6	
	$^cH^{4,5}$	3.7°	281°	0.79	0.61	11°	280°	93°	10°		
	$W^{4,5}$	8.7°	319°	0.75	0.57	8°	322°	14°	10°	0.59	
	$Y^{4,5}$	3.0°	324°	0.77	0.64	3°	333°	18°	10°	0.54	
	$Y^{4,5}$					15°	321°	124°	5°	0.63	
DOPC	L^4W^5	6.0°	323°	0.87	0.57	9°	321°	48°	9°	0.7	[22]
	$F^{4,5}$	6.0°	332°	0.92	0.9	10°	329°	54°	9°	1.6	[22]
	$A^{4,5}$	8.0°	329°	0.78	0.2	8°	330°	20°	10°	0.4	[24]
	$*A^{4,5}$	8.0°	328°	0.79	0.3	17°	329°	72°	10°	0.3	This work
	$G^{4,5}$	6.0°	325°	0.82	0.64	8°	324°	44°	10°	0.61	
	$^cH^{4,5}$	1.3°	7°	0.83	0.25	6°	8°	114°	10°		This work
	$W^{4,5}$	5.3°	340°	0.81	0.42	6°	341°	29°	10°	0.25	
	$Y^{4,5}$	3.0°	359°	0.82	1.1	6°	344°	72°	13°	0.9	[20 22]
	$Y^{4,5}$					13°	344°	122°	5°	0.86	This work

[a] The analysis methods were described previously [22]. The units for RMSD are kHz. Unless otherwise noted, each analysis is based on the deuterium (^2H) quadrupolar splittings for the CD_3 side chains of six central alanine residues 7, 9, 11, 13, 15 and 17 in the core helix of the transmembrane peptide.

[b] For the modified Gaussian analysis [22, 30], $\sigma\tau$ was assigned the fixed value noted in the table; S_{zz} was assigned the fixed value of 0.88. Where noted ($*A^{4,5}$), a GALA fit and a full Gaussian analysis (varying also $\sigma\tau$) were performed based on eight data points (DOPC) or seven data points (DMPC, without A17).

[c] Residue A7 of $H^{4,5}$GWALP23 does not fit the quadrupolar wave plot in DMPC or DOPC and was omitted from the analysis. Curiously, residue A3 of $H^{4,5}$GWALP23 **does fit** the quadrupolar wave plot in DMPC (but not in DOPC).

5.9 **Figure Legends**

Figure 1. Model to illustrate unwinding of peptide terminals for the helix of $G^{4,5}$GWALP23, showing the observed tilted orientation of the core helix in DLPC bilayers. The locations of Trp19 and residues 4 and 5 are illustrated on a ribbon helix, drawn using PyMOL [47]. The deuterated alanine methyl groups are shown as space filling and are colored black for core alanines (that underlie the tilt analysis) or red for the juxta-terminal alanines 3 and 21. The depicted side-chain orientations are arbitrary

Figure 2. Deuterium NMR spectra for ^{2}H-labeled core alanines A7 (50% deuterated) and A17 (100%) in $G^{4,5}$GWALP23 and $A^{4,5}$GWALP23 in oriented bilayers of DLPC. Spectra for $\beta = 90°$ and $\beta = 0°$ sample orientations are shown. Peptide:lipid ratio, 1:60; temperature, 50 °C

Figure 3. Quadrupolar wave analysis of tilted peptide helices in DLPC, DMPC and DOPC bilayer membranes. A. Results for $G^{4,5}$GWALP23. B. Results for the parent GWALP23 peptide with L4 and W5 (core alanine data points from [17]). The $|\Delta\nu_q|$ values for alanines 3 and 21 (numbered, shown as circles) generally fail to fit the helix wave plots. In some cases (i.e., GWALP in DOPC) the $\Delta\nu_q$ value for A3 fits on the helical wave, while that for A21 stays off the curve

Figure 4**.** Deuterium NMR spectra for ^{2}H-labeled core alanines A15 and A17 in $H^{4,5}$GWALP23 and $W^{4,5}$GWALP23; and A11 and A15 in $F^{4,5}$GWALP23 and $Y^{4,5}$GWALP23 peptides in oriented bilayers of DLPC. Spectra for $\beta = 90°$ and $\beta = 0°$ sample orientations are shown. Peptide:lipid ratio, 1:60; temperature, 50 °C.

Figure 5. Quadrupolar wave analysis of $H^{4,5}$GWALP23 (A), $W^{4,5}$GWALP23 (B) and $Y^{4,5}$GWALP23 (C) helices in DLPC (black), DMPC (red) and DOPC (blue) bilayer membranes. The $|\Delta\nu_q|$ values for alanines 3 and 21 (numbered, shown as circles) generally fail to fit the helix wave plots. In $H^{4,5}$GWALP23, A7 of the core helix (numbered) is off the curves for all three lipid membranes. suggesting extended helix unwinding at N-terminal end up to residue 7**.**

Figure 6. Deuterium NMR spectra for labeled A3 (50% deuterated) and A21 (100% deuterated) of $X^{4,5}$GWALP23 peptides, where X= G, Y, H and W. Spectra are shown for oriented samples in DLPC , DMPC and DOPC lipid bilayers. Peptide:lipid ratio, 1:60; temperature, 50 °C; sample orientation, $\beta = 90°$.

Figure 7. Contour plots for solutions of helix tilt τ and azimuthal rotation ρ for selected $X^{4,5}$ derivatives of GWALP23 in bilayers of DLPC (black), DMPC (red), and DOPC (blue). Contour levels are drawn from 0 to 3 kHz with increments of 0.6.

Figure 8. Deuterium NMR spectra for labeled alanines 4 and 5 (50% and 100% deuterated, respectively) of $A^{4,5}$GWALP23 in oriented bilayers of DLPC, DMPC and DOPC. Peptide:lipid ratio, 1:60; temperature, 50 °C; sample orientation, $\beta = 90°$.

Figure 9. GALA quadrupolar wave plots for $A^{4,5}$GWALP23 in DLPC (black), DMPC (red), and DOPC (blue) bilayer membranes. The $|\Delta\nu_q|$ values are shown as triangles for d_4-labeled core

alanines, as squares for A4 and A5 and as circles for A3 and A21, with the color of the respective lipid bilayer. The $\Delta\nu_q$ values of alanines 3 and 21 are off of the wave plot regardless of the lipid thickness. The $\Delta\nu_q$ values of alanines 4 and 5 are off of the wave plot in DLPC, but on the wave plot for the core helix in DMPC and DOPC. Alanine 17 deviates from the wave plot in DMPC

Figure 10. Contour plots showing preferred ranges of $\sigma\tau$ and $\sigma\rho$ for the $A^{4,5}$GWALP23 helix in bilayers of DLPC (upper), DMPC (middle) and DOPC (lower). Contours for RMSD are drawn from 1.2 kHz (dark blue) to 6.0 kHz in increments of 1.2 kHz (other colors).

Figure 11. Deviation of experimental value from fitted value for juxta-terminal alanines 3 and 21 for several transmembrane peptide helices. A. Quadrupolar splitting, $\Delta\nu_q$, deviation in kHz. B. Theta angle, θ, deviation in degrees. Results are shown for GWALP23 peptides having $G^{4,5}$, $A^{4,5}$, $F^{4,5}$ or the parent L^4W^5 sequence

5.10 **Figures**

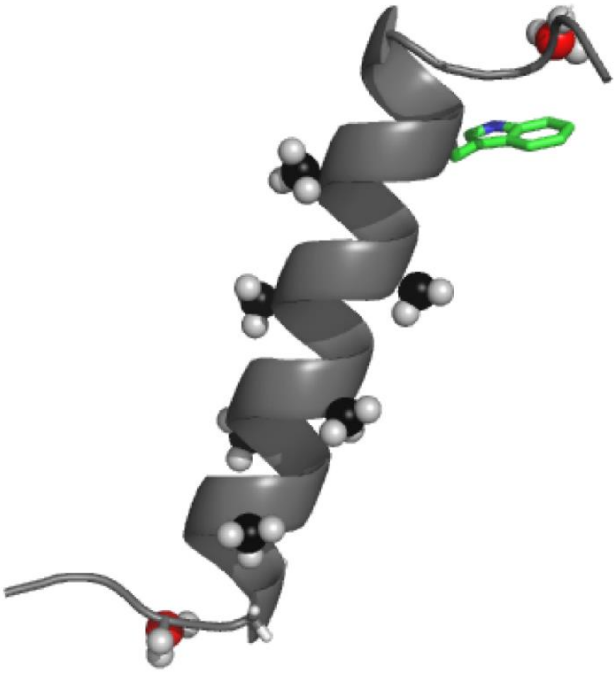

Figure 1. Model to illustrate unwinding of peptide terminals for the helix of $G^{4,5}$GWALP23, showing the observed tilted orientation of the core helix in DLPC bilayers. The locations of Trp19 and residues 4 and 5 are illustrated on a ribbon helix, drawn using PyMOL [47]. The deuterated alanine methyl groups are shown as space filling and are colored black for core alanines (that underlie the tilt analysis) or red for the juxta-terminal alanines 3 and 21. The depicted side-chain orientations are arbitrary

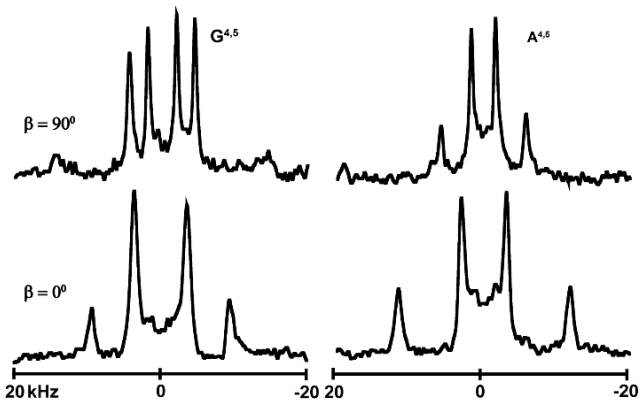

Figure 2. Deuterium NMR spectra for ^{2}H-labeled core alanines A7 (50% deuterated) and A17 (100%) in $G^{4,5}$GWALP23 and $A^{4,5}$GWALP23 in oriented bilayers of DLPC. Spectra for β = 90° and β = 0° sample orientations are shown. Peptide:lipid ratio, 1:60; temperature, 50 °C

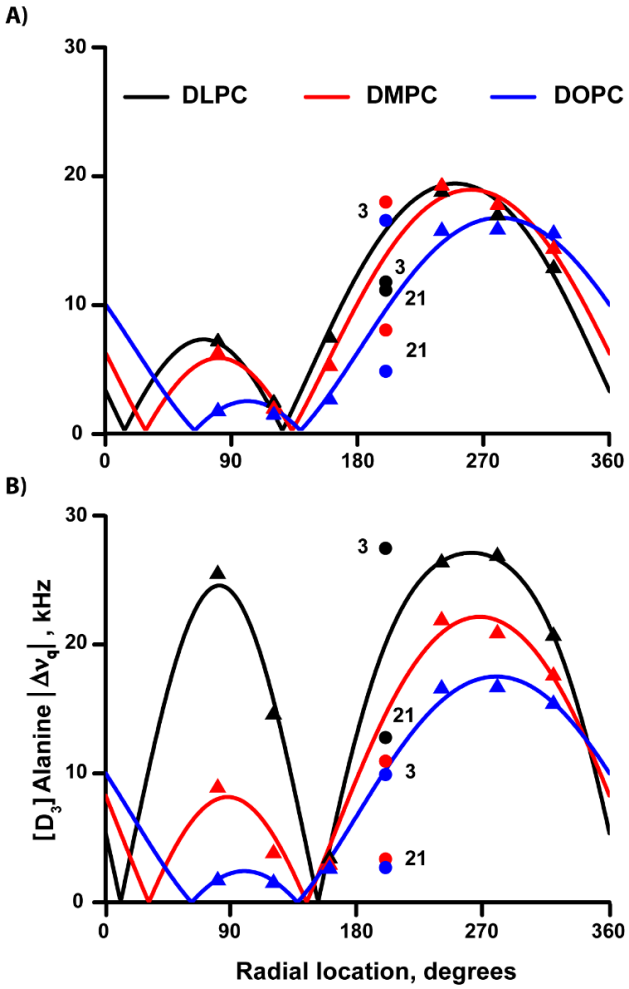

Figure 3. Quadrupolar wave analysis of tilted peptide helices in DLPC, DMPC and DOPC bilayer membranes. A. Results for $G^{4,5}$GWALP23. B. Results for the parent GWALP23 peptide with L4 and W5 (core alanine data points from [17]). The $|\Delta\nu_q|$ values for alanines 3 and 21 (numbered, shown as circles) generally fail to fit the helix wave plots. In some cases (i.e., GWALP in DOPC) the $\Delta\nu_q$ value for A3 fits on the helical wave, while that for A21 stays off the curve.

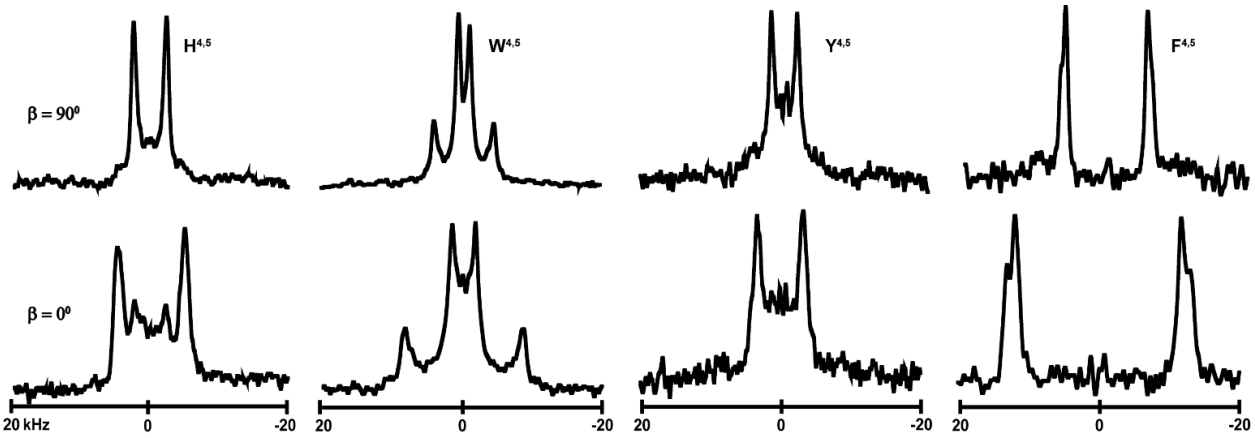

Figure 4**.** Deuterium NMR spectra for ^{2}H-labeled core alanines A15 and A17 in $H^{4,5}$GWALP23 and $W^{4,5}$GWALP23; and A11 and A15 in $F^{4,5}$GWALP23 and $Y^{4,5}$GWALP23 peptides in oriented bilayers of DLPC. Spectra for β = 90° and β = 0° sample orientations are shown. Peptide:lipid ratio, 1:60; temperature, 50 °C.

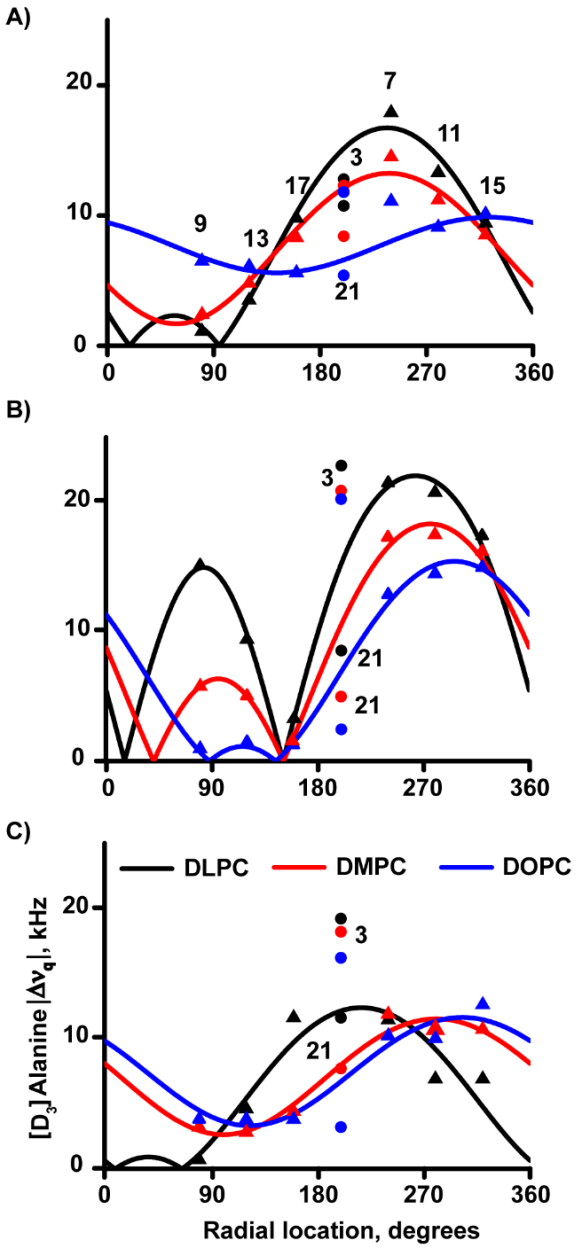

Figure 5. Quadrupolar wave analysis of $H^{4,5}$GWALP23 (A), $W^{4,5}$GWALP23 (B) and $Y^{4,5}$GWALP23 (C) helices in DLPC (black), DMPC (red) and DOPC (blue) bilayer membranes. The $|\Delta\nu_q|$ values for alanines 3 and 21 (numbered, shown as circles) generally fail to fit the helix wave plots. In $H^{4,5}$GWALP23, A7 of the core helix (numbered) is off the curves for all three lipid membranes. suggesting extended helix unwinding at N-terminal end up to residue 7**.**

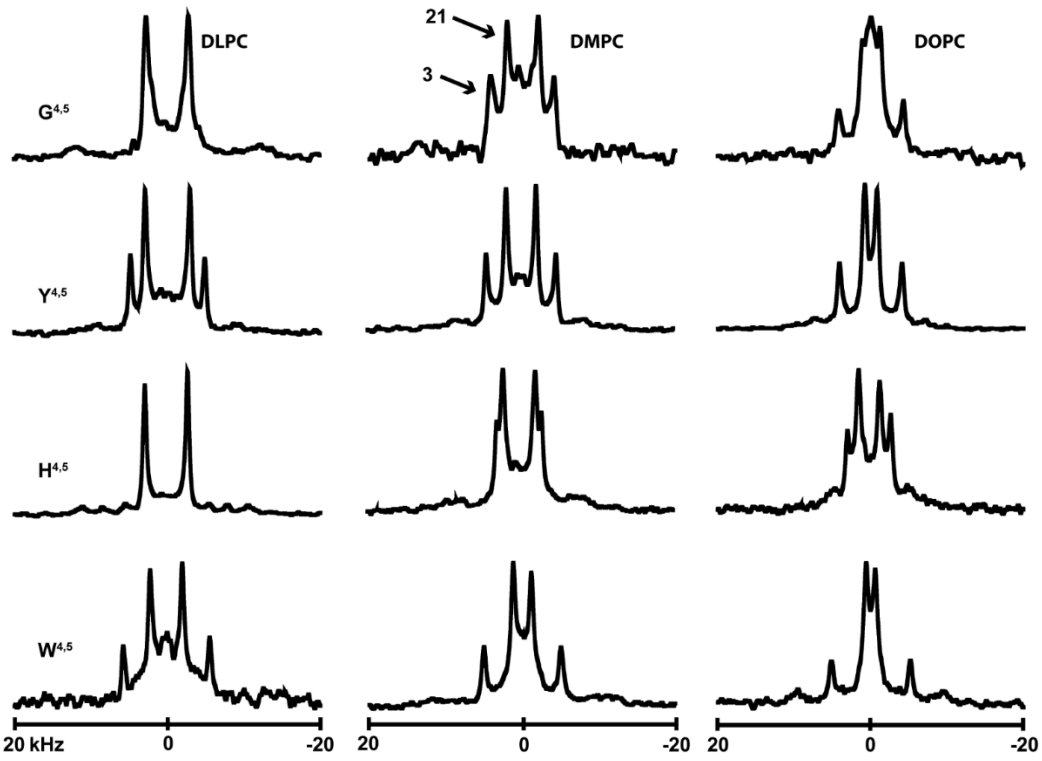

Figure 6. Deuterium NMR spectra for labeled A3 (50% deuterated) and A21 (100% deuterated) of $X^{4,5}$GWALP23 peptides, where X= G, Y, H and W. Spectra are shown for oriented samples in DLPC , DMPC and DOPC lipid bilayers. Peptide:lipid ratio, 1:60; temperature, 50 °C; sample orientation, $\beta = 90°$.

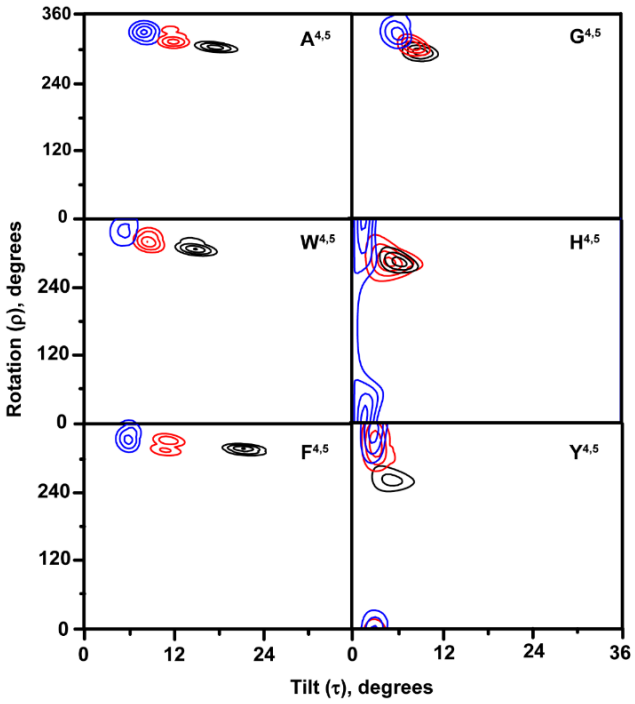

Figure 7. Contour plots for solutions of helix tilt τ and azimuthal rotation ρ for selected $X^{4,5}$ derivatives of GWALP23 in bilayers of DLPC (black), DMPC (red), and DOPC (blue). Contour levels are drawn from 0 to 3 kHz with increments of 0.6.

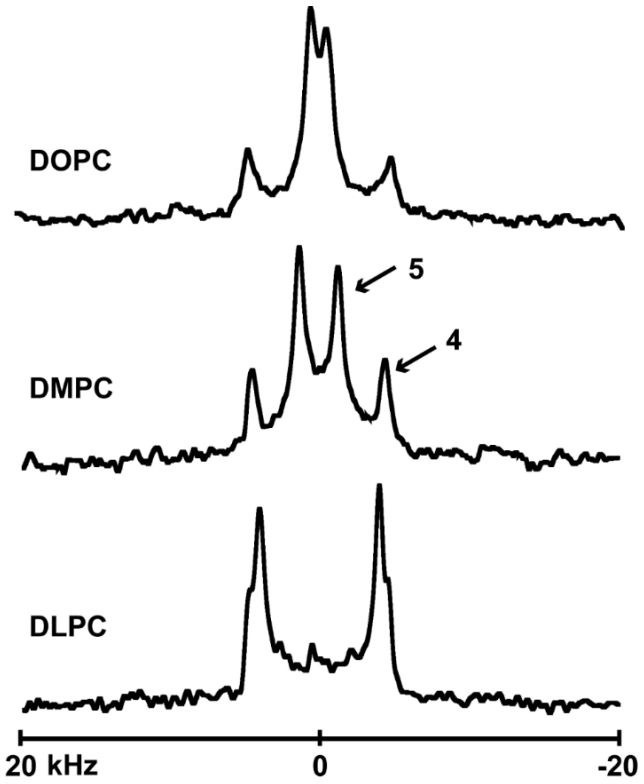

Figure 8. Deuterium NMR spectra for labeled alanines 4 and 5 (50% and 100% deuterated, respectively) of $A^{4,5}$GWALP23 in oriented bilayers of DLPC, DMPC and DOPC. Peptide:lipid ratio, 1:60; temperature, 50 °C; sample orientation, $\beta = 90°$.

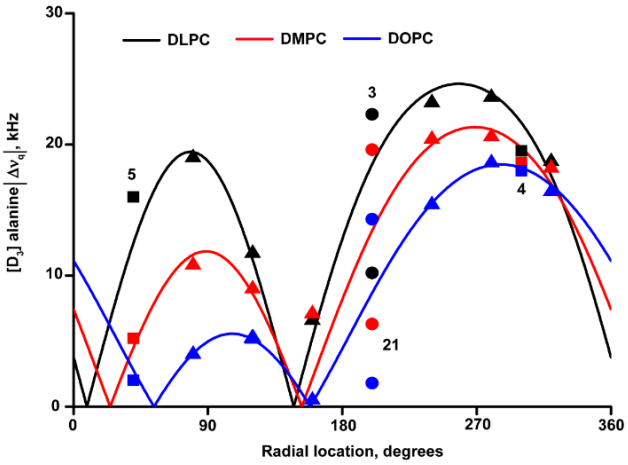

Figure 9. GALA quadrupolar wave plots for $A^{4,5}$GWALP23 in DLPC (black), DMPC (red), and DOPC (blue) bilayer membranes. The $|\Delta\nu_q|$ values are shown as triangles for d_4-labeled core alanines, as squares for A4 and A5 and as circles for A3 and A21, with the color of the respective lipid bilayer. The $\Delta\nu_q$ values of alanines 3 and 21 are off of the wave plot regardless of the lipid thickness. The $\Delta\nu_q$ values of alanines 4 and 5 are off of the wave plot in DLPC, but on the wave plot for the core helix in DMPC and DOPC. Alanine 17 deviates from the wave plot in DMPC

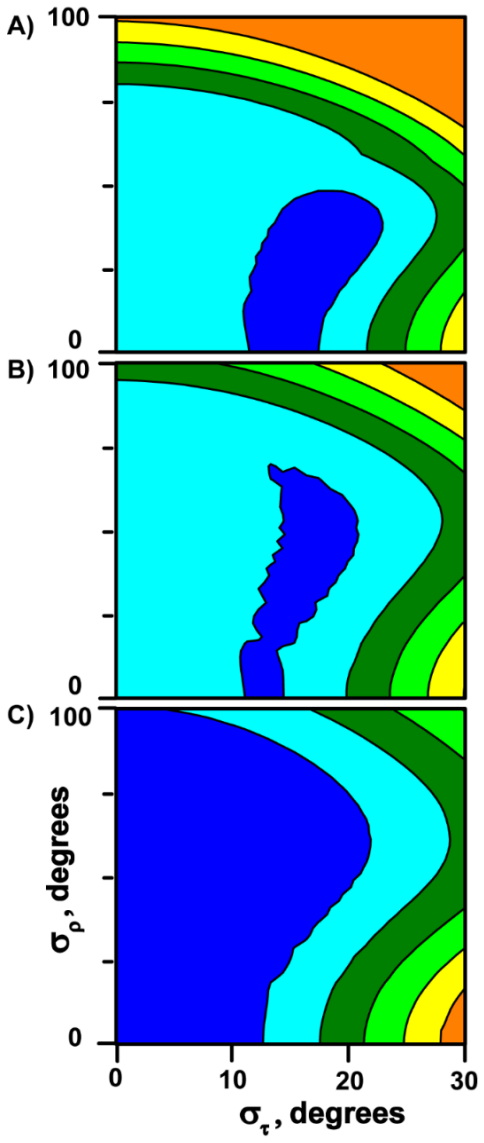

Figure 10. Contour plots showing preferred ranges of στ and σρ for the $A^{4,5}$GWALP23 helix in bilayers of DLPC (upper), DMPC (middle) and DOPC (lower). Contours for RMSD are drawn from 1.2 kHz (dark blue) to 6.0 kHz in increments of 1.2 kHz (other colors).

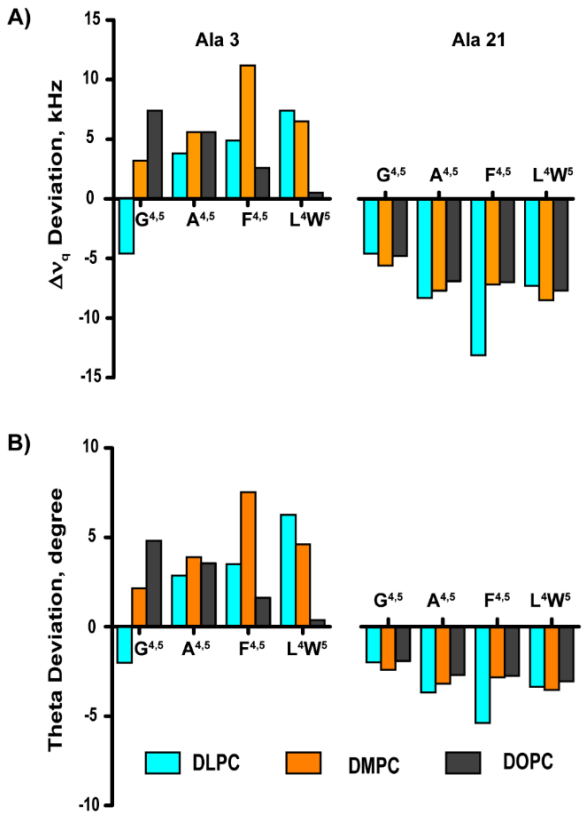

Figure 11. Deviation of experimental value from fitted value for juxta-terminal alanines 3 and 21 for several transmembrane peptide helices. A. Quadrupolar splitting, $\Delta\nu_q$, deviation in kHz. B. Theta angle, θ, deviation in degrees. Results are shown for GWALP23 peptides having $G^{4,5}$, $A^{4,5}$, $F^{4,5}$ or the parent L^4W^5 sequence

5.11 **Supporting Figures**

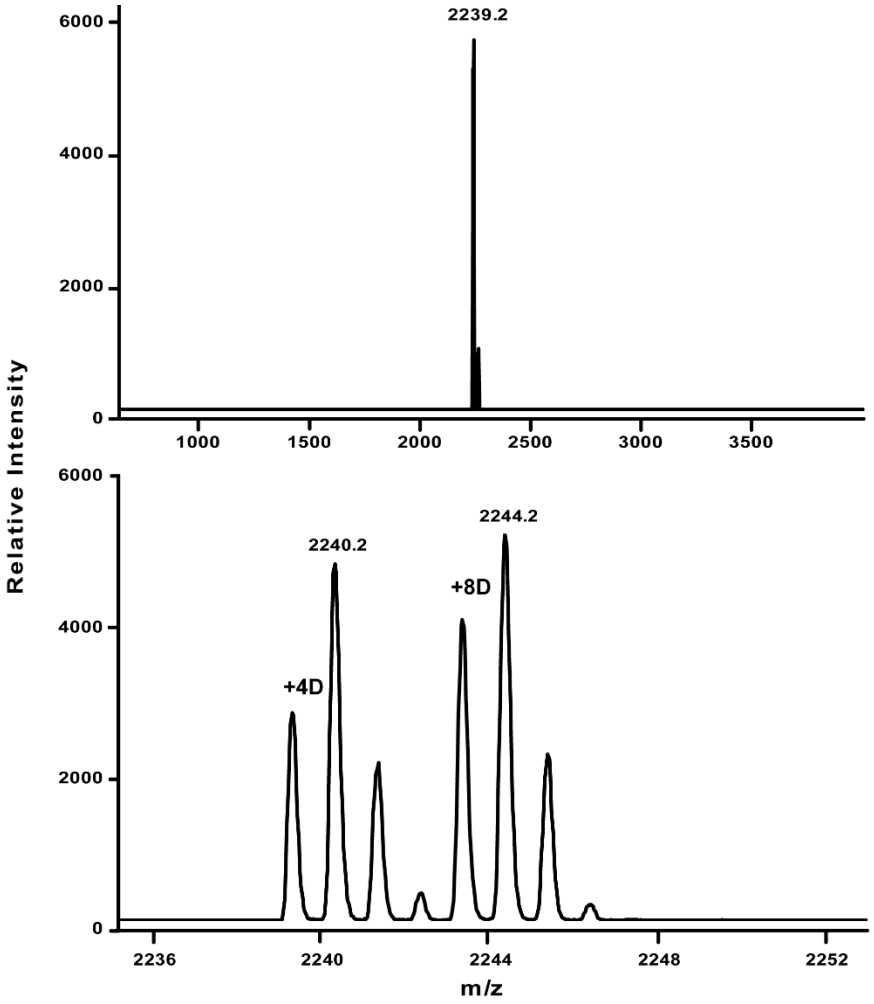

Figure S1: Mass spectrum of the synthesized $H^{4,5}$GWALP23 peptide. The expected monoisotopic mass is 2235.7 Da. Addition of a ^{13}C and eight deuterons gives 2244.7 Da, which agrees with the observed mass of the most prominent isotopic peak in the population. Successive peaks differ by one Da in m/z based on the natural abundance of ^{13}C.

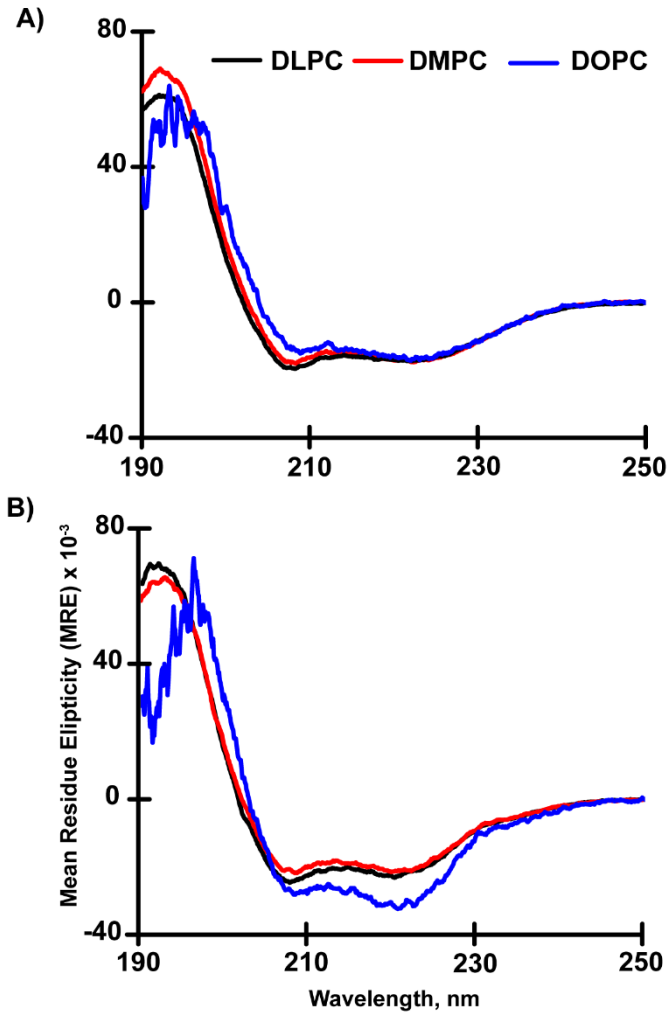

Figure S2: Circular Dichorism spectra of A) $H^{4,5}$GWALP23 and B) $W^{4,5}$GWALP23 in DLPC (black), DMPC (red) and DOPC (blue) lipid vesicles. Peptide to lipid ratio was 1:60, recorded at ambient temperature of 22°C. The y-axis units for mean residue ellipticity (MRE) are deg cm^2 $dmol^{-1}$.

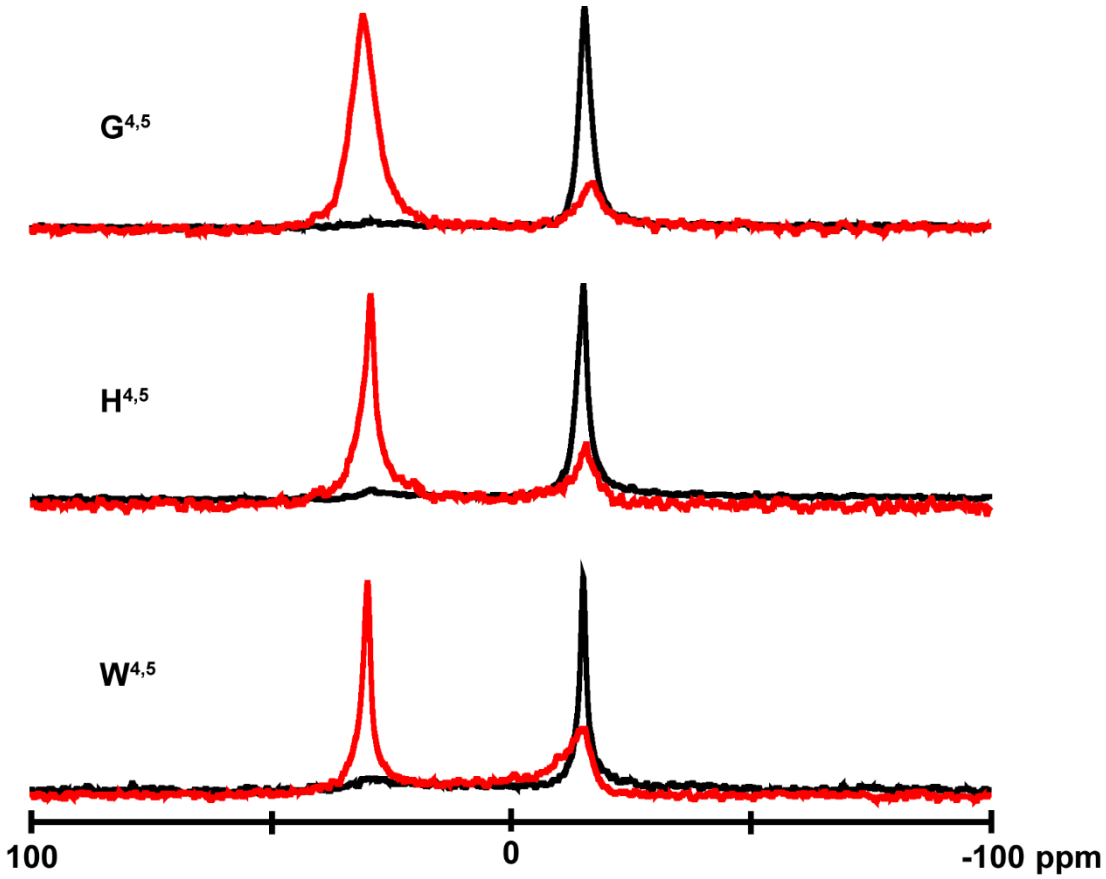

Figure S3: ^{31}P NMR spectra for aligned sample of DLPC with $G^{4,5}$, $H^{4,5}$ and $W^{4,5}$ peptides incorporated at 1/60 peptide/lipid ratio

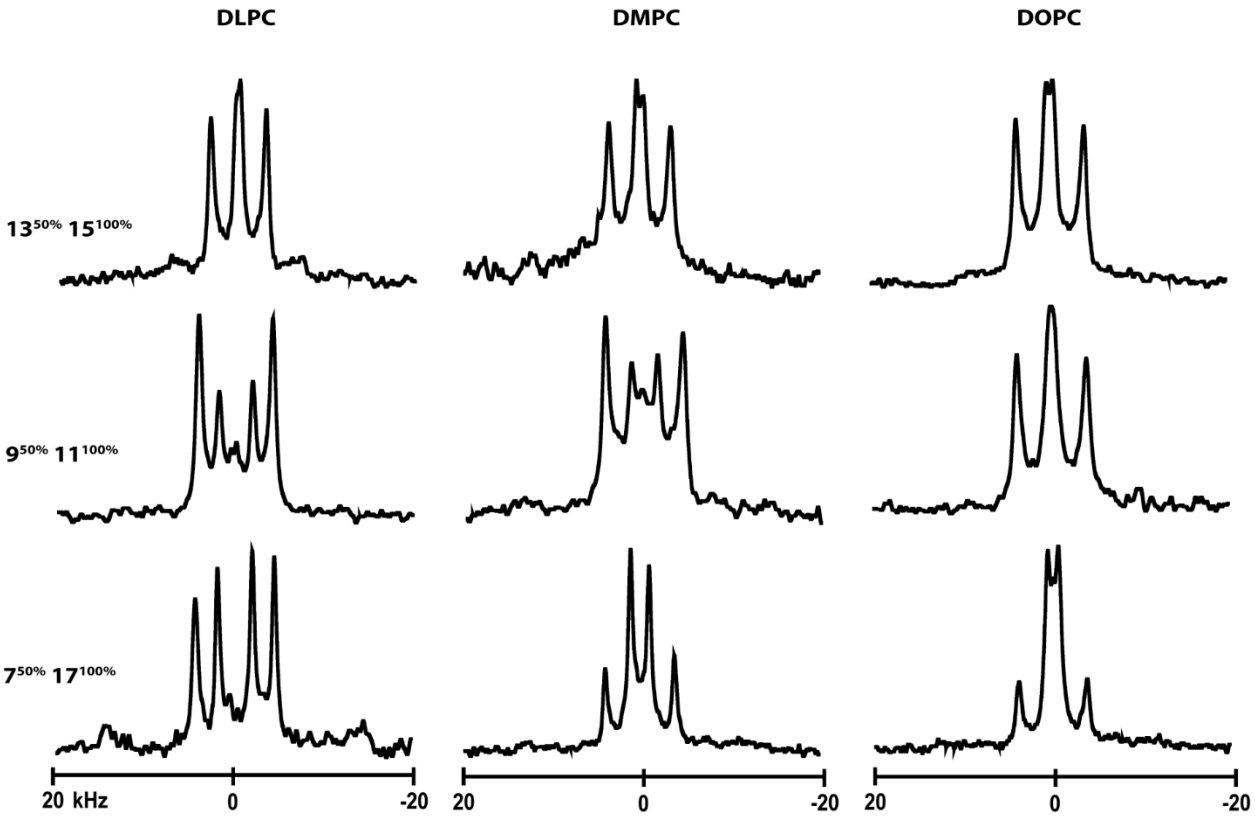

Figure S4: Deuterium NMR spectra for labeled core alanines of $G^{4,5}$GWALP23 peptide. Spectra shown are at $\beta = 90^0$ sample orientation.

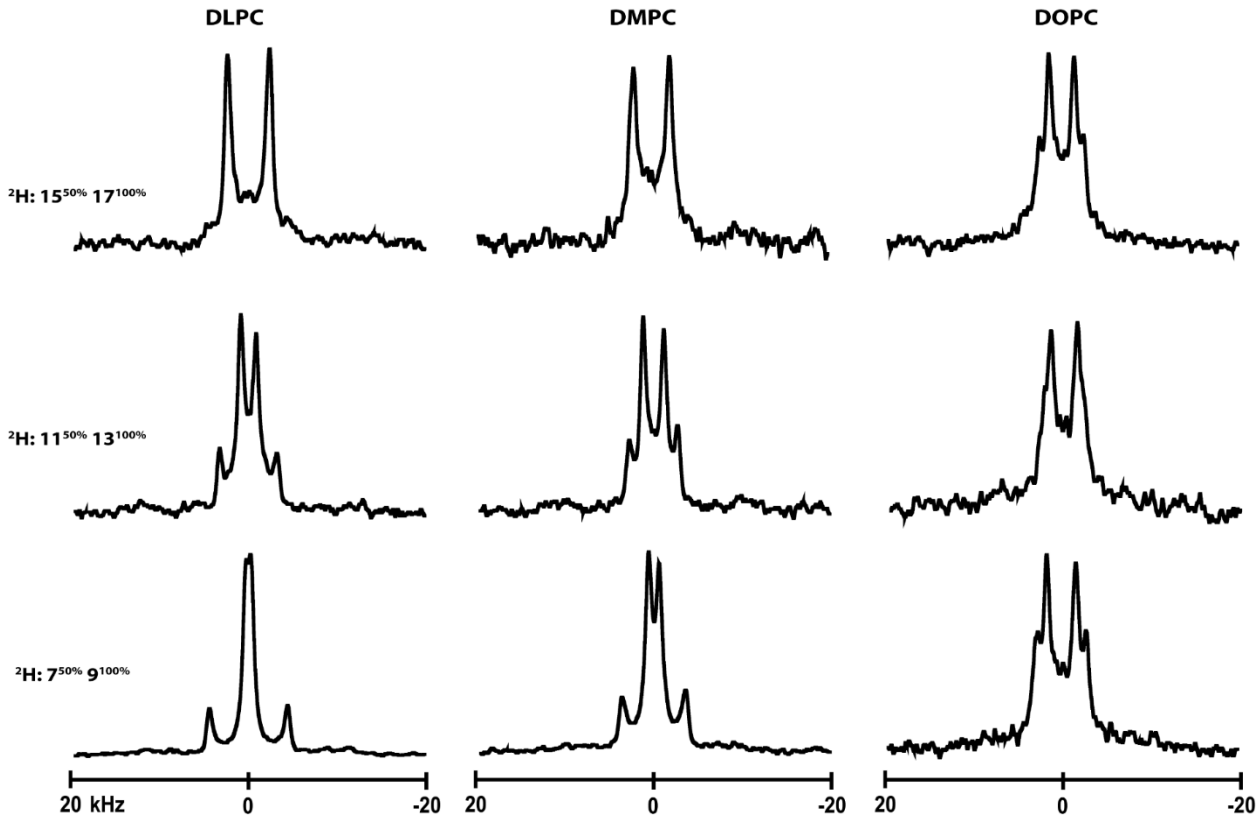

Figure S5: Deuterium NMR spectra for labeled core alanines of $H^{4,5}$GWALP23 peptide. Spectra shown are at $\beta = 90^0$ sample orientation.

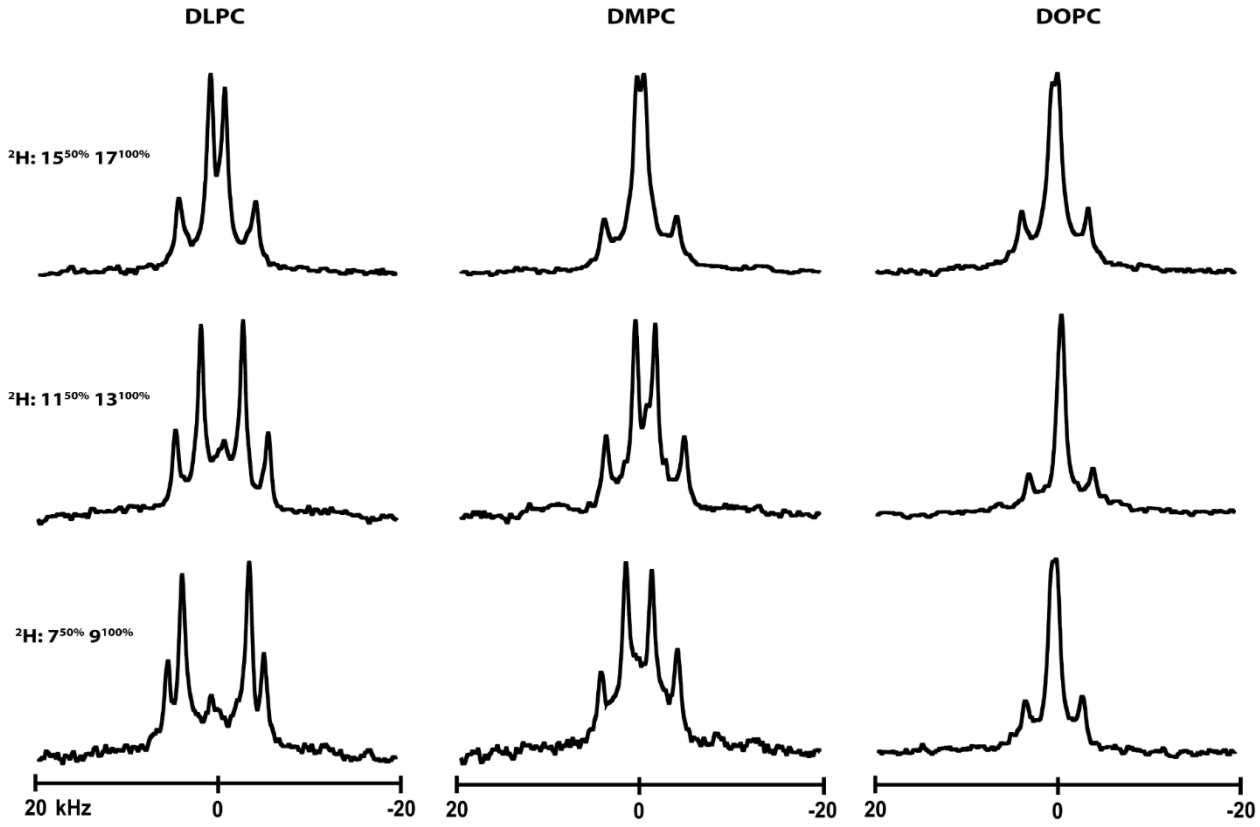

Figure S6: Deuterium NMR spectra for labeled core alanines of $W^{4,5}$GWALP23 peptide. Spectra shown are at $\beta = 90^0$ sample orientation.

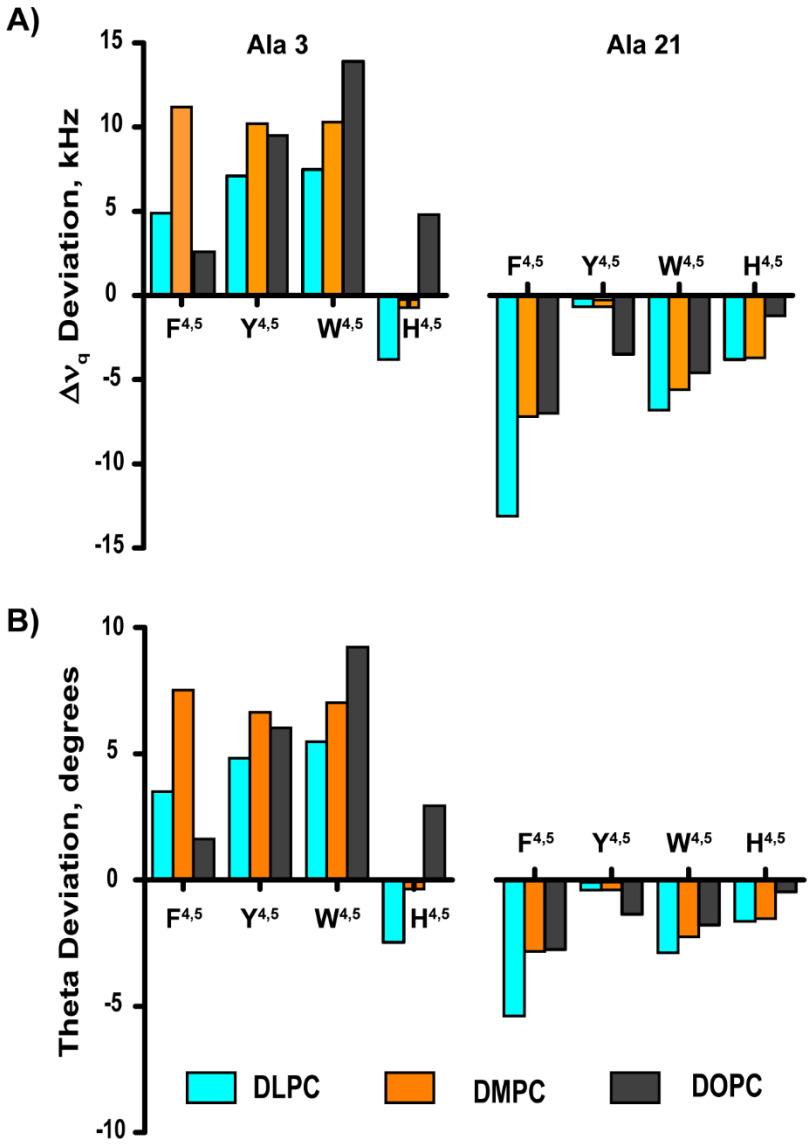

Figure S7: Representation of experimental value deviation of A) quadrupolar splittings, $\Delta\nu_q$ and B) angle theta (θ) for alanine 3 and 21 of $F^{4,5}$, $Y^{4,5}$, $W^{4,5}$ and $H^{4,5}$.

6. Chapter 6: Conclusion

This dissertation focuses on studying the orientations and some dynamic aspects of transmembrane peptides carrying single or multiple histidine residues when present in various depth of the lipid bilayer. Two locations of the histidine residue/s reported in this work are near membrane-water interfaces and one at the core of the bilayer. For the double histidine mutants, the distance between two histidine residues gradually decreases from -$H^{2,22}$ to -$H^{5,19}$ to -$H^{8,16}$ peptides. The effects of adjacent histidine residues at the N-terminal of the transmembrane helix is also addressed.

Through the use of model peptide framework GWALP23, I have characterized a number of important protein-lipid interactions involving histidine residues. Incorporation of histidine residues at the membrane water interface (at positions 2 and/or 22) along with tryptophan residues, either one or both, does not increase the peptide motional averaging like tryptophan, rather the transmembrane orientation of peptide is retained with modest dynamic properties. Hence, some exemptions are observed when a single histidine is present at the C-terminal end of the helix (Chapter 2). When the pair of histidine residues are moved inside the membrane, but still close to the interface, by removing tryptophan residues (5 and 19), the tilt of the -$H^{5,19}$ peptide slightly increases in DOPC lipid membrane compared to the -$H^{2,22}$ analog. Histidine residues successfully maintain a tilted orientation without any issue with motional averaging. However, residue A7 is found to deviate from the helical geometry occasionally (Chapter 3). For further analysis, the histidines were further pushed into the hydrophobic core of the peptide, replacing two leucine residues L8 and L16 (Chapter 4). Such modification causes the helix to adopt two different orientations depending on bilayer thickness. In thinner lipid, the helix remains transmembrane with significant amount of tilt, while in DMPC a portion of peptide fails

to retain this tilted orientation and exit the bilayer. When the bilayer thicknesses are further increased with the use of DPoPC and DOPC lipids, the surface orientation dominates for the -$H^{8,16}$ peptide. Removal of H16 from this helix leaves only on histidine residues H8 and this single histidine peptide is observed to have similar bilayer thickness dependent orientation transition with some adaptation. Unlike other single or double histidine mutants, GWALP23-H^{8} significantly responded with pH change and two pKa values were calculated (Chapter 4). Finally, the effects of two adjacent histidine residues in the molecular orientation, conformation stability and dynamics are addressed (Chapter 5). As seen for $H^{4,5}$GWALP23, these two histidines not only increases the dynamics averaging, but also induces the overall orientation. The helix with two adjacent histidine is highly dynamic and has a very low tilt angle.

Appendix I

Current List of Additional Publications

Peer Reviewed:

Sara J Sustich, **Fahmida Afrose***, Denise V Greathouse, Roger E. Koeppe II, (2019) Influence of interfacial tryptophan residues on an arginine-flanked transmembrane helix. BBA Biomembranes (In press)

Karli Lipinski, Matthew J. McKay, **Fahmida Afrose***, Ashley N. Martfeld, Denise V. Greathouse, Roger E. Koeppe II. (2019). Influence of lipid saturation, hydrophobic length and cholesterol on double-arginine-containing helical peptides in bilayer membranes. ChemBioChem. 20 (41): 2784-2792

Matthew J. McKay, **Fahmida Afrose***, Denise V. Greathouse, Roger E. Koeppe. (2018). Helix formation and stability in membranes. BBA Biomembranes 1860(10):2108-2117